# CHAPTER – 4

# RESULTS AND DISCUSSIONS

The chapter starts with cross-sectional micrographs of various yarn samples to measure their perimeter and cross-sectional area, which are necessary for the analysis of bond behaviour of yarn bundles with cementitious mortar and bond stress calculation during yarn pull-out test. The second section presents the tensile test results of yarn and fabric samples of AR glass, basalt, and carbon (uncoated, epoxy-coated, and hybrid yarn). The subsequent sections present cube compression and cylinder split tensile behaviour, yarn pull-out behaviour of yarn-reinforced cementitious mortar (YRCM), and yarn pull-out behaviour of fabric-reinforced cementitious mortar (FRCM). Later sections address the uniaxial tensile behaviour of FRCM and the flexural behaviour of FRCM.

## 4.1 Cross-section micrograph of yarn specimens

To obtain cross-sectional micrographs of yarn specimens, samples are prepared and polished before being examined under a microscope equipped with a camera and image processing software. The software tool facilitates measurement of the perimeter and areas of different cross-sectional shapes of the specimens. The non-roundness factor (shape factor) of different yarn specimens was calculated using Bueno et al.'s method [151] (*Equation 2*)(Chapter 3, Section 3.5.2).

### 4.1.1 Cross-section micrographs of DREF spun core-sheath yarn

The microstructural behaviour can be analysed by examining the cross-sectional micrograph of the Basalt-PP DREF spun hybrid (core-sheath) yarn and the thermally treated Basalt-PP hybrid yarn in shown in Figure 4.1. The micrographs reveal that the DREF-spun Basalt-PP yarn has a nearly circular geometry, with polypropylene fibres loosely wound around a core of basalt filaments. In contrast, the thermally treated DREF Basalt-PP yarn exhibits an elliptical shape, where the partially melted polypropylene encapsulates, uniformly covers,

and binds the outer filaments of the basalt roving bundle. This encapsulation prevents the peeling off of the PP sheath fibres due to yarn-metal friction during the weaving process while ensuring the minimum flexibility required for fabric formation on the loom. Additionally, this encapsulation enhances adhesion between the PP sheath and the high-performance filament core, thereby improving the mechanical properties of both the yarn and the fabric.

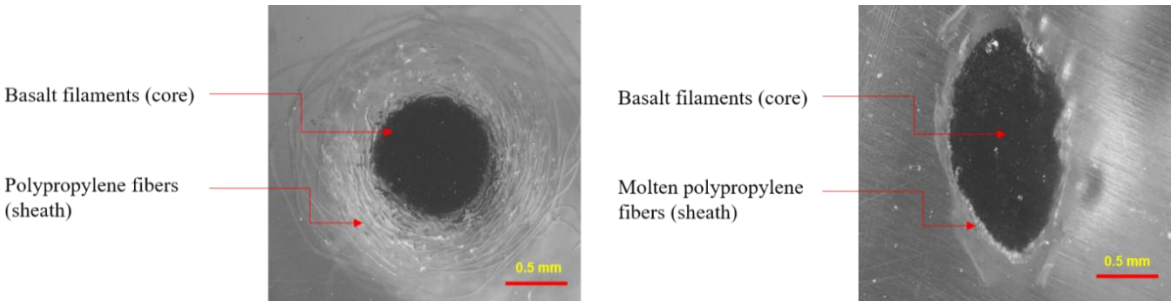


*Figure 4.1 Cross-sectional micrograph of the Basalt-PP DREF spun yarn (left) and thermal treated Basalt-PP yarn (right) at 6x magnification.*

### 4.1.2 Cross-section micrographs of parent, epoxy coated and hybrid yarn

The micrographs of the parent yarn, epoxy-coated yarn, and hybrid yarn configurations are shown in Figure 4.2 for AR glass yarn, Figure 4.3 for basalt yarn, and Figure 4.4 for carbon yarn.

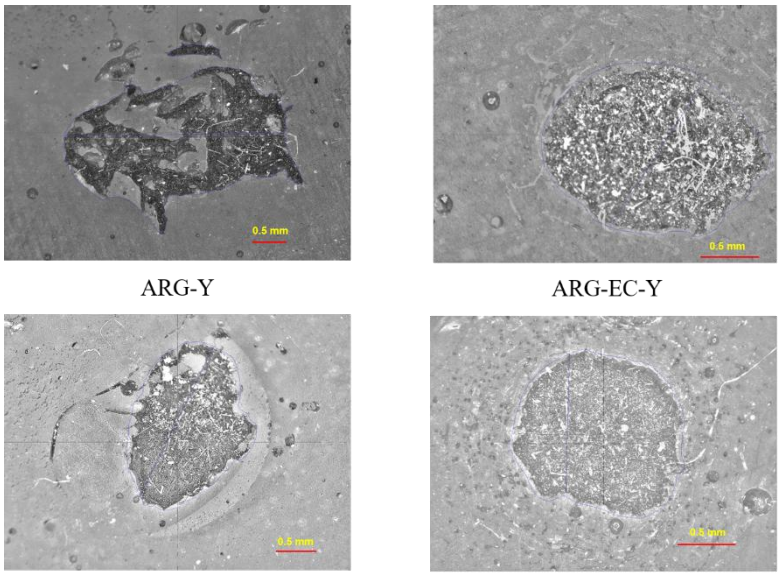

*Figure 4.2 Microscopic cross-sectional image of parent AR glass yarn and hybrid AR glass yarn structures.*

It can be observed that the parent roving bundle comprises of multifilament with smooth surface which relatively poor inter-filament cohesion and likely to spreads in mortar matrix resulting in a flattened cross-section while the epoxy coated are less likely to spread out and making them oval or elliptical cross-section. Similarly, the hybrid yarn cross-sections are also oval or circular in cross-section because they are held by the polypropylene sheath fibres and wrapper PET filaments. The cross-sectional configuration of yarn is important as it decides the filament-mortar interfacial contact region which is likely to influence bonding between filament bundle and mortar matrix and will affect the bond stress.

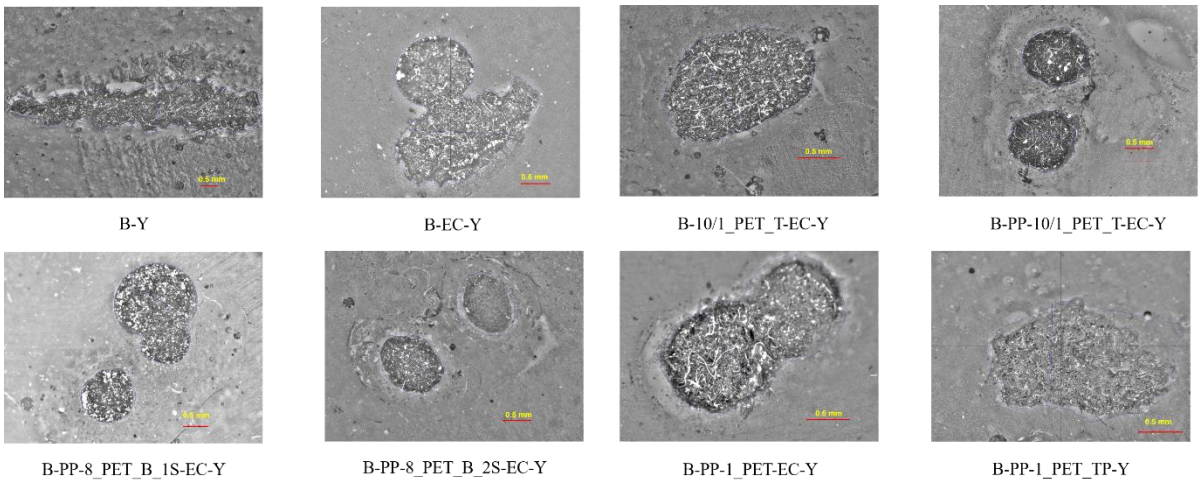


*Figure 4.3 Microscopic cross-sectional image of parent basalt yarn and hybrid basalt yarn structures.*

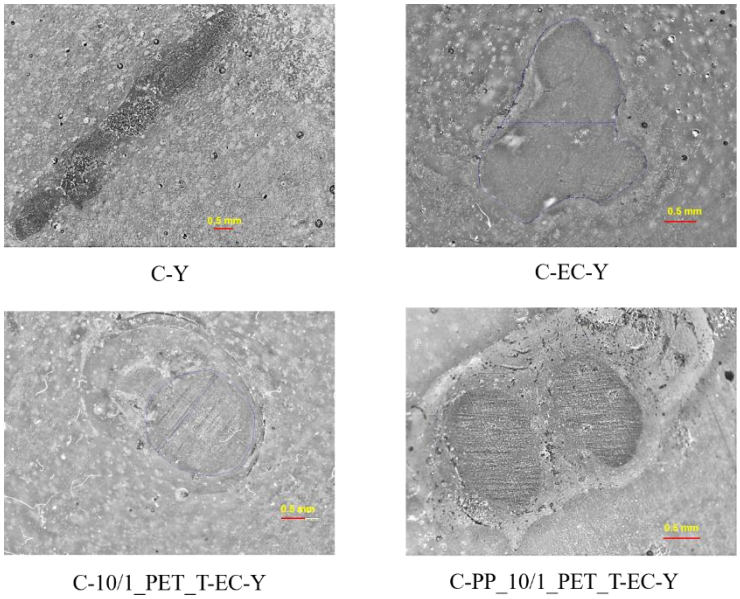


*Figure 4.4 Microscopic cross-sectional images of parent carbon yarn and hybrid carbon yarn structures.*

The cross-sectional perimeter,and areaof various yarn specimens used in this research are measured using the software integrated with the microscope and the values are listed in Table 4.1. The cross-sectional perimeter is also required to calculate the bond stress values of during yarn pull-out test (*Equation 1*). The non-roundness factor (shape factor) of different yarn specimens were calculated using the *Equation 2* and are listed in Table 4.1.

*Table 4.1 Measured perimeter, cross-sectional area and shape factor of yarn specimens using microscope.*

| Yarn specimen code | Perimeter *P* (mm) | Cross sectional area *S*($mm^2$) | Shape factor (non-roundness factor, *k*) |
|---|---|---|---|
| ARG-Y | 10.78 | 5.42 | 1.31 |
| ARG-EC-Y | 5.47 | 2.20 | 1.04 |
| ARG-10/1_PET_T-EC-Y | 6.18 | 2.57 | 1.09 |
| ARG-PP-10/1_PET_T-EC-Y | 4.82 | 1.70 | 1.04 |
| B-Y | 15.56 | 6.39 | 1.74 |

| | | | |
|---|---|---|---|
| B-EC-Y | 10.27 | 4.04 | 1.44 |
| B-10/1_PET_T-EC-Y | 9.82 | 3.41 | 1.50 |
| B-PP-10/1_PET_T-EC-Y | 7.22 | 1.98 | 1.45 |
| B-PP-8_PET_B_1S-EC-Y | 9.81 | 3.55 | 1.47 |
| B-PP-8_PET_B_2S-EC-Y | 6.81 | 1.76 | 1.45 |
| B-PP-1_PET-EC-Y | 6.12 | 2.32 | 1.13 |
| B-PP-1_PET_TP-Y | 6.25 | 2.35 | 1.15 |
| C-Y | 18.21 | 8.17 | 1.80 |
| C-EC-Y | 9.62 | 5.18 | 1.19 |
| C-10/1_PET_T-EC-Y | 7.31 | 4.15 | 1.01 |
| C-PP_10/1_PET_T-EC-Y | 9.12 | 4.89 | 1.16 |

It can be observed that the non-coated parent multifilament bundle (AR glass, basalt, carbon roving/tow) has a higher shape factor, indicating a greater deviation from a round cross-section. This deviation results from the spreading of filaments over a larger surface area, attributed to the absence of twist and inter-filament cohesion.

However, when the same multifilament bundle is covered with PP sheath fibres and PET wrapping (hybrid yarn structure), a binding effect is introduced, preventing filament spreading. Consequently, the shape factor decreases and tends to move toward a more circular cross-section.The shape factor is highest for the parent carbon multifilament bundle (1.80), followed by basalt (1.74) and AR glass (1.31). This trend is linked to the finer carbon filament diameter (7 µm) and the larger number of carbon filaments. The carbon bundle contains the highest number of fine filaments (7 × 6000 = 42,000 filaments), which, due to its higher fineness compared to basalt and AR glass, covers a larger surface area.Basalt follows next, as its bundle consists of a higher number of filaments and finer filaments (13 µm diameter) compared to AR glass (14 µm diameter).Additionally, the AR glass bundle consists of 30 strands of 82 tex, with each strand containing multiple filaments coated with zirconium

to enhance alkaline resistance. This coating causes each filament strand to behave like a monofilament system, preventing filament spreading.Similarly, coating the filament bundle with epoxy resin prevented filament spreading, resulting in a reduced shape factor for the carbon strand (1.19), followed by basalt (1.44) and AR glass (1.04). Furthermore, the introduction of PP fibres as a sheath and PET yarn wrapping around the core strand of carbon, AR glass, and basalt multifilament bundles also led to a reduction in shape factor.

## 4.2 Tensile behaviour of yarn and fabric specimens

Based on the tensile testing of yarn and fabric specimens, the results for average peak load and average displacement at peak load for ARG, basalt, and carbon parent yarns, epoxy-coated yarns, and hybrid yarns are listed in Table 4.2. The corresponding results for fabric specimens are listed in Table 4.3.

*Table 4.2 Tensile load and displacement values of uncoated, epoxy coated and hybrid yarns of ARG, basalt, and carbon.*

| Yarn specimen name | Average peak load (N)(±S.D.) | Average displacement at peak load (mm) (±S.D.) |
|---|---|---|
| ARG-Y | 189.62 (±13.94) | 1.32 (±0.09) |
| ARG-EC-Y | 696.98 (±7.94) | 1.96 (±0.18) |
| ARG-10/1_PET_T-EC-Y | 771.1 (±46.29) | 2.91 (±0.14) |
| ARG-PP-10/1_PET_T-EC-Y | 908.71 (±24.6) | 2.77 (±0.18) |
| B-Y | 297.12 (±22.87) | 1.69 (±0.26) |
| B-EC-Y | 793 (±50.62) | 2.21 (±0.12) |
| B-10/1_PET_T-EC-Y | 1248.9 (±61.21) | 3.61 (±0.18) |

| | | |
|---|---|---|
| B-PP-10/1_PET_T-EC-Y | 1607.44 (±8.6) | 5.29 (±0.34) |
| B-PP-8_PET_B_1S-EC-Y | 1750.42 (±21.96) | 5.58 (±0.23) |
| B-PP-8_PET_B_2S-EC-Y | 1865.48 (±14.48) | 6.5 (±0.38) |
| C-Y | 614.49 (±49.92) | 2.51 (±0.01) |
| C-EC-Y | 1420.61 (±38.44) | 1.48 (±0.19) |
| C-10/1_PET_T-EC-Y | 1626.73 (±41.86) | 1.7 (±0.28) |
| C-PP_10/1_PET_T-EC-Y | 2341.20 (±137.08) | 2.73 (±0.19) |

*Table 4.3 Tensile load and displacement values of uncoated, epoxy coated and hybrid yarn-based fabrics of ARG, basalt, and carbon.*

| Fabric specimen name | Average peak load (N)(±S.D.) | Average displacement at peak load (mm)(±S.D.) |
|---|---|---|
| ARG-F | 541.87 (±42.01) | 2.58 (±0.07) |
| ARG-EC-F | 719.54 (±38.96) | 3.06 (±0.43) |
| ARG-10/1_PET_T-EC-F | 1902.94 (±55.21) | 2.12 (±0.2) |
| ARG-PP-10/1_PET_T-EC-F | 1950.95 (±45.6) | 1.71 (±0.18) |
| B-F | 1342.77 (±61.63) | 2.56 (±0.34) |
| B-EC-F | 2320.4 (±110.33) | 7.72 (±0.52) |
| B-PP-1_PET-EC-F | 2383.63 (±261.94) | 5.71 (±0.74) |

| | | |
|---|---|---|
| B-10/1_PET_T-EC-F | 2598.99 (±93.51) | 5.14 (±0.31) |
| B-PP-10/1_PET_T-EC-F | 3631.92 (±178.19) | 4.08 (±0.52) |
| B-PP-8_PET_B_1S-EC-F | 3634.03 (±176.9) | 5.06 (±0.56) |
| B-PP-8_PET_B_2S-EC-F | 4581.04 (±244.88) | 5.14 (±0.47) |
| B-PP-1_PET_TP-F (10 mm x 12 mm) | 1293.92 (±29.66) | 2.89 (±0.18) |
| B-PP-1_PET_TP-F (6 mm x 7 mm) | 1491.2 (±113.84) | 6.08 (±0.46) |
| C-F | 1977.12 (±78.06) | 1.36 (±0.13) |
| C-EC-F | 2852.04 (±98.86) | 1.86 (±0.64) |
| C-10/1_PET_T-EC-F | 3658.4 (±169.46) | 2.05 (±0.3) |
| C-PP-10/1_PET_T-EC-F | 4177.8 (±153.7) | 2.54 (±0.26) |

### 4.2.1 Tensile behaviour of parent AR glass yarn, hybrid yarn and fabric specimens

The various ARG fabric specimens used in this study and subjected to tensile testing are depicted in Figure 4.5. The fabric construction details are listed in Table 3.6 (Chapter 3, Section 3.3).

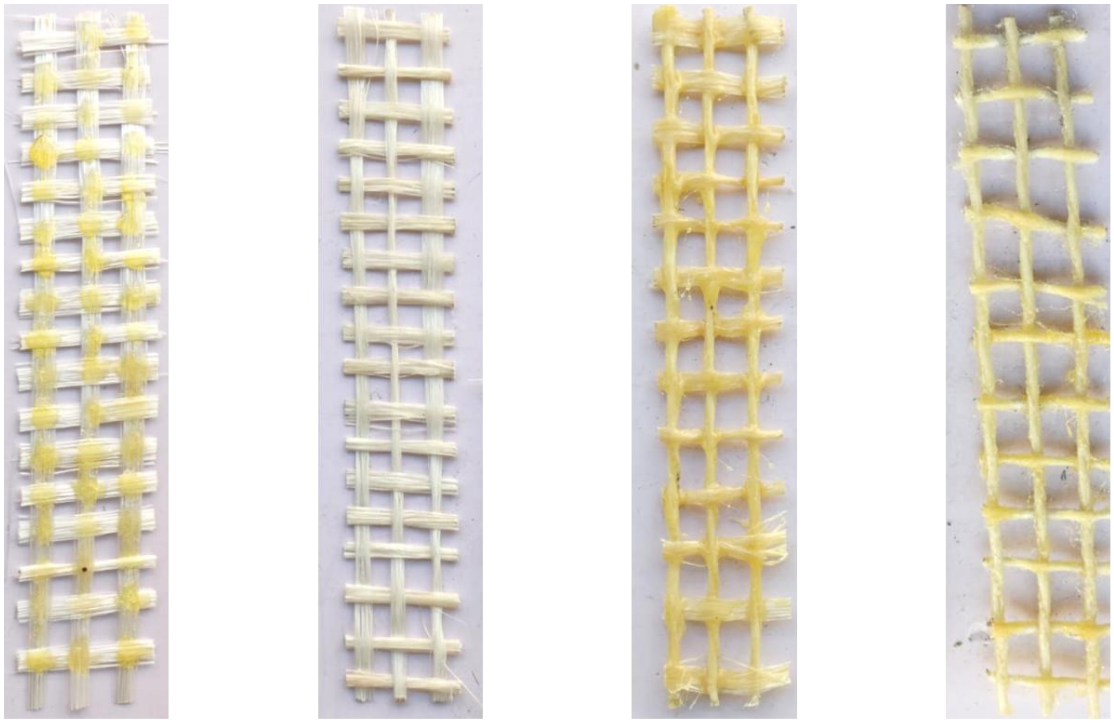

(a) ARG-F (b) ARG-EC-F (c) ARG-10/1_PET_T_EC_F (d) ARG-PP-10/1_PET_T_EC_F

*Figure 4.5 AR glass fabric specimens for tensile test.*

The tensile load-displacement plot for the parent ARG, epoxy-coated ARG, and hybrid ARG yarns is depicted in Figure 4.6(a). The average peak load values from Table 4.2 reveal that the peak load increased from 189.62 N ($\sigma$ = 13.94) for the parent uncoated ARG yarn to 696.98 N ($\sigma$ = 7.94) with epoxy coating. Further enhancement was observed with helical wrapping of PET filament and epoxy coating, reaching 771.1 N ($\sigma$ = 46.29). Hybridization, which involved covering a sheath of low modulus PP fibres on the core of the ARG filament strand and helically wrapping it with twisted PET filament combined with epoxy coating, achieved 908.71 N ($\sigma$ = 24.6). The AR glass hybrid yarn (ARG-PP-10/1_PET_T-EC-Y) exhibited a 379% increase in peak load compared to the parent AR glass yarn (ARG-Y). These improvements facilitated better fibre activation, enhancing load-bearing capacity and ensuring proper load transfer under tensile load application. Additionally, the displacement of hybrid yarns (ARG-PP-10/1_PET_T-EC-Y and ARG-10/1_PET_T-EC-Y) indicates improved ductility, as they exhibit higher displacement at failure compared to the parent and epoxy-coated yarns. This suggests that incorporating ductile fibres such as PP and PET filaments into the hybrid yarn structure enhances ductile behaviour (displacement/elongation) under tensile load. The results demonstrate that the

ductile properties of PP and PET fibres are effectively transferred to the hybrid yarns, leading to increased displacement.

The tensile load-displacement plot for the corresponding fabric specimens is shown in Figure 4.6(b). The average peak load values from Table 4.3 indicate similar improvements in both load and ductility (elongation/displacement) for the fabric specimens, consistent with the trends observed in the yarn specimens.

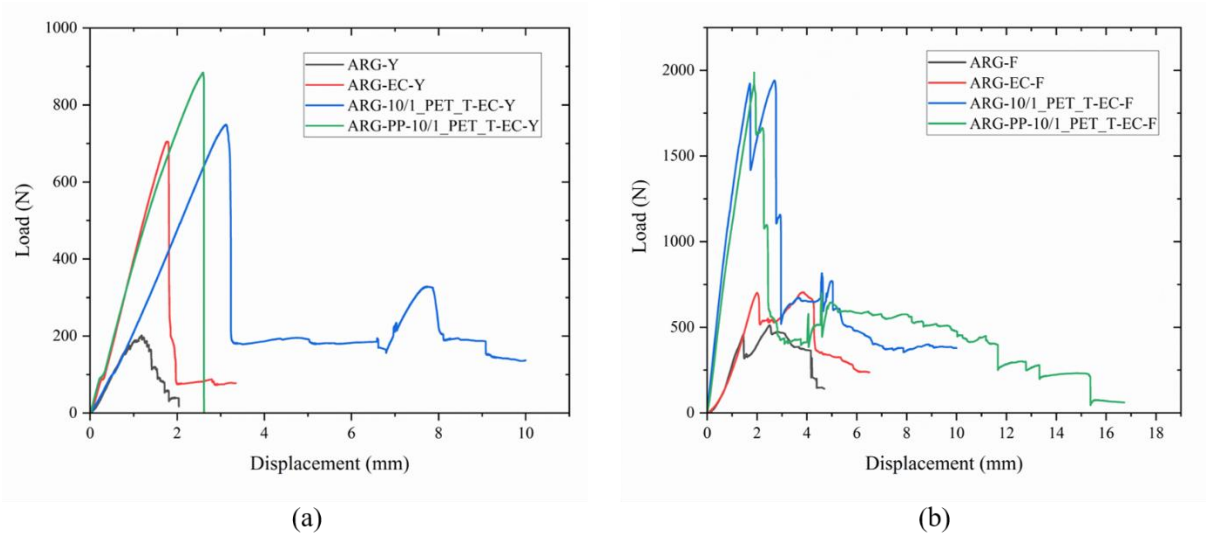


*Figure 4.6 Load displacement plot of (a) AR glass yarn, epoxy coated AR glass yarn, and AR glass hybrid yarn, (b) AR glass fabric, epoxy coated AR glass fabric and AR glass hybrid yarn-based fabrics.*

The tensile test of the ARG-based fabric specimens revealed that the peak load for uncoated ARG fabric was 541.87 N ($\sigma$ = 42.01). This value increased to 719.54 N ($\sigma$ = 38.96) with epoxy coating. Further improvement was seen in the fabric with the incorporation of ARG yarn helically wrapped with PET filament and epoxy coating as the warp yarn, reaching a tensile load of 1902.94 N ($\sigma$ = 55.21). Finally, fabric made from DREF yarn with an ARG core, a sheath of PP fibres, helically wrapped with PET yarn, and epoxy coating as the warp yarn achieved a peak load of 1950.95 N ($\sigma$ = 45.6). The AR glass hybrid yarn-based fabric (ARG-PP-10/1_PET_T-EC-F) exhibited a 260% increase in peak load compared to the parent AR glass yarn-based fabric (ARG-F). As observed in the ARG-based hybrid yarn specimens, fibre hybridization through the incorporation of ductile fibres such as PP and PET filaments resulted in a synergistic effect, enhancing both tensile load and ductility (elongation) in the fabric specimens (ARG-10/1_PET_T-EC-F and ARG-PP-10/1_PET_T-EC-F). This

demonstrates that the improved mechanical behaviour of hybrid yarns is effectively transferred to the corresponding fabric specimens.

### 4.2.2 Tensile behaviour of parent basalt yarn, hybrid yarn and fabric specimens

The various basalt fabric specimens used in this study and subjected to tensile testing are depicted in Figure 4.7. The fabric construction details are listed in Table 3.6 (Chapter 3, Section 3.3).

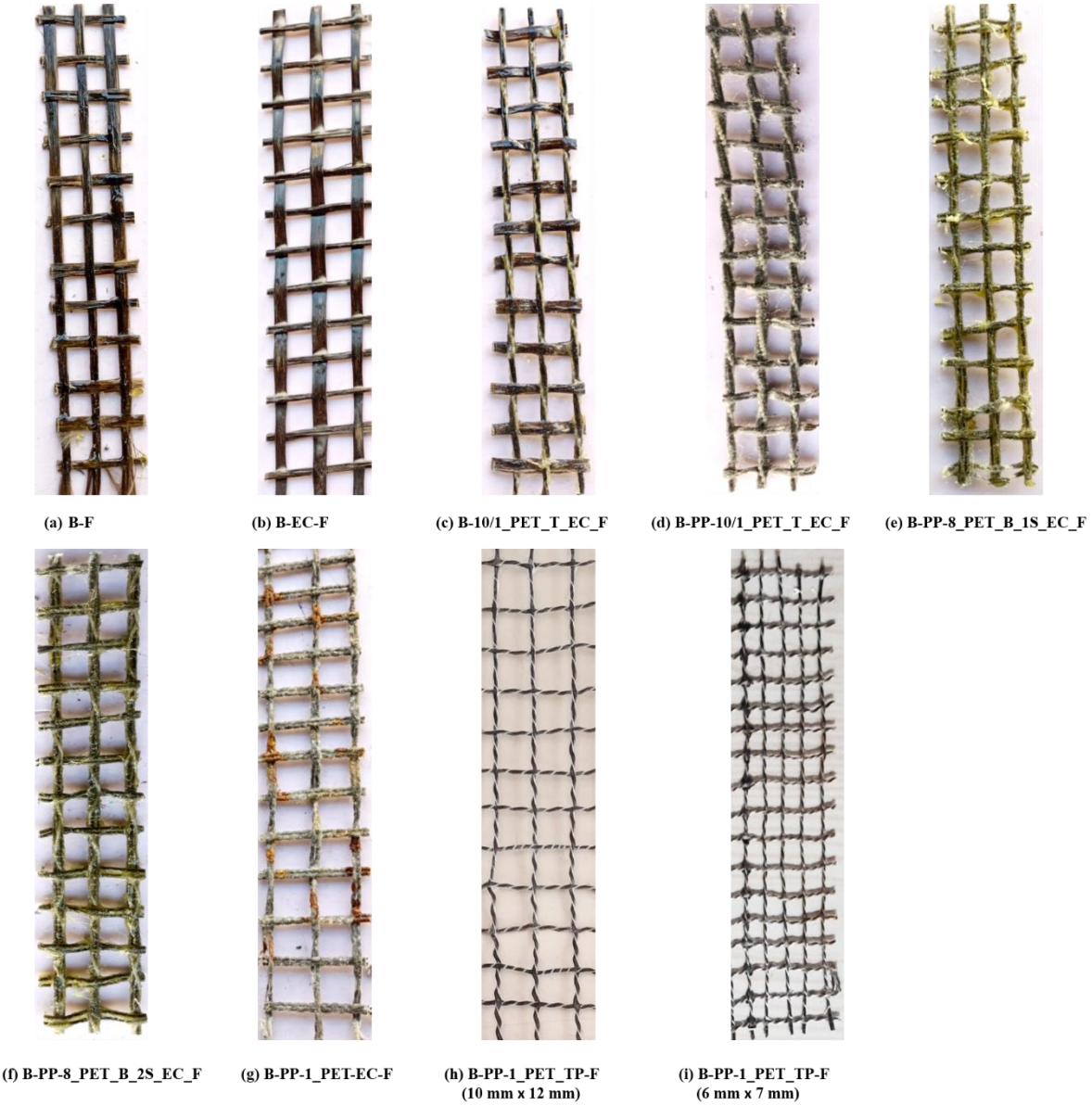


*Figure 4.7 Basalt fabric specimens for tensile test.*

The tensile load-displacement plot for the parent basalt, epoxy-coated basalt, and hybrid basalt yarns is depicted in Figure 4.8(a).The average peak load values from Table 4.2 reveal

that the peak load value increased from 297.12 N (σ = 22.87) for the parent uncoated basalt yarn to 793 N (σ = 50.62) with epoxy coating. Further enhancement was observed with the helical wrapping of PET filament and epoxy coating, reaching 1248.9 N (σ = 61.21). Hybridization, which involved covering a sheath of low modulus PP fibres on the core of the basalt filament strand and helically wrapping it with twisted PET filament combined with epoxy coating, achieved 1607.44 N (σ = 8.6). These improvements facilitated better fibre activation, enhancing load-bearing capacity and ensuring proper load transfer under tensile load application. Additionally, the incorporation of ductile fibres such as PP and PET filaments in the hybrid yarn structure improved ductile behaviour (elongation). Similarly, helical wrapping using a braided PET structure over the core of the basalt-PP DREF yarn combined with epoxy coating improved the peak load to 1750.42 N (σ = 21.96). When two braided PET strands are helically wrapped over the basalt-PP DREF yarn (core strand), crossing each other and epoxy coated, the peak load further increased to 1865.48 N (σ = 14.48). The hybrid yarns – B-PP-10/1_PET_T-EC-Y and B-PP-8_PET_B_2S-EC-Y exhibited a 440% and 527% increase in peak load, respectively, compared to the parent basalt yarn (B-Y).The reasons for the improvement in tensile load and ductility (elongation/displacement) in the basalt-based hybrid yarn specimens (B-10/1_PET_T-EC-Y, B-PP-10/1_PET_T-EC-Y, B-PP-8_PET_B_1S-EC-Y, and B-PP-8_PET_B_2S-EC-Y) are the same as those stated for the ARG hybrid yarn specimens discussed in Section 4.2.1.

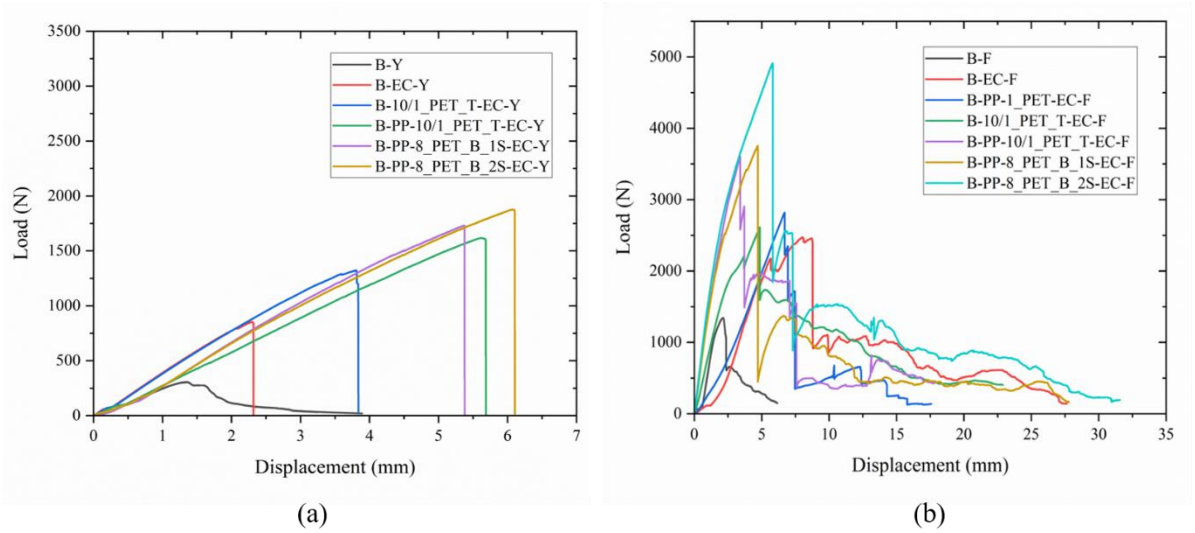


*Figure 4.8 Load displacement plot of – (a) Basalt yarn, epoxy coated basalt yarn, and basalt hybrid yarn, (b) Basalt fabric, epoxy coated basalt fabric and basalt hybrid yarn-based fabrics.*

The tensile load-displacement plot for the fabric specimens is shown in Figure 4.8(b). The average peak load values from Table 4.3 indicate similar improvements in both load and ductility (elongation/displacement) for the fabric specimens, consistent with the trends observed in the yarn specimens.It reveals that the uncoated basalt fabric had a peak load of 1342.77 N ($\sigma$ = 61.63), which improved to 2320.4 N ($\sigma$ = 110.33) with epoxy coating. Further enhancement was seen when basalt yarn with helical wrapping of PET filament and epoxy coating was used as the warp yarn, increasing the fabric tensile load to 2598.99 N ($\sigma$ = 93.51). Finally, fabric made of warp yarn with a DREF yarn core of basalt and a sheath of PP fibres, helically wrapped by PET yarn and epoxy coated, improved the peak load to 3634.92 N ($\sigma$ = 178.19). Additionally, fabric with warp yarn comprising helical wrapping using a braided PET structure over the core of the basalt-PP DREF yarn combined with epoxy coating improved the peak load to 3634.03 N ($\sigma$ = 176.9). When warp yarn had two braided PET strands helically wrapped over the basalt-PP DREF yarn (core strand), crossing each other and epoxy coated, the peak load further increased to 4581.04 N ($\sigma$ = 244.88). The basalt hybrid yarn-based fabrics – B-PP-10/1_PET_T-EC-F and B-PP-8_PET_B_2S-EC-F exhibited a 170% and 241% increase in peak load, respectively, compared to the parent basalt yarn-based fabric (B-F).The reasons for the improvement in tensile load and ductility (elongation/displacement) in the basalt hybrid yarnbased fabric specimens (B-10/1_PET_T-EC-F, B-PP-10/1_PET_T-EC-F, B-PP-8_PET_B_1S-EC-F, and B-PP-8_PET_B_2S-EC-F) are the same as those stated for the ARG hybrid yarnbased fabric specimens discussed in Section 4.2.1.

### 4.2.3 Effect of mesh opening on tensile behaviour of hybrid yarn based thermoplastic fabric composite specimens

The tensile load-displacement plot for the thermoplastic fabric composite specimens is shown in Figure 4.9. The initial non-linearity in the tensile load-displacement plot is attributed to yarn waviness (crimp) caused by the interlacement of warp and weft yarns during the weaving process. This results in a small initial increase in load and higher displacement due to crimp removal from the warp yarn, followed by a further increase in load (linear behaviour) as the warp yarns straighten and begin to contribute to load-bearing. Subsequently, a sudden decrease in load occurs due to warp yarn rupture, after which the load is redistributed among the remaining warp yarns, leading to a slight increase in load. This process continues until all the load-bearing warp yarns break, significantly reducing the load-bearing capacity and causing substantial elongation of the specimen[162].

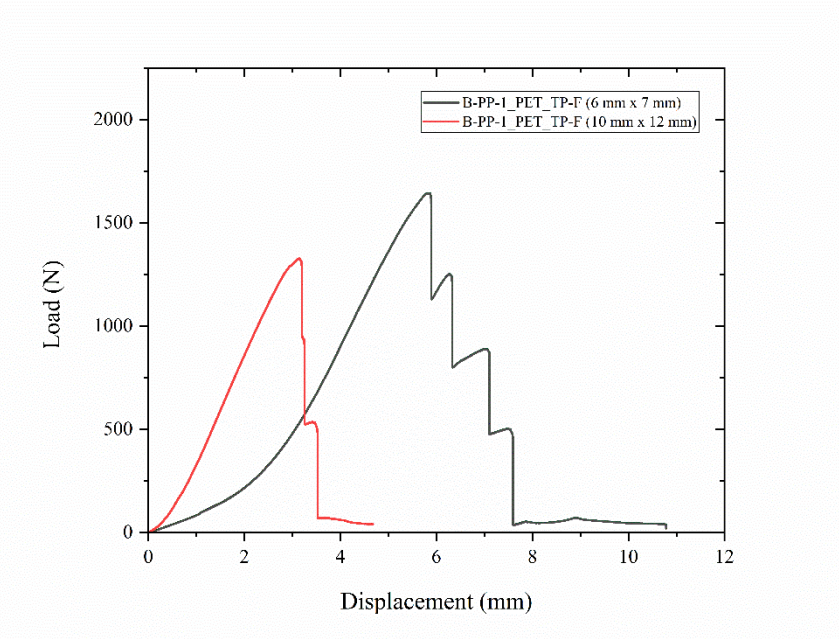


*Figure 4.9 Load displacement plot of basalt fabric thermoplastic composites with mesh openings 6 mm x 7 mm and 10 mm x 12 mm.*

The tensile test results of two thermoplastic fabric composites, one with a mesh size of 6 mm x 7 mm and the other with a mesh size of 10 mm x 12 mm, indicate that the fabric composite with the smaller mesh opening has a higher load-bearing ability [491.2 N ($\sigma$ = 113.84)] and greater elongation compared to the fabric composite with the larger mesh opening [1293.92 ($\sigma$ = 29.66)]. A decrease in mesh opening size from 10 mm x 12 mm to 6 mm x 7 mm improves the peak load value by 15.24%. This difference is due to the number of warp yarns participating in load bearing, with three warp yarns in the 10 mm x 12 mm mesh size and five in the smaller 6 mm x 7 mm mesh size. The higher number of warp yarns in the fabric specimen with a smaller mesh size contributed to its greater tensile load-bearing capacity and elongation.

### 4.2.4 Tensile behaviour of parent carbon yarn, hybrid yarn and fabric specimens

The various carbon fabric specimens used in this study and subjected to tensile testing are depicted in Figure 4.10. The fabric construction details are listed in Table 3.6 (Chapter 3, Section 3.3).

(a) C-F (b) C-EC-F (c) C-10/1_PET_T_EC_F (d) C-PP-10/1_PET_T_EC_F

*Figure 4.10 Carbon fabric specimens for tensile test.*

The tensile load-displacement plot for the parent basalt, epoxy-coated basalt, and hybrid basalt yarns is depicted in Figure 4.11(a).The average peak load values from Table 4.2 reveal that the peak load value increased from 614.49 N ($\sigma$ = 49.92) for the parent uncoated carbon yarn to 1420.61 N ($\sigma$ = 38.44) with epoxy coating. Further enhancement was observed with helical wrapping of PET filament and epoxy coating, reaching 1626.73 N ($\sigma$ = 41.86). Hybridization, which involved covering a sheath of low modulus PP fibres on the core of the carbon multi-filament strand and helically wrapping it with twisted PET filament combined with epoxy coating, achieved 2341.20 N ($\sigma$ = 137.08). The carbon hybrid yarn (C-PP-10/1_PET_T-EC-Y) exhibited a 280% increase in peak load compared to the parent carbon yarn (C-Y). These improvements facilitated better fibre activation, enhancing load-bearing capacity and ensuring proper load transfer under tensile load application. Additionally, the incorporation of ductile fibres such as PP and PET filaments in the hybrid yarn structure improved ductile behaviour (elongation). The reasons for the improvement in tensile load and ductility (elongation/displacement) in the carbon-based hybrid yarn specimens (C-10/1_PET_T-EC-Y, and C-PP-10/1_PET_T-EC-Y) are the same as those stated for the ARG hybrid yarn specimens discussed in Section 4.2.1.

The tensile load-displacement plot for the fabric specimens is shown in Figure 4.11(b).

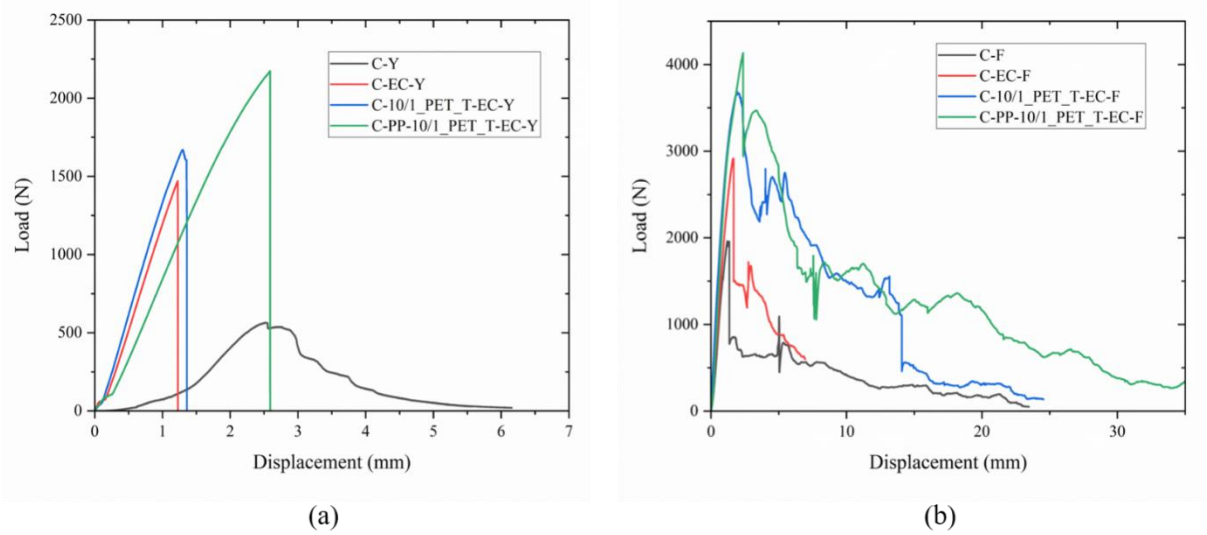


*Figure 4.11 Load displacement plot of – (a) Carbon yarn, epoxy coated carbon yarn, and carbon hybrid yarn, (b) Carbon fabric, epoxy coated carbon fabric and carbon hybrid yarn-based fabrics.*

The average peak load values from Table 4.3 indicate similar improvements in both load and ductility (elongation/displacement) for the fabric specimens, consistent with the trends observed in the yarn specimens.It reveals thatthe peak load for uncoated carbon fabric was 1977.12 N (σ = 78.06). This value increased to 2852.04 N (σ = 98.86) with epoxy coating. Further improvement was seen in the fabric with the incorporation of carbon yarn helically wrapped with PET filament and epoxy coating as the warp yarn, reaching a tensile load of 3658.4 N (σ = 169.46). Finally, fabric made from DREF yarn with a carbon core, a sheath of PP fibres, helically wrapped with PET yarn, and epoxy coating as the warp yarn achieved a peak load of 4177.8 N (σ = 153.7). The carbon hybrid yarn-based fabric (C-PP-10/1_PET_T-EC-F) exhibited a 111% increase in peak load compared to the parent carbon yarn-based fabric (C-F).The reasons for the improvement in tensile load and ductility (elongation/displacement) in the carbon hybridyarn-based fabric specimens (C-10/1_PET_T-EC-F, and C-PP-10/1_PET_T-EC-F) are the same as those stated for the ARG hybridyarn-based fabric specimens discussed in Section 4.2.1.

### 4.2.5 Comparison of tensile behaviour of parent and hybrid AR glass, basalt, carbon yarn and fabric specimens

When comparing the tensile behaviour (load-displacement plot) of parent AR glass, basalt, and carbon yarns (for filament bundle strands with nearly equivalent tex), it is evident that the peak load is highest for carbon, followed by basalt, and lowest for AR glass (Figure 4.12a& Table 4.2), reflecting their inherent mechanical properties. The peak load for parent carbon yarn (C_Y) and parent basalt yarn (B_Y) was 224% and 56% higher than that of parent AR glass yarn (ARG_Y), respectively. This trend continues in hybrid yarns made from these materials, particularly for yarn bundle strands with nearly equivalent tex.The peak load for carbon hybrid yarn (C-PP-10/1_PET_T-EC-Y) and basalt hybrid yarn (B-PP-10/1_PET_T-EC-Y) was 157% and 105% higher than that of AR glass hybrid yarn (ARG-PP-10/1_PET_T-EC-Y), respectively. The corresponding fabrics (with similar geometry and mesh openings made up of nearly equivalent yarn tex) also exhibit similar tensile behaviour, as shown in Figure 4.12 (b).

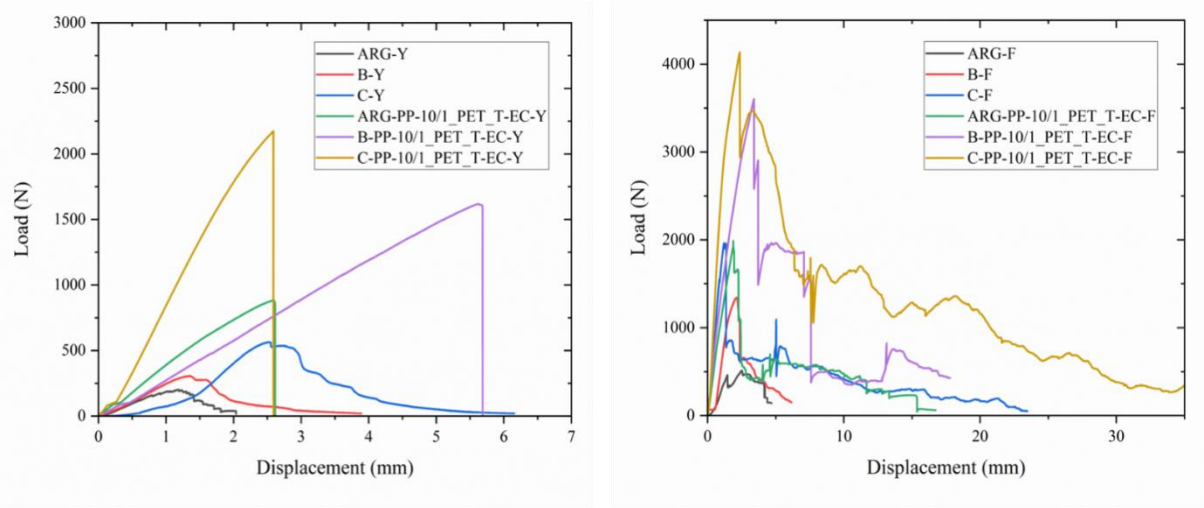


*Figure 4.12 Comparison of load displacement plot of (a) AR glass, basalt, carbon yarn, and their hybrid yarns, (b) AR glass, basalt, carbon fabric, and their hybrid yarn-based fabrics.*

The peak load for parent carbon yarn-based fabric (C_F) and parent basalt yarn-based fabric (B_F) was 264% and 147% higher than that of parent AR glass yarn-based fabric (ARG_F), respectively. The peak load for carbon hybrid yarn-based fabric (C-PP-10/1_PET_T-EC-F) and basalt hybrid yarn-based fabric (B-PP-10/1_PET_T-EC-F) was 114% and 86% higher than that of AR glass hybrid yarn-based fabric (ARG-PP-

10/1_PET_T-EC-F), respectively.The superior tensile load-bearing capacity of carbon, followed by basalt, and the lowest for AR glass in both yarn and fabric specimens is attributed to the inherent tensile strength of the fibres (carbon > basalt > AR glass), as listed in Table 3.1.

### 4.2.6 Discussion on tensile behaviour of parent yarn, hybrid yarn and fabric specimens

The parent ARG, basalt, and carbon yarn bundle consist of numerous individual filaments, with only a small fraction being loaded or fractured at any given time. High-performance filament bundles often contain surface imperfections and defects in some filaments, leading to stress concentration in weaker regions and subsequent fractures during tensile loading. Due to the high sensitivity of these filaments, fractures initiate and propagate from individual filaments. Uncoated high-performance filaments exhibit non-linear tensile behaviour as individual fibres break without causing the complete failure of the multifilament bundle. Initially, the load increases linearly with elongation, followed by limited non-linearity until the peak load is reached. As more fibres fracture, the load gradually decreases with further elongation, leading to inferior tensile performance compared to their theoretical potential, with pull-out failures being predominantly observed. However, research suggests that applying a controlled amount of coating and sizing can effectively improve surface characteristics and enhance the tensile behaviour of high-performance multifilament bundles [163].

Yarn hybridization and epoxy coating have significantly improved the tensile performance of ARG, basalt, and carbon yarns. In DREF spun yarn, the PP fibre sheath acts as a binding element, securing the high-performance multifilament core strand. This binding effect is further reinforced by thermal treatment and the helical wrapping of PET twisted yarn. The application of epoxy resin on the hybrid yarn provides surface coating and facilitates resin impregnation within the bundle, enhancing its stiffness and allowing it to behave more like a monofilament system[138]. This results in improved fibre activation, better load transfer, and enhanced load-sharing performance under tensile forces compared to uncoated, non-hybrid parent high-performance yarns. The core strand of the high-performance roving bundle is responsible for load-bearing behaviour, while the low-modulus ductile fibres (PP and PET) contribute to improved ductility. This leads to a synergistic effect, increasing the peak load capacity while enhancing ductile behaviour (elongation/displacement) due to the incorporation of PP and PET filaments in the hybrid yarn structure[23].

Under tensile loading, fabric specimens initially exhibit a non-linear response, with a slow increase in load as displacement occurs due to fabric crimp (waviness). Once the crimp is removed, the load increases linearly with displacement until the peak load is reached[162]. This is followed by the detachment of the weft yarn (fabric distortion) and the rupture of the warp yarn that either bears the highest load or is the weakest among the warp yarns. This rupture results in a sudden drop in load, which is then redistributed among the remaining warp yarns, causing a slight increase in load. This process continues until all load-bearing warp yarns fail, significantly reducing the fabric's load-bearing capacity and causing substantial elongation of the specimen.

## 4.3 Compression behaviour of Mortar Cubes

The average reading of three mortar cube specimens of size 150 mm x 150 mm x 150 mm (length x width x height) was considered for compressive strength. The mean compressive strength and the standard deviation were 64.6 MPa ($\sigma$ = 2.05). The image of the cube specimen after compression test is depicted in Figure 4.13.

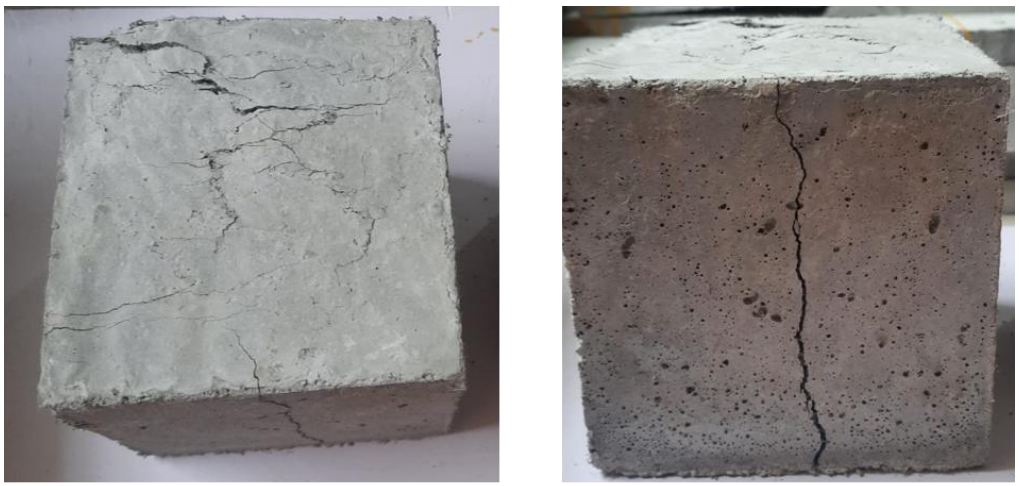

(a) (b)

*Figure 4.13 Mortar cube specimen after compression test.*

## 4.4 Cylinder split tensile behaviour of Mortar Cylinders

The average reading of three mortar cylinder specimens, each with a diameter of 150 mm and a height of 300 mm, was used to determine the split tensile strength. The mean split tensile strength for the unreinforced cylinder was 6.73 MPa ($\sigma$ = 0.21), while for the basalt

thermoplastic fabric composite [B-PP-1_PET_TP-F (10 mm x 12 mm)] reinforced cylinder, it was 7.55 MPa (σ = 0.31), suggesting an improvement of 12%. This demonstrates that incorporating fabric reinforcement in mortar cylinder specimens enhances resistance to splitting under compressive loading and highlights the effectiveness of fabric reinforcement in handling the tensile forces induced during the split tensile test. The images of the cylinder specimens, both unreinforced and thermoplastic fabric composite (single layer) reinforced, after the split tensile test are depicted in Figure 4.14. The fabric reinforced specimens have undergone fabric rupture and pull-out as shown in the Figure 4.14 (b).

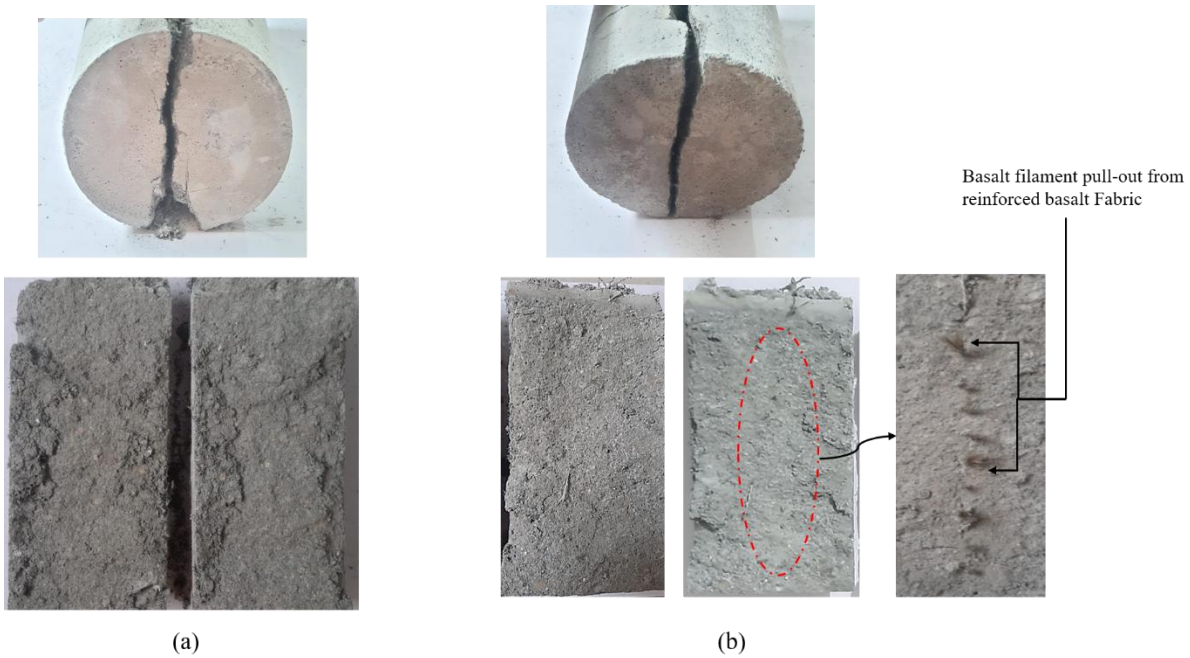


*Figure 4.14 Mortar cylinder specimens after split tensile test – (a) unreinforced mortar, (b) reinforced with a single layer of basalt thermoplastic FRCM.*

## 4.5 Yarn pull-out behaviour of yarn reinforced cementitious mortar specimens

The yarn pull-out behaviour of yarn-reinforced cementitious mortar (YRCM), comprising different yarns – parent (uncoated) AR glass, basalt, carbon, and their epoxy coated and hybrid yarn structures is discussed. The yarn-reinforced mortar is cast in the form of plate specimens with dimensions of 15 mm x 60 mm x 500 mm. The test procedure is described in Section 3.10, Chapter 3. The pull-out load versus slip behaviour, along with the average bond stress and energy absorbed, is plotted and analysed.

### 4.5.1 Yarn pull-out behaviour of AR glass YRCM specimens

The graph in Figure 4.15(a) illustrates the yarn pull-out load versus bond slip behaviour of different AR glass yarn-based specimens – uncoated, epoxy-coated, and hybrid, with a yarn embedment length of 25 mm. The uncoated AR glass yarn had a lower average peak pull-out load of 619 N (σ = 21), which increased to 716 N (σ = 20) with epoxy coating. The addition of twisted PET yarn helically wrapped around the AR glass yarn core, combined with epoxy coating, further increased the load to 743 N (σ = 30). Finally, the DREF yarn, consisting of an AR glass filament core, a PP fibre sheath, helically wrapped twisted PET yarn, and an epoxy coating, achieved the highest peak load of 1070 N (σ = 31), representing a 72% increase in yarn pull-out load compared to the parent uncoated AR glass YRCM specimen. This improvement suggests that incorporating a hybrid yarn structure and epoxy coating enhances fibre activation, facilitates better load transfer, and improves load-sharing performance, along with providing strong mechanical anchorage within the cementitious matrix(a detailed description is provided in Section 4.6.6, Figure 4.30).

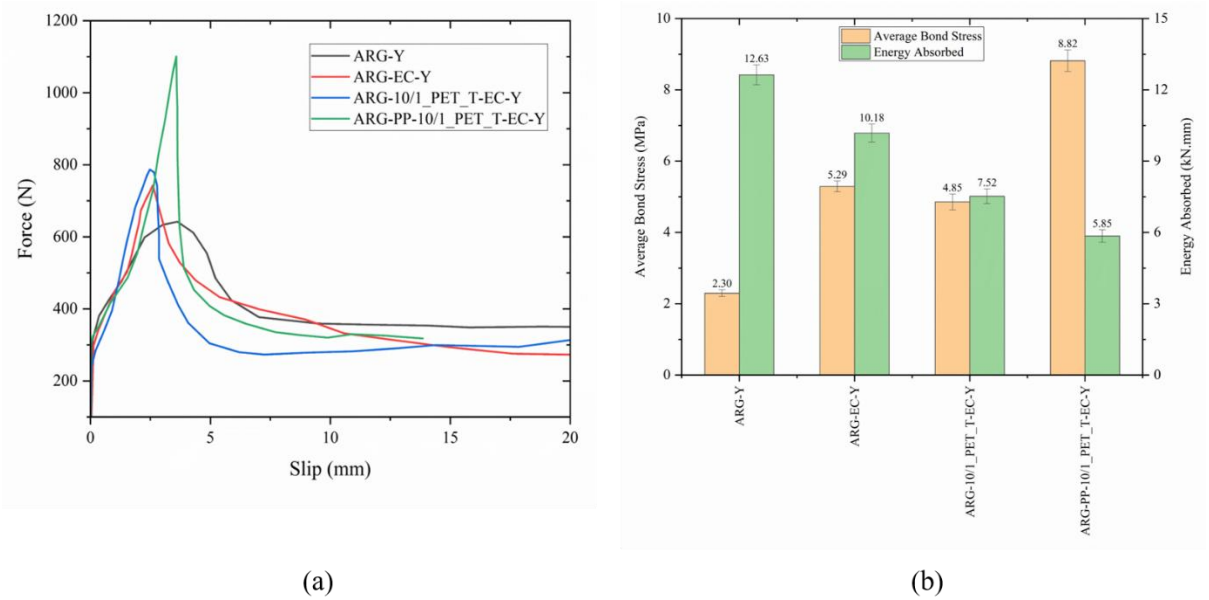


(a) (b)

*Figure 4.15 (a) Pull-out force and slip behaviour of parent, epoxy-coated, and hybrid AR glass YRCM specimens, (b) plot representing average bond stress and energy absorbed by AR glass YRCM specimens during the yarn pull-out test.*

Figure 4.15(b) illustrates the average bond stress and energy absorbed by the specimens. As shown in the graph, bond stress, which depends on the yarn perimeter in contact with the mortar, significantly increases from the parent yarn (2.30 MPa) to the epoxy-

coated (5.29 MPa) and hybrid yarns (4.85 MPa and 8.82 MPa). The uncoated parent yarn, being flattened and less consolidated, has a larger contact perimeter with the mortar, resulting in lower bond stress (yarn cross-sectional area, perimeter, and shape factor values are provided in Table 4.4).In contrast, epoxy-coated and hybrid yarns exhibit a smaller contact perimeter with improved consolidation due to epoxy resin impregnation and structural binding by PP fibres and PET filaments during hybrid yarn production. The hybrid yarn structure, featuring a surface-twisted PET yarn secured by an epoxy resin coating, enhances mechanical anchorage within the mortar matrix, resulting in higher peak load and bond stress (a detailed description is provided in Section 4.6.6, Figure 4.30).

Further, Figure 4.15(b) illustrates the energy absorption values of different AR glass-based YRCM specimens, calculated from the area under the load-slip curve. The parent AR glass yarn exhibits the highest value, followed by the epoxy-coated yarn, while hybrid yarn structures show the lowest energy absorption.

The images of AR glass yarn-based specimens after the yarn pull-out test are shown in Figure 4.16.

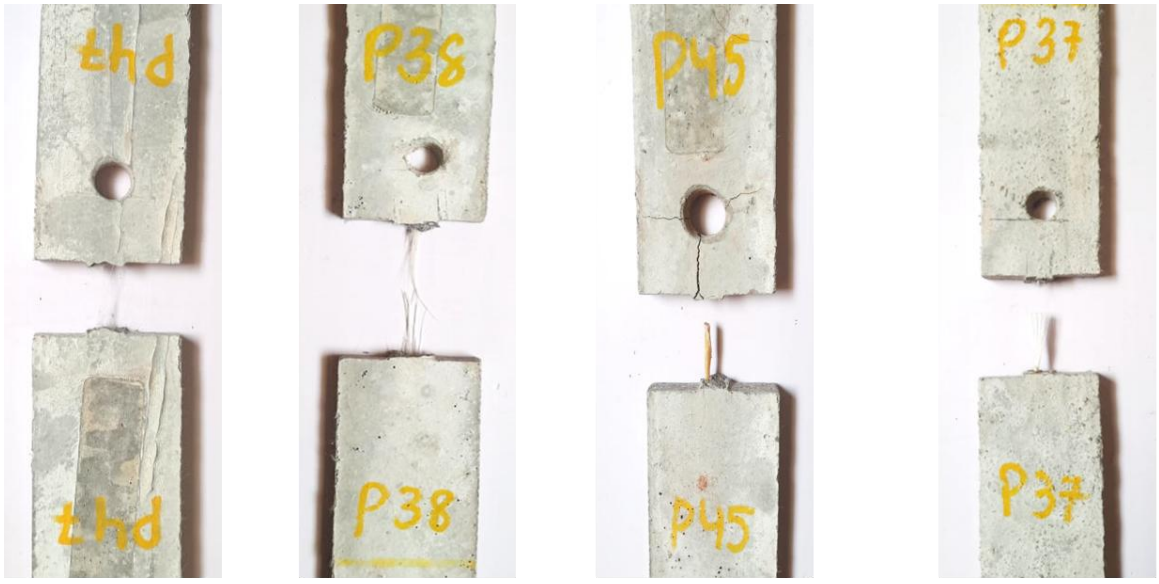


(a) ARG-Y (b) ARG-EC-Y (c) ARG-10/1_PET_T-EC-Y (d) ARG-PP-10/1_PET_T-EC-Y

*Figure 4.16 Photographs of different YRCM specimens reinforced with AR glass yarn, epoxy coated AR glass yarn, and AR glass hybrid yarns following yarn pull-out test.*

The parent AR glass yarn (ARG_Y) and epoxy-coated AR glass yarn (ARG_EC_Y) exhibit failure through a combination of fibre fracture and pull-out. The twisted PET helically

wrapped ARG yarn specimen (ARG-10/1_PET_T-EC-Y) shows pull-out behaviour, with significant mortar damage indicated by major cracks, signifying strong bonding with the mortar matrix. The hybrid yarn specimen (ARG-PP-10/1_PET_T-EC-Y), featuring an ARG-PP DREF spun yarn core, exhibited telescopic failure under pull-out loading. This failure mode suggests that epoxy resin penetration through the PP sheath was inadequate in the hybrid ARG yarn. Additionally, the zirconium coating on the AR glass bundle hindered effective bonding between the filaments and the resin, resulting in poor wetting of the AR glass filaments. Consequently, the inner core filaments slipped out, leaving the outer PP sleeve embedded in the mortar during the pull-out test. As a result, no significant crack development, damage, or spalling was observed in the concrete specimen during the yarn pull-out test of hybrid ARG yarn-based YRCM specimens.

### 4.5.2 Yarn pull-out behaviour of Basalt YRCM specimens

The graph in Figure 4.17(a) illustrates the yarn pull-out load versus bond slip behaviour of different basalt YRCM specimens: uncoated, epoxy-coated, and hybrid, with a yarn embedment length of 25 mm. The uncoated basalt yarn had an average peak pull-out load of 688 N ($\sigma$ = 12), which increased to 703 N ($\sigma$ = 5) with epoxy coating. Wrapping a single PET yarn over Basalt-PP DREF yarn with epoxy coating improved the pull-out load to 747 N ($\sigma$ = 25). The addition of twisted PET yarn (10/1_PET) helically wrapped around the basalt yarn core, combined with epoxy coating, further enhanced the load to 757 N ($\sigma$ = 14). The DREF yarn with a basalt filament core, a sheath of PP fibres, helically wrapped with twisted PET yarn (10/1_PET) and epoxy coating, achieved a peak load of 1038 N ($\sigma$ = 47). Similarly, helical wrapping using a braided PET structure over the core of the basalt-PP DREF yarn combined with epoxy coating improved the peak pull-out load to 1186 N ($\sigma$ = 25), while helical wrapping with two braided PET structures crossing each other increased the peak pull-out load to 1310 N ($\sigma$ = 57), representing a 90% increase in yarn pull-out load over the parent uncoated basalt yarn reinforced mortar specimen(a detailed description is provided in Section 4.6.6, Figure 4.30).The reasons for the improvement in pull-out load in the basalt hybrid yarn based YRCM specimens are the same as those stated for the ARG hybrid yarn-based fabric specimens discussed in Section 4.5.1.

Figure 4.17(b) shows the average bond stress and energy absorbed by the specimens. The average bond stress shows a substantial increase from parent yarn (1.78 MPa) to epoxy-coated (2.74 MPa) and hybrid yarns (ranges between 3.09 MPa to 12.54 MPa). The core

basalt strand, helically wrapped with twisted and braided PET yarn, and secured by epoxy resin coating, improves the mechanical anchorage (bonding) between the yarn surface and the cementitious mortar. This enhancement results in higher pull-out load and bond stress values. The reasons for the improvement in average bond stress values in the basalt hybrid yarn based YRCM specimens are the same as those stated for the ARG hybrid yarn-based fabric specimens discussed in Section 4.5.1.The energy absorbed during yarn pull-out is highest for the basalt hybrid yarns B-PP-10/1_PET_T-EC-Y and B-PP-8_PET_B_2S-EC-Y, followed by the parent basalt yarn (B-Y), then B-PP-1_PET-EC-Y, the epoxy-coated yarn (B-EC-Y), and finally B-10/1_PET_T-EC-Y, which has the lowest energy absorption.

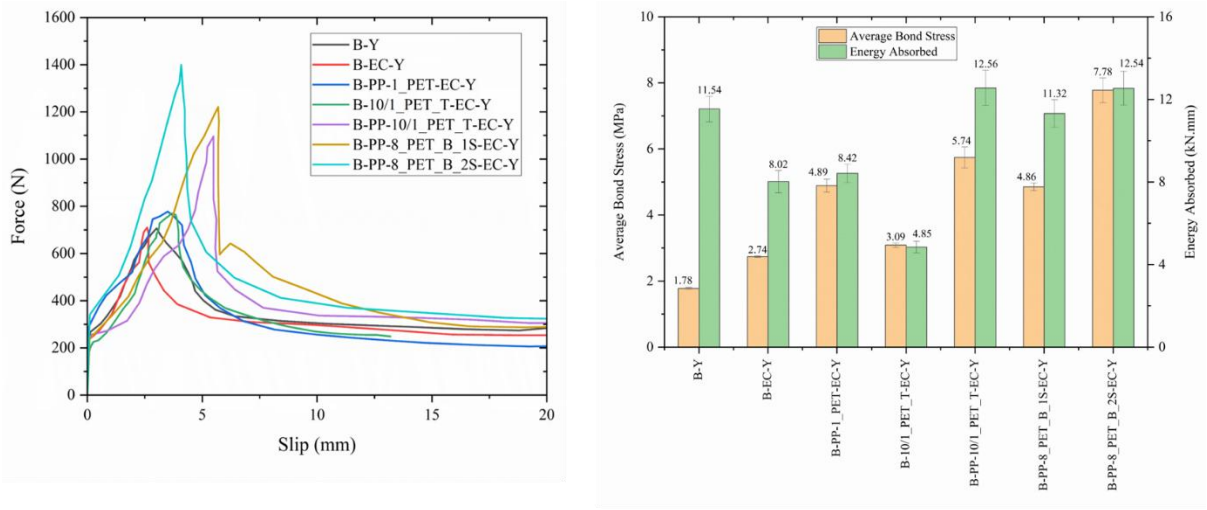


(a) (b)

*Figure 4.17 (a) Pull-out force and slip behaviour of parent, epoxy-coated, and hybrid basalt YRCM specimens, (b) plot representing average bond stress and energy absorbed by basalt YRCM specimens during the yarn pull-out test.*

The images of basalt yarn-based specimens after the yarn pull-out test are shown in Figure 4.18. The parent basalt yarn (B_Y) and epoxy-coated basalt yarn (B_EC_Y) exhibit failure through a combination of fibre fracture and pull-out. All the basalt hybrid yarn reinforced specimens (B-PP-1_PET-EC-Y, B-10/1_PET_T-EC-Y, B-PP-10/1_PET_T-EC-Y, B-PP-8_PET_B_1S-EC-Y, B-PP-8_PET_B_2S-EC-Y) displayed yarn pull-out behaviour, with significant mortar damage indicated by major cracks, especially for specimens B-PP-1_PET-EC-Y, B-PP-10/1_PET_T-EC-Y, and B-PP-8_PET_B_2S-EC-Y. This signifies strong bonding with the mortar matrix, which is also reflected in the higher energy absorption capabilities of these specimens.

(a) B-Y (b) B-EC-Y (c) B-PP-1_PET_EC-Y (d) B-10/1_PET_T-EC-Y

(e) B-PP-10/1_PET_T-EC-Y (f) B-PP-8_PET_B_1S-EC-Y (g) B-PP-8_PET_B_2S-EC-Y

*Figure 4.18 Photographs of different YRCM specimens reinforced with basalt yarn, epoxy coated basalt yarn, and basalt hybrid yarns subjected to a yarn pull-out test.*

### 4.5.3 Yarn pull-out behaviour of Carbon YRCM specimens

The graph in Figure 4.19(a) illustrates the yarn pull-out load versus bond slip behaviour of different carbon YRCM specimens: uncoated, epoxy-coated, and hybrid, with a

yarn embedment length of 25 mm. The uncoated carbon yarn had an average peak pull-out load of 878 N (σ = 24), which increased to 1145 N (σ = 37) with epoxy coating. Adding twisted PET yarn (10/1_PET) helically wrapped around the carbon yarn core, combined with epoxy coating, further enhanced the load to 1310 N (σ = 46). Finally, DREF yarn with a carbon filament core, a sheath of PP fibres, helically wrapped with twisted PET yarn (10/1_PET) and epoxy coating, achieved a peak load of 1392 N (σ = 16), representing a 58% increase in yarn pull-out load over the parent uncoated carbon yarn reinforced mortar specimen(a detailed description is provided in Section 4.6.6, Figure 4.30).The reasons for the improvement in pull-out load in the carbon hybrid yarn based YRCM specimens are the same as those stated for the ARG hybrid yarn-based fabric specimens discussed in Section 4.5.1.

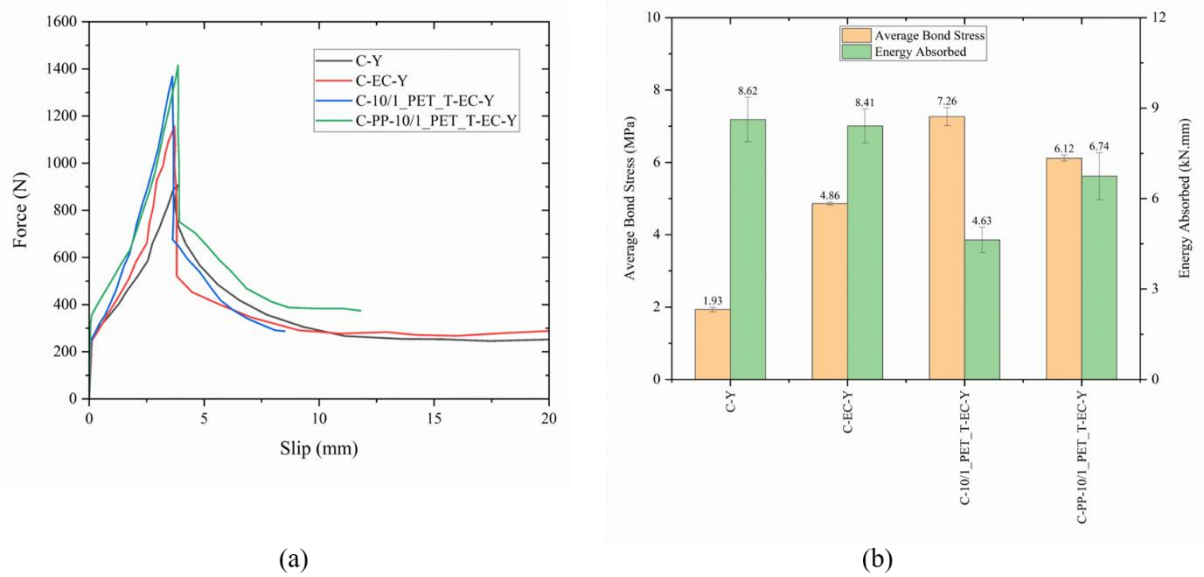


(a) (b)

*Figure 4.19 (a) Pull-out force and slip behaviour of parent, epoxy-coated, and hybrid carbon YRCM specimens, (b) plot representing average bond stress and energy absorbed by carbon YRCM during the yarn pull-out test.*

Figure 4.19(b) shows the average bond stress and energy absorbed by these specimens which shows that the average bond stress substantially increased from parent yarn to epoxy-coated and hybrid yarn. The core carbon strand, helically wrapped with twisted PET yarn and secured by epoxy resin coating, improved the mechanical anchorage (bonding) between the yarn surface and the cementitious mortar, resulting in higher pull-out load and bond stress values. The reasons for the improvement in average bond stress values in the carbon hybrid yarn based YRCM specimens are the same as those stated for the ARG hybrid yarn-based fabric specimens discussed in Section 4.5.1.Further, the energy absorbed during yarn pull-out

was highest for the parent carbon yarn (C_Y), followed by epoxy-coated yarn (C_EC_Y), then C-PP-10/1_PET_T-EC-Y, and lowest for C-10/1_PET_T-EC-Y.

The images of carbon YRCM specimens after the yarn pull-out test are shown in Figure 4.20. All specimens reinforced with parent carbon yarn, epoxy-coated, and hybrid yarns exhibited failure through partial pull-out with significant mortar damage indicated by major cracks, even with separation. This signifies strong bonding with the mortar matrix, and the small pull-out of yarn along with low slip behaviour resulted in lower energy absorption capabilities for these specimens.

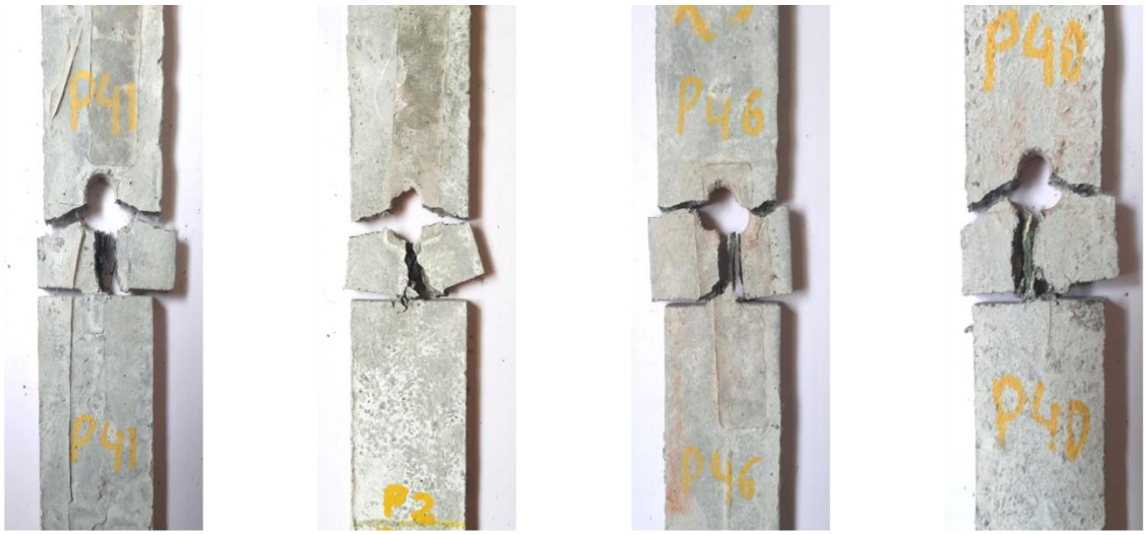


(a) C-Y (b) C-EC-Y (c) C-10/1_PET_T-EC-Y (d) C-PP_10/1_PET_T-EC-Y

*Figure 4.20 Photographs of different YRCM specimens reinforced with parent carbon yarn, epoxy coated carbon yarn, and carbon hybrid yarns subjected to a yarn pull-out test.*

### 4.5.4 Comparison of yarn pull-out behaviour of different YRCM specimens

The graph in Figure 4.21(a) illustrates the yarn pull-out load versus bond slip behaviour of various parent (uncoated) and hybrid AR glass, basalt, and carbon YRCM specimens. It reveals that highest pull-out load for carbon yarn (C-Y) at 878 N ($\sigma$ = 24), followed by basalt (B-Y) at 688 N ($\sigma$ = 12), and the lowest for AR glass (ARG-Y) at 618 N ($\sigma$ = 20). For hybrid yarn-reinforced mortar, the highest pull-out load is exhibited by carbon yarn (C-PP-10/1_PET_T-EC-Y) at 1392 N ($\sigma$ = 16), followed by AR glass (ARG-PP-10/1_PET_T-EC-Y) at 1070 N ($\sigma$ = 30), and the lowest for basalt (B-PP-10/1_PET_T-EC-Y) at 1038 N ($\sigma$ = 46).

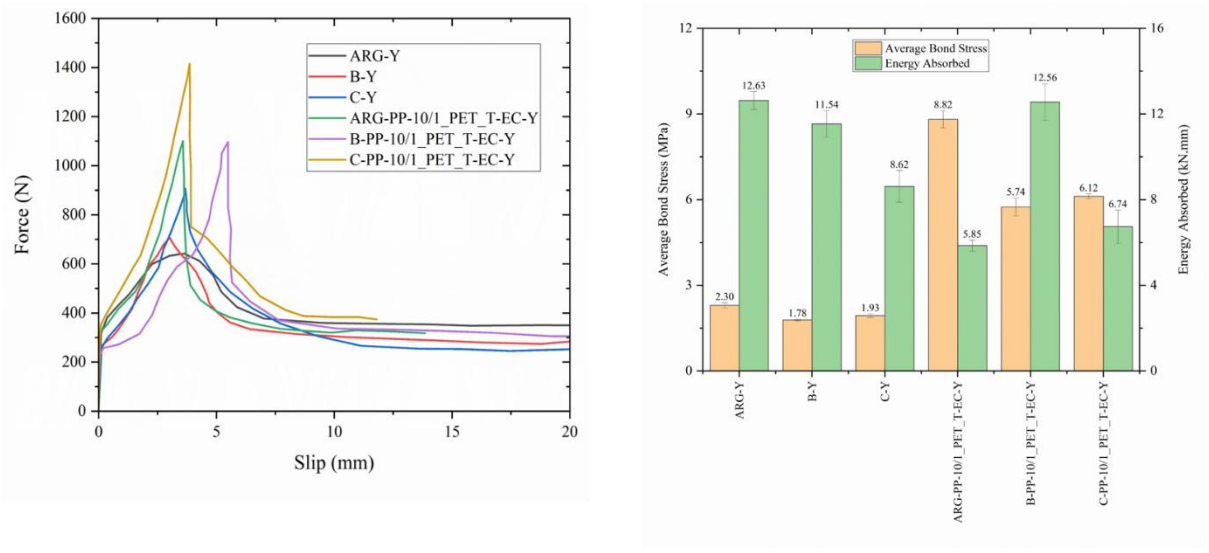


(a) (b)

*Figure 4.21 (a) Pull-out force and slip behaviour of AR glass, basalt and carbon parent, and hybrid YRCM specimens, (b) plot representing average bond stress and energy absorbed by these specimens during the yarn pull-out test.*

Figure 4.21(b) shows the average bond stress and energy absorbed by these specimens. Among the bond stress values of parent (uncoated) and hybrid YRCM specimens, AR glass yarn specimens exhibit the highest values, followed by carbon, and the lowest for basalt yarn specimens. For energy absorbed values, parent (uncoated) yarn-reinforced mortar specimens show the highest values for AR glass, followed by basalt, and the lowest for carbon yarn specimens. However, for hybrid YRCM specimens, basalt yarn specimens exhibit the highest energy absorption, followed by carbon, and the lowest for AR glass yarn specimens.

## 4.6 Yarn pull-out behaviour of FRCM specimens

This section discusses the yarn pull-out behaviour from FRCM specimens (plate specimen, dimensions – 15 mm x 60 mm x 500 mm). The test procedure is described in Section 3.24, Chapter 3. The specimens are reinforced with various fabrics made of parent (uncoated) AR glass, basalt, carbon, and their epoxy coated and hybrid yarn structures. The pull-out load versus slip behaviour, along with the average bond stress and energy absorbed, is plotted and analysed.

### 4.6.1 Yarn pull-out behaviour of AR glass FRCM specimens

The graph in Figure 4.22(a) illustrates the yarn pull-out load versus bond slip behaviour of different AR glass FRCM specimens: uncoated, epoxy-coated, and hybrid yarn structures. The uncoated AR glass fabric had a lower average yarn peak pull-out load of 862 N ($\sigma$ = 17), which increased to 987 N ($\sigma$ = 67) with epoxy coating. The fabric made of twisted PET yarn helically wrapped around the AR glass yarn core, combined with epoxy coating, further enhanced the load to 1110 N ($\sigma$ = 35). Finally, the fabric made of DREF yarn with an AR glass filament core, a sheath of PP fibres, helically wrapped with twisted PET yarn and epoxy coating, achieved the highest peak load of 1270 N ($\sigma$ = 5), representing a 47% increase in yarn pull-out load over the parent uncoated AR glass FRCM specimen(a detailed description is provided in Section 4.6.6, Figure 4.30).

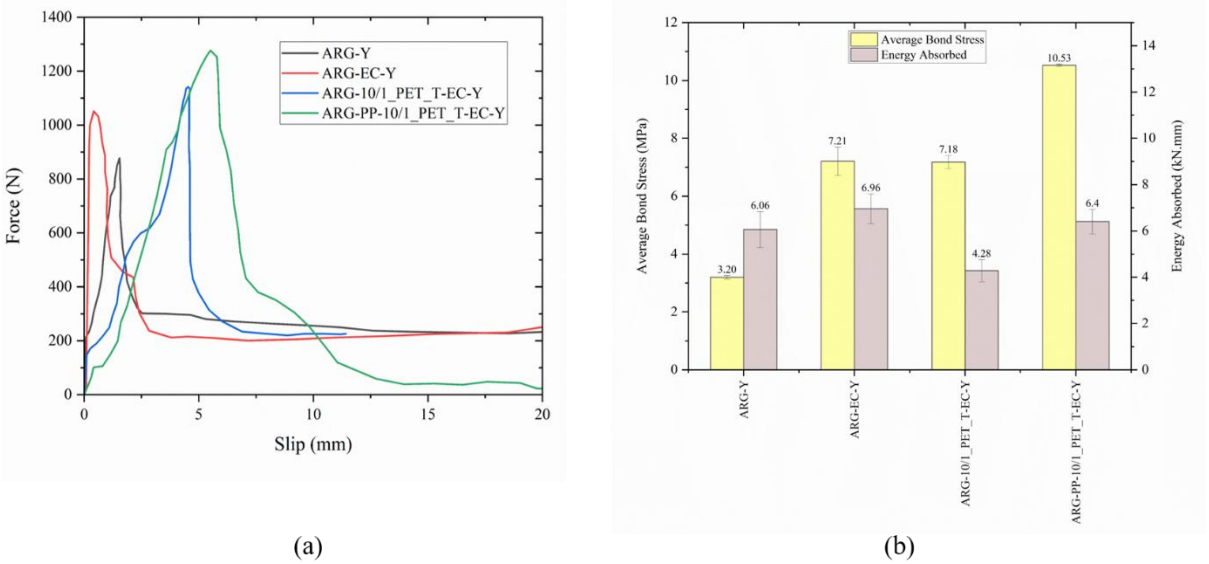


(a) (b)

*Figure 4.22 (a) Yarn pull-out force and slip behaviour of parent, epoxy-coated, and hybrid AR glass FRCM specimens, (b) plot representing average bond stress and energy absorbed by these specimens during the yarn pull-out test.*

Figure 4.22(b) shows the average bond stress and energy absorbed by the specimens. The average bond stress significantly increases from fabric made with parent AR glass yarn to epoxy-coated and hybrid yarn. The core AR glass strand, helically wrapped with twisted PET yarn and secured by epoxy resin coating, enhances the mechanical anchorage between the yarn surface and the cementitious mortar, resulting in higher pull-out load and bond stress

values. The energy absorbed during yarn pull-out is highest for the fabric with epoxy-coated yarn (ARG-EC-Y), followed by AR glass hybrid yarns (ARG-PP-10/1_PET_T-EC-Y), parent basalt yarn-based fabric (ARG-Y), and finally ARG-10/1_PET_T-EC-Y, which has the lowest energy absorption.

Figure 4.23 shows images of AR glass yarn-based FRCM specimens after the yarn pull-out test. The parent AR glass yarn (ARG-Y), epoxy-coated AR glass yarn (ARG-EC-Y), and twisted PET helically wrapped ARG yarn specimen (ARG-10/1_PET_T-EC-Y) exhibit failure through a combination of fibre fracture and pull-out. The hybrid yarn specimen (ARG-PP-10/1_PET_T-EC-Y), with an ARG-PP DREF spun yarn core, exhibited telescopic failure under pull-out loading. This failure mode suggests that epoxy resin penetration through the PP sheath was inadequate in the hybrid ARG yarn. Additionally, the zirconium coating on the AR glass bundle hindered effective bonding between the filaments and the resin, resulting in poor wetting of the AR glass filaments. Consequently, the inner core filaments slipped out, leaving the outer PP sleeve embedded in the mortar during the pull-out test. As a result, no significant crack development, damage, or spalling was observed in the concrete specimen during the yarn pull-out test of hybrid ARG yarn-based FRCM specimens.


*Figure 4.23 Photographs of different FRCM specimens reinforced with AR glass fabric, epoxy coated AR glass fabric, and hybrid yarn-based AR glass fabrics subjected to a yarn pull-out test.*

### 4.6.2 Yarn pull-out behaviour of Basalt FRCM specimens

The graph in Figure 4.24(a) illustrates the yarn pull-out load versus bond slip behaviour of different basalt FRCM specimens: uncoated, epoxy-coated, and hybrid yarn structures. The uncoated basalt fabric had an average yarn peak pull-out load of 1230 N (σ = 45), which increased to 1335 N (σ = 55) with epoxy coating. The fabric formed by wrapping a single PET yarn over Basalt-PP DREF yarn with epoxy coating improved the load to 1798 N (σ = 22). The fabric incorporating twisted PET yarn (10/1_PET) helically wrapped around the basalt yarn core, combined with epoxy coating, further enhanced the load to 1725 N (σ = 40). The fabric made of DREF yarn with a basalt filament core, a sheath of PP fibres, helically wrapped with twisted PET yarn (10/1_PET) and epoxy coating, achieved a peak load of 1820 N (σ = 25). Similarly, fabric made with a braided PET structure over the core of the basalt-PP DREF yarn, combined with epoxy coating, improved the load to 2298 N (σ = 56), while fabric made with two braided PET structures crossing each other increased the load to 2550 N (σ = 55), representing a 107% increase in yarn pull-out load over the parent uncoated basalt FRCM specimen(a detailed description is provided in Section 4.6.6, Figure 4.30).

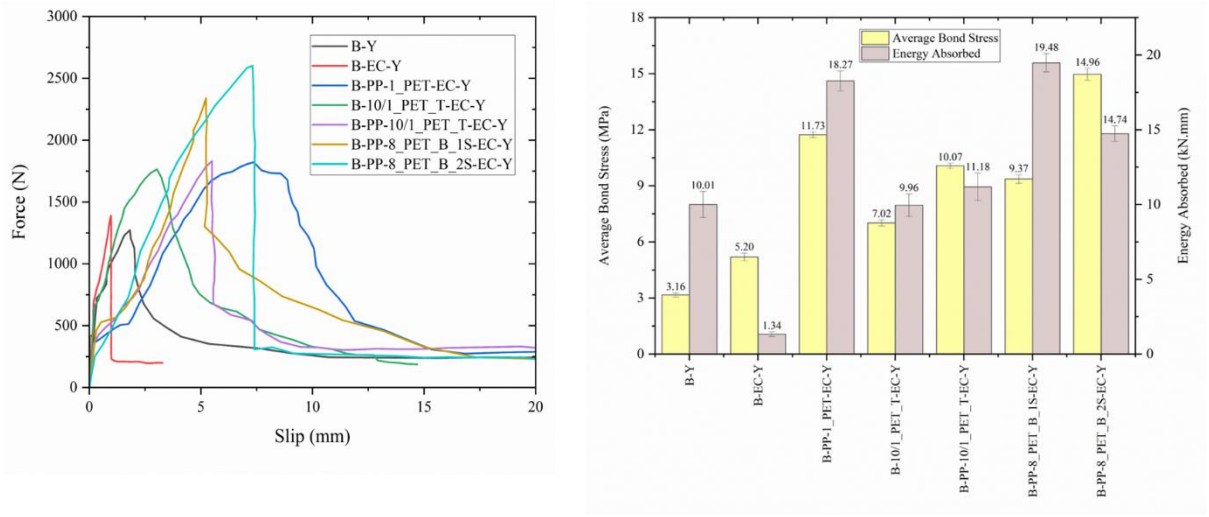


(a) (b)

*Figure 4.24 (a) Yarn pull-out force and slip behaviour of parent, epoxy-coated, and hybrid basalt FRCM specimens, (b) plot representing average bond stress and energy absorbed by these specimens during the yarn pull-out test.*

Figure 4.24(b) shows the average bond stress and energy absorbed by these specimens. It demonstrates that the average bond stress of FRCM specimens increases significantly from those made with parent basalt yarn to epoxy-coated and hybrid yarn. The core basalt strand, helically wrapped with twisted and braided PET yarn, and secured by

epoxy resin coating, improves the mechanical anchorage between the yarn surface and the cementitious mortar. This enhancement results in higher pull-out load and bond stress values. Further, energy absorbed during yarn pull-out is highest for the basalt hybrid yarns B-PP-8_PET_B_1S-EC-Y, followed by B-PP-1_PET-EC-Y, B-PP-8_PET_B_2S-EC-Y, B-PP-10/1_PET_T-EC-Y, parent basalt yarn (B-Y), B-10/1_PET_T-EC-Y, and finally epoxy-coated yarn (B-EC-Y), which has the lowest energy absorption.

Figure 4.25 shows images of basalt FRCM specimens after the yarn pull-out test.


(a) B-Y (b) B-EC-Y (EL – 25 mm) (c) B-EC-Y (EL – 50 mm) (d) B-PP-1_PET_TP-Y

(e) B-10/1_PET_T-EC-Y (f) B-PP-10/1_PET_T-EC-Y (g) B-PP-8_PET_B_1S-EC-Y (h) B-PP-8_PET_B_2S-EC-Y

*Figure 4.25 Photographs of different FRCM specimens reinforced with basalt fabric, epoxy coated basalt fabric, and hybrid yarn-based basalt fabrics subjected to a yarn pull-out test.*

The parent basalt yarn (B-Y) and epoxy-coated AR glass yarn (B-EC-Y) exhibit failure through a combination of fibre fracture and pull-out. All hybrid yarn specimens show yarn pull-out behaviour from the FRCM specimens with significant mortar damage indicated by major cracks and spalling, especially for FRCM specimens B-PP-1_PET-EC-Y, B-PP-8_PET_B_1S-EC-Y, and B-PP-10/1_PET_T-EC-Y. This indicates strong bonding of yarn as well as the assistance provided by the weft yarn of the fabric, reflected in the higher energy absorption capabilities of these specimens.

### 4.6.3 Yarn pull-out behaviour from Carbon FRCM specimens

The graph in Figure 4.26(a) illustrates the yarn pull-out load versus bond slip behaviour of different carbon FRCM specimens: uncoated, epoxy-coated, and hybrid yarn structures. The uncoated carbon fabric had an average yarn peak pull-out load of 1190 N ($\sigma$ = 35), which increased to 2238 N ($\sigma$ = 22) with epoxy coating. The fabric incorporating twisted PET yarn (10/1_PET) helically wrapped around the carbon yarn core, combined with epoxy coating, further enhanced the load to 2415 N ($\sigma$ = 110). Finally, the fabric made of DREF yarn with a carbon filament core, a sheath of PP fibres, helically wrapped with twisted PET yarn (10/1_PET) and epoxy coating, achieved a peak load of 3362 N ($\sigma$ = 112), representing a 182% increase in yarn pull-out load over the parent uncoated carbon FRCM specimen(a detailed description is provided in Section 4.6.6, Figure 4.30).

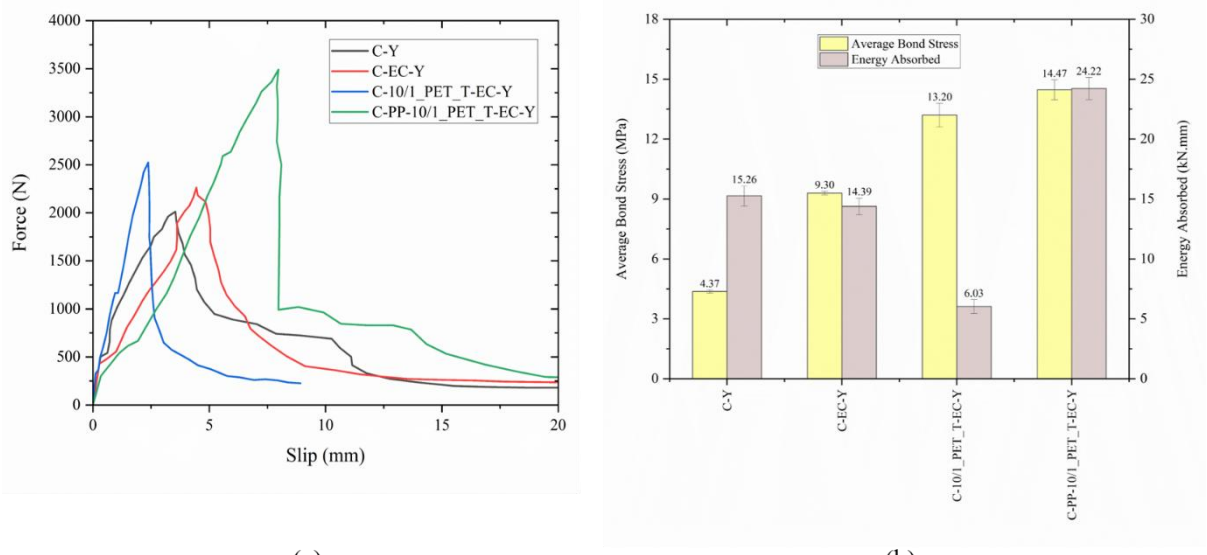


(a) (b)

*Figure 4.26 (a) Yarn pull-out force and slip behaviour of parent, epoxy-coated, and hybrid carbon FRCM specimens, (b) plot representing average bond stress and energy absorbed by these specimens during the yarn pull-out test.*

Figure 4.26(b) shows the average bond stress and energy absorbed by the carbon specimens. It shows that the average bond stress significantly increases from fabric made with parent carbon yarn to epoxy-coated and hybrid yarn. The core carbon strand, helically wrapped with twisted and braided PET yarn and secured by epoxy resin coating, improves the mechanical anchorage between the yarn surface and the cementitious mortar. This enhancement results in higher pull-out load and bond stress values. Additionally, energy absorbed during yarn pull-out is highest for the carbon hybrid yarn C-PP-10/1_PET_T-EC-Y, followed by parent carbon yarn (C-Y), then epoxy-coated yarn (C-EC-Y), and finally C-10/1_PET_T-EC-Y, which has the lowest energy absorption.

Figure 4.27 shows images of carbon FRCM specimens after the yarn pull-out test. The parent basalt yarn (B-Y) exhibits a higher number of fibres showing pull-out and few fibre failures through fracture, while the epoxy-coated carbon yarn (C-EC-Y) shows failure through a combination of fibre fracture and pull-out. All hybrid yarn specimens demonstrate yarn pull-out behaviour from the FRCM specimens with mortar damage indicated by cracks and spalling, especially for FRCM specimens C-PP-10/1_PET_T-EC-Y and C-10/1_PET_T-EC-Y. This indicates strong bonding of the yarn and the assistance provided by the weft yarn of the fabric.


(a) C-Y (b) C-EC-Y (c) C-10/1_PET_T-EC-Y (d) C-PP_10/1_PET_T-EC-Y

*Figure 4.27 Photographs of different FRCM specimens reinforced with carbon fabric, epoxy coated carbon fabric, and hybrid yarn-based carbon fabrics subjected to a yarn pull-out test.*

### 4.6.4 Influence of yarn embedment length on pull-out behaviour

Figure 4.28(a) illustrates the yarn pull-out load versus bond slip behaviour of AR glass and basalt epoxy-coated FRCM at 25 mm and 50 mm yarn embedment lengths. It shows that the average yarn peak pull-out load for AR glass epoxy-coated FRCM at a 25 mm yarn embedment length is 987 N (σ = 67), increasing to 1201 N (σ = 43) at a 50 mm embedment length. For basalt epoxy-coated FRCM, the load increases from 1335 N (σ = 55) to 1515 N (σ = 30). The increase in embedment length from 25 mm to 50 mm results in a 21% improvement in peak pull-out load for AR glass and a corresponding 13% improvement for basalt. The higher pull-out load observed for the basalt epoxy-coated yarn (B-EC-Y) compared to the ARG epoxy-coated yarn (ARG-EC-Y) is attributed to the larger surface perimeter contact of the basalt bundle with the concrete (10.27 mm for B-EC-Y vs. 5.47 mm for ARG-EC-Y, as shown in Table 4.4).It was also found that as the embedment length is increased from 25 mm to 50 mm the peak pull-out load for the AR glass and basalt specimen are attained at a higher deformation (slip), also the load increase is gradual unlike the specimens at short embedment length. It was also found that the peak pull-out load for AR glass and basalt specimens occurs at higher deformation (slip) with a more gradual load increase when the embedment length increases from 25 mm to 50 mm.

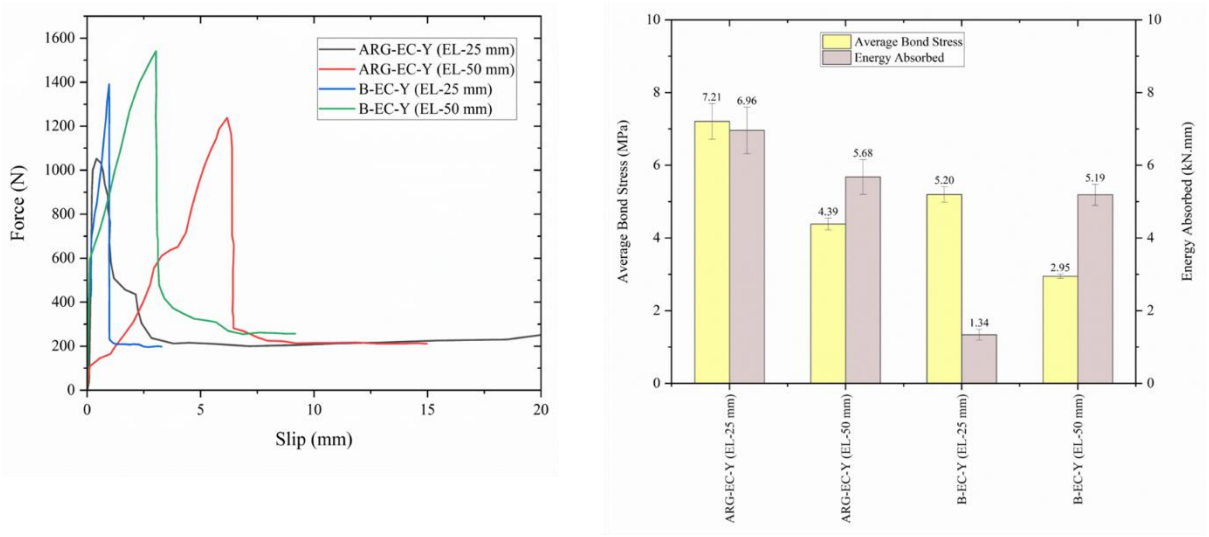


(a) (b)

*Figure 4.28. (a) Pull-out force and slip behaviour of AR glass and basalt epoxy-coated FRCM at 25 mm and 50 mm yarn embedment lengths, (b) plot representing average bond stress and energy absorbed by these specimens during the yarn pull-out test.*

Figure 4.28(b) shows the average bond stress and energy absorbed by these fabrics at the same embedment lengths. It indicates that bond stress and energy absorbed for AR glass

epoxy-coated FRCM decrease as embedment length increases, while for basalt epoxy-coated FRCM, bond stress decreases but energy absorption increases. Images of the specimens after the pull-out test show failure through a combination of fibre fracture and pull-out, regardless of the embedment length.

### 4.6.5 Comparison of yarn pull-out behaviour from different FRCM specimens

The graph in Figure 4.29(a) illustrates the yarn pull-out load versus bond slip behaviour of various parent (uncoated) and hybrid AR glass, basalt, and carbon FRCM specimens. The yarn pull-out load of parent (uncoated) AR glass, basalt, and carbon FRCM specimens shows the highest pull-out load for carbon yarn (C-Y) at 1990 N (σ = 35), followed by basalt (B-Y) at 1230 N (σ = 45), and the lowest for AR glass (ARG-Y) at 862 N (σ = 18). Similarly, for hybrid FRCM specimens, the highest pull-out load is exhibited by carbon yarn (C-PP-10/1_PET_T-EC-Y) at 3362 N (σ = 112), followed by basalt (B-PP-10/1_PET_T-EC-Y) at 1820 N (σ = 25), and the lowest for AR glass (ARG-PP-10/1_PET_T-EC-Y) at 1270 N (σ = 5).In the hybrid FRCM specimens, the highest pull-out load observed for the carbon bundle, followed by basalt and the lowest for ARG, is attributed to the greater number of carbon filaments participating in the load-sharing process, the effective bonding between carbon filaments due to epoxy coating, and the larger surface perimeter contact of the carbon bundle with the concrete (9.12 mm for hybrid carbon yarn, 7.22 mm for hybrid basalt yarn, and 4.82 mm for hybrid ARG yarn, as shown in Table 4.4).

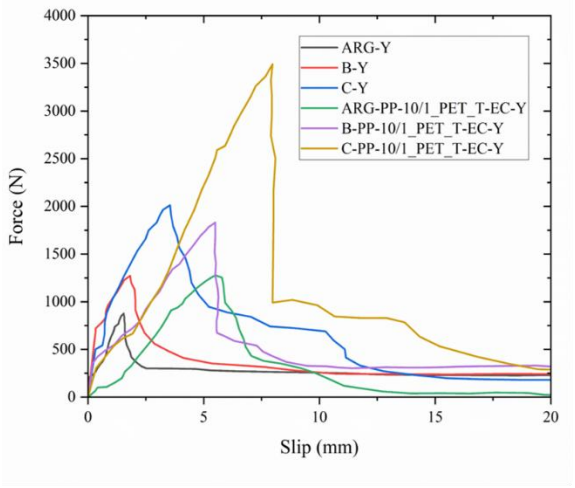


(a)

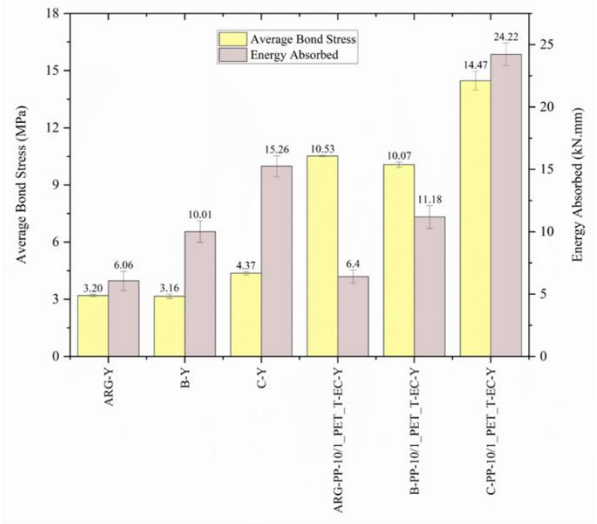


(b)

*Figure 4.29 (a) Pull-out force and slip behaviour of AR glass, basalt and carbon parent, and hybrid yarn-based FRCM specimens, (b) plot representing average bond stress and energy absorbed by these specimens during the yarn pull-out test.*

Figure 4.29(b) shows the average bond stress and energy absorbed by the specimens. Among the bond stress values of parent (uncoated) and hybrid FRCM specimens, carbon yarn specimens exhibit the highest values, while AR glass and basalt FRCM specimens have comparable bond stress values. For energy absorbed values, both parent (uncoated) and hybrid FRCM specimens show the highest values for carbon, followed by basalt, and the lowest for AR glass yarn specimens.The superior performance of carbon yarn in terms of average bond stress and energy absorbed can be attributed to the same factors discussed in the previous paragraph for pull-out load.

### 4.6.6 Discussion on yarn pull-out behaviour of YRCM and FRCM specimens

Two types of mortar plate specimens were tested for yarn pull-out behaviour: one using yarn reinforcement (YRCM) and the other with fabric reinforcement (FRCM). The pull-out behaviour of parent (uncoated), epoxy-coated, and hybrid yarn and fabric specimens made of AR glass, basalt, and carbon yarn reinforced in mortar was evaluated in terms of peak pull-out load, bond stress, and energy absorbed.

Figure 4.30 presents a schematic representation of the interaction between cementitious mortar and different yarn specimens: (a) uncoated parent high-performance yarn bundle, (b) epoxy-coated high-performance yarn bundle, and (c) epoxy-coated hybrid yarn.

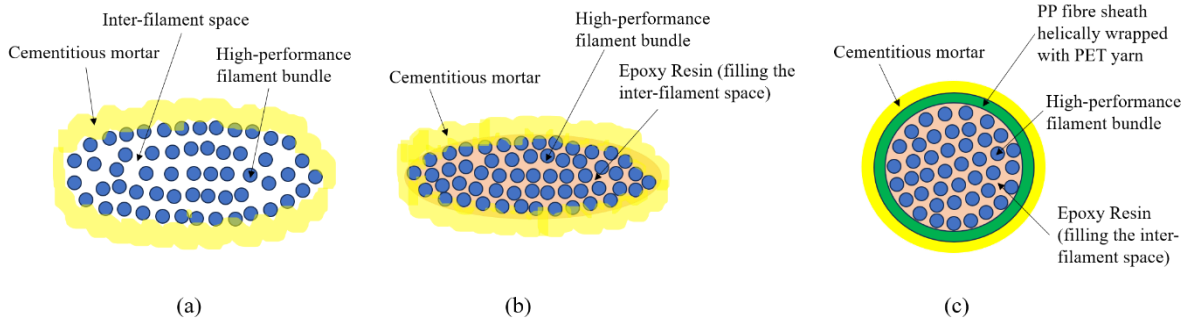


Figure 4.30. Schematic showing the interaction of cementitious mortar with different yarn specimens: (a) parent (uncoated) high performance yarn bundle, (b) epoxy coated high performance yarn bundle, and (c) epoxy coated hybrid yarn.

The uncoated parent yarn, being flattened and less consolidated, has a larger contact perimeter with the mortar, resulting in lower bond stress (yarn cross-sectional area, perimeter, and shape factor values are provided in Table 4.4). In contrast, epoxy-coated yarns (with an elliptical cross-section) and hybrid yarns (with a nearly circular cross-section) exhibit a smaller contact perimeter with improved structural consolidation due to epoxy resin impregnation and the binding effect of PP fibres and PET filaments during hybrid yarn production. The hybrid yarn structure, featuring surface-twisted PET yarn secured by an epoxy resin coating, enhances mechanical anchorage within the mortar matrix, leading to a higher peak pull-out load and bond stress. This improvement suggests that incorporating a hybrid yarn structure and epoxy coating promotes fibre activation, facilitates efficient load transfer, enhances load-sharing performance, and provides strong mechanical anchorage within the cementitious matrix.

The peak pull-out load for all hybrid YRCM specimens exceeded that of the parent YRCM specimens, indicating that yarn hybridization positively influences pull-out behaviour. The helically wrapped twisted and braided PET yarns enhance surface roughness, improving mechanical anchorage with the mortar matrix. Additionally, the epoxy coating and PP sheath fibres help bind and secure the core high-performance filaments within the PET-wrapped yarn.

When comparing the pull-out load of YRCM specimens to FRCM specimens, the FRCM specimens demonstrated superior pull-out behaviour. This improvement is attributed to the combined effect of surface roughness from the helically wrapped twisted and braided PET yarns, epoxy coating, and the contribution of the woven fabric structure-specifically, the weft yarns-which introduce undulations that enhance bonding with the mortar matrix. In YRCM specimens, the primary contributors to the pull-out load are the increased surface roughness from the PET yarn wrapping and epoxy coating, which enhance bond performance.

Unlike the basalt and carbon hybrid yarn specimens, the AR glass hybrid yarn specimen (ARG-PP-10/1_PET_T-EC-Y) exhibited telescopic failure under pull-out loading. This failure mode suggests that epoxy resin penetration through the PP sheath was inadequate in the hybrid ARG yarn. Additionally, the zirconium coating on the AR glass bundle hindered effective bonding between the filaments and the resin, resulting in poor wetting of the AR glass filaments. Consequently, the inner core filaments slipped out, leaving the outer sleeve

embedded in the mortar during the pull-out test. As a result, no significant crack development, damage, or spalling was observed in the concrete specimen during the yarn pull-out test of AR glass yarn and fabric specimens.

The effect of embedment length (25 mm and 50 mm) in FRCM specimens indicates that increasing the embedment length improves the peak pull-out load, likely due to greater surface perimeter contact between the yarn bundle and the mortar matrix. However, no clear improvement in bond stress or energy absorption was observed with varying embedment lengths for AR glass and basalt specimens.

A comparison of peak pull-out load, bond stress, and energy absorption among different FRCM specimens reveals that the hybrid carbon yarn (C-PP-10/1_PET_T-EC-Y) outperforms the hybrid AR glass and basalt yarns (ARG-PP-10/1_PET_T-EC-Y and B-PP-10/1_PET_T-EC-Y). Similarly, the parent (uncoated) carbon yarn (C-Y) exhibits superior performance compared to the parent (uncoated) ARG and basalt yarns (ARG-Y and B-Y). Fiber pull-out incidents are more prevalent in carbon FRCM specimens, which can be attributed to the numerous fine filaments in the carbon yarn bundle, as well as the inherently superior tensile properties of carbon filaments compared to AR glass and basalt filaments.

## 4.7 Uniaxial tensile behaviour of FRCM specimens

This section discusses the uniaxial tensile behaviour of FRCM specimens (plate specimen, dimensions – 15 mm x 60 mm x 500 mm). In this test, each FRCM specimen is reinforced with two layers of fabric, except for the specimens used for comparison (one layer and two layers), the details of which are mentioned. The test procedure is described in Section 3.11, Chapter 3. The specimens are reinforced with various fabrics made of uncoated parent AR glass, basalt, carbon, and their epoxy coated and hybrid yarn structures. The tensile load versus displacement behaviour, along with the average tensile strength and energy absorbed, are plotted and analysed. It was observed during the test that as the tensile test begins and the tensile load increases, the crack size (width) also increases. However, after the test, upon the removal of the tensile load, the crack size (width) reduces, making it difficult to locate in the tested specimen. Consequently, individual microcracks are challenging to identify in the images. Therefore, colour markings have been used to highlight the cracks, facilitating the identification and analysis of the number of cracks, crack spacing, and crack patterns.

### 4.7.1 Uniaxial tensile behaviour of AR glass FRCM specimens

The graph in Figure 4.31(a) illustrates the tensile load versus displacement behaviour of different ARG yarn-based FRCM specimens: uncoated, epoxy-coated, and hybrid. Figure 4.31 (b) represents the average tensile strength and energy absorbed by these specimens. The parent (uncoated) ARG yarn based FRCM specimen exhibited an average tensile load of 3.78 kN ($\sigma$ = 0.08), which increased to 4.54 kN ($\sigma$ = 0.13) with epoxy coating. The addition of twisted PET yarn helically wrapped around the AR glass yarn core, along with epoxy coating, further enhanced the load to 5.26 kN ($\sigma$ = 0.03). Finally, the DREF yarn with an ARG filament core, a sheath of PP fibres, helically wrapped with twisted PET yarn and epoxy coating, achieved the highest peak load of 6.15 kN ($\sigma$ = 0.14), representing a 62% increase in tensile load over the parent uncoated AR glass FRCM specimen.

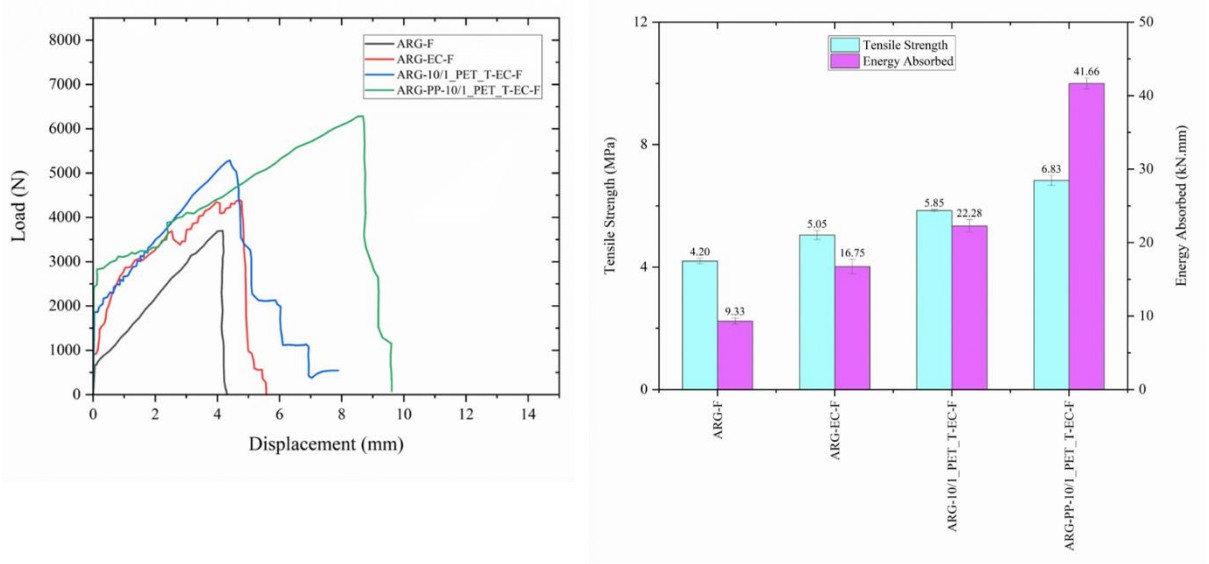


(a) (b)

*Figure 4.31 (a) Tensile load versus displacement plot for AR glass, epoxy coated AR glass fabric, and AR glass hybrid yarn-based fabric reinforced FRCM specimens, (b) plot representing average tensile strength and energy absorbed by these FRCM specimens during the uniaxial tensile test.*

Figure 4.31(b) shows that the average tensile strength and energy absorbed significantly increase from fabric made with parent ARG yarn to epoxy-coated and hybrid yarn. The ARG hybrid yarn-based FRCM specimen (ARG-PP-10/1_PET_T-EC-F) exhibits a 62% increase in tensile strength and a 346% increase in energy absorbed compared to the parent (uncoated) ARG FRCM specimen (ARG-F).

Based on the tensile load versus displacement plot (Figure 4.31a), all ARG yarn-based FRCM specimens exhibit deflection-hardening (strain-hardening) behaviour. After the first crack formation (matrix cracking), the FRCM specimens continue to sustain increasing load with the development of fine multiple cracks, preventing sudden localized failure (catastrophic failure). The tensile load is then transferred to the fabric, which bears the applied tensile forces during the uniaxial tensile test. This behaviour is characterized by progressive stress redistribution, multiple crack formations, and enhanced load-bearing capacity, ultimately improving ductility and energy absorption.

The FRCM specimen with a hybrid yarn structure, featuring surface-twisted PET yarn secured by an epoxy resin coating, enhances mechanical anchorage within the mortar matrix, leading to higher tensile load capacity, tensile strength and energy absorption. This improvement suggests that incorporating a hybrid yarn structure and epoxy coating promotes fibre activation, facilitates efficient load transfer, and enhances load-sharing performance. The helically wrapped twistedPET yarns further contribute by increasing surface roughness, thereby improving the mechanical anchorage of the yarn within the mortar matrix.

Additionally, the woven fabric structure – specifically the weft yarns – introduces undulations that enhance bonding with the mortar matrix. These undulations are more pronounced (higher crimp) in fabrics woven with hybrid yarns, which have a nearly circular cross-section (low shape factor, see Table 4.4), compared to parent yarns that exhibit a flatter cross-sectional geometry. The higher undulation in hybrid yarns results in greater surface contact between the weft yarn and the cementitious matrix, leading to improved bond behaviour and enhanced tensile strength in FRCM specimens.

Furthermore, the inclusion of low-modulus ductile fibres (PP and PET) in hybrid yarn-based FRCM specimens enhances their ductility during uniaxial tensile test. Fabrics incorporating hybrid yarns exhibit greater displacement before failure, significantly improving ductility compared to parent uncoated ARG FRCM specimens. This enhanced ductility also contributes to improved energy absorption in hybrid yarn-based FRCM specimens.

Figure 4.32 presents images of ARG FRCM specimens after the uniaxial tensile test. Similar to the pull-out test, FRCM specimens reinforced with fabrics made from parent AR glass yarn (ARG-F), epoxy-coated AR glass yarn (ARG-EC-F), and twisted PET helically wrapped ARG yarn (ARG-10/1_PET_T-EC-F) exhibited failure through a combination of

fibre fracture (fabric rupture) and fibre pull-out.However, the FRCM specimen reinforced with fabric made from hybrid yarn (ARG-PP-10/1_PET_T-EC-F), featuring an ARG-PP DREF spun yarn core, exhibited telescopic failure under uniaxial tensileloading. This failure mode indicates that epoxy resin penetration through the PP sheath was inadequate in the hybrid ARG yarn. Additionally, the zirconium coating on the AR glass bundle impeded effective bonding between the filaments and the resin, resulting in poor wetting of the AR glass filaments. Consequently, the inner core filaments slipped out, leaving the outer PP sleeve embedded in the mortar during the uniaxial tensiletest. Due to this failure mechanism, no significant crack development, damage, or spalling was observed in the concrete specimen during the uniaxial tensile test of hybrid ARG yarn-based FRCM specimens.

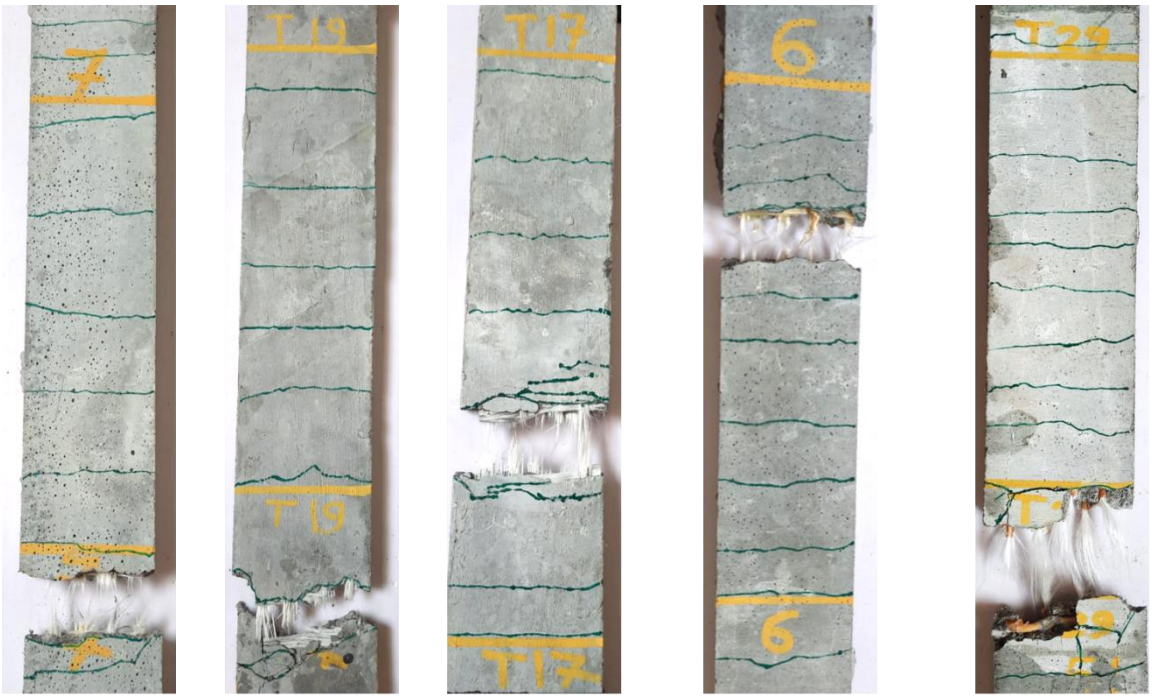


*Figure 4.32 Photographs of various failed FRCM specimens reinforced with AR glass fabric, epoxy-coated AR glass fabric, and hybrid yarn-based AR glass fabrics subjected to a uniaxial tensile test.*

### 4.7.2 Uniaxial tensile behaviour of Basalt FRCM specimens

The graph in Figure 4.33(a) illustrates the tensile load versus displacement behaviour of different basalt yarn-based FRCM specimens: uncoated, epoxy-coated, and hybrid. The parent (uncoated) basalt yarn based FRCM specimen exhibited an average tensile load of

5.58 kN (σ = 0.04), which increased to 6.64 kN (σ = 0.02) with epoxy coating. The fabric incorporating twisted PET yarn (10/1_PET) helically wrapped around the basalt yarn core, combined with epoxy coating, further enhanced the load to 7.98 kN (σ = 0.09). The fabric made of DREF yarn with a basalt filament core, a sheath of PP fibres, helically wrapped with twisted PET yarn (10/1_PET) and epoxy coating, achieved a peak load of 9.41 kN (σ = 0.31). Similarly, fabric made with a braided PET structure over the core of the basalt-PP DREF yarn, combined with epoxy coating, demonstrated a tensile load of 9.40 kN (σ = 0.52), while fabric made with two braided PET structures crossing each other increased the load to 11.12 kN (σ = 0.17), representing a 99% increase in tensile load over the parent (uncoated) basalt FRCM specimen. FRCM specimens reinforced with hybrid basalt yarn-based fabrics exhibited larger displacement before failure, enhancing ductility compared to parent uncoated basalt FRCM specimens.

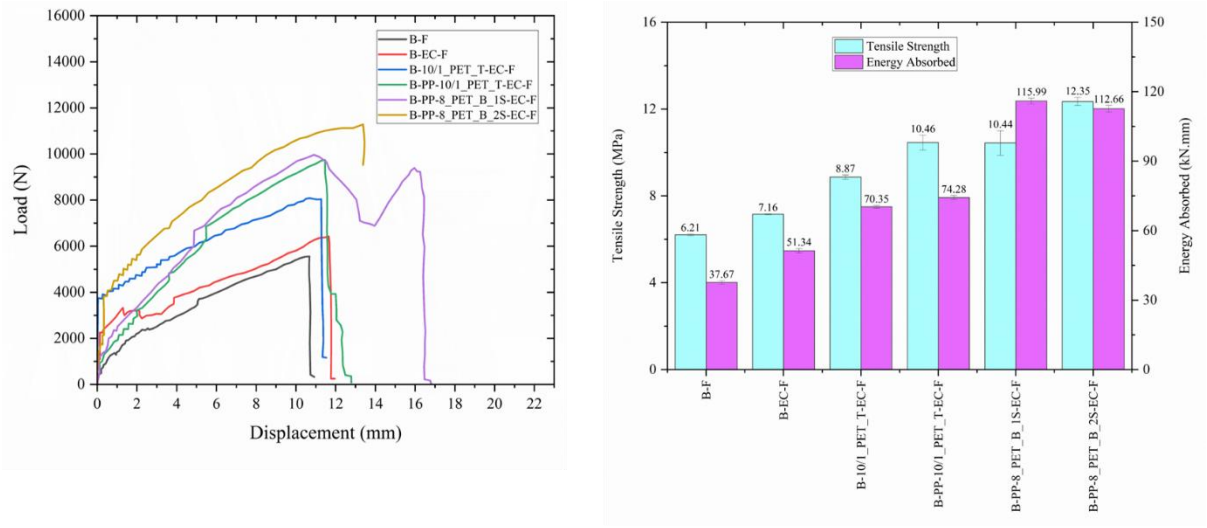


(a) (b)

*Figure 4.33 (a) Tensile load versus displacement plot for basalt, epoxy coated basalt fabric, and basalt hybrid yarn-based fabric reinforced FRCM specimens, (b) plot representing average tensile strength and energy absorbed by these FRCM specimens during the uniaxial tensile test.*

Figure 4.33(b) represents the average tensile strength and energy absorbed by various basalt FRCM specimens. It shows that the average tensile strength and energy absorbed markedly increase from fabric made with parent basalt yarn to epoxy-coated and hybrid yarn. The hybrid yarn-based fabric reinforced FRCM specimen (B-PP-10/1_PET_T-EC-F) exhibits a 68% increase in tensile strength and a 97% increase in energy absorbed compared to the

parent (uncoated) basalt-based FRCM specimen (B-F). Similarly, another basalt hybrid yarn-based fabric reinforced FRCM specimen (B-PP-8_PET_B_2S-EC-F) shows a 99% increase in tensile strength and a 199% increase in energy absorbed compared to the parent (uncoated) basalt-based FRCM specimen (B-F). The reasons for this improvement in tensile load, tensile strength, ductility (displacement), and energy absorption are similar to those discussed for ARG yarn-based FRCM specimens (see section 4.7.1).Figure 4.34 displays images of basalt yarn-based FRCM specimens after the uniaxial tensile test.

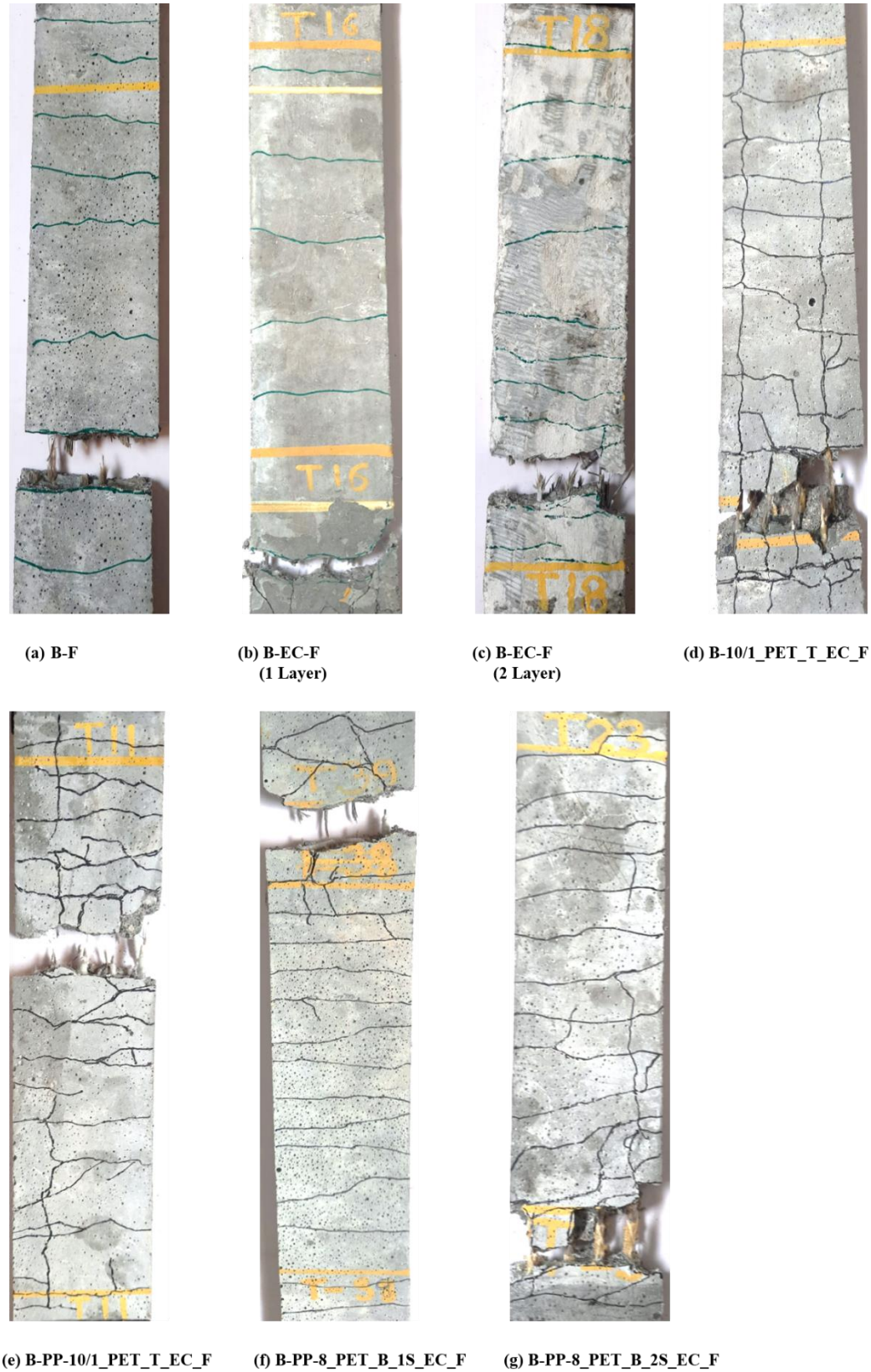


(a) B-F (b) B-EC-F (1 Layer) (c) B-EC-F (2 Layer) (d) B-10/1_PET_T_EC_F

(e) B-PP-10/1_PET_T_EC_F (f) B-PP-8_PET_B_1S_EC_F (g) B-PP-8_PET_B_2S_EC_F

*Figure 4.34 Photographs of various failed FRCM specimens reinforced with basalt fabric, epoxy-coated basalt fabric, and hybrid yarn-based basalt fabrics subjected to a uniaxial tensile test.*

The specimens reinforced with parent basalt (B-F), epoxy-coated basalt (B-EC-F), and hybrid yarns all exhibit failure through a combination of fibre fracture (fabric rupture) and fibre pull-out. Some hybrid yarn-based FRCM specimens like B-10/1_PET_T-EC-Y, B-PP-8_PET_B_2S-EC-Y, and B-PP-10/1_PET_T-EC-Y show mortar damage with cracks running in both axial and transverse directions, along with minor spalling. This suggests strong bonding of warp-weft yarn in fabric and highlights the assistance provided by the fabric's weft yarn.

### 4.7.3 Comparison of tensile behaviour of parent basalt fabric, hybrid yarn-based basalt TP and TS fabric composite based FRCM specimens

The graph in Figure 4.35(a) illustrates the tensile load versus displacement behaviour of different basalt yarn-based FRCM specimens: parent (uncoated), epoxy-coated thermoset (TS) fabric composite, and hybrid yarn-based thermoplastic(TP) fabric composite. Among the three basalt specimens, the epoxy-coated basalt-based TS fabric composite (B-PP-1_PET-EC-F) exhibited the highest average tensile load of 6.80 kN ($\sigma$ = 0.11), followed by the basalt hybrid yarn-based TP fabric composite (B-PP-1_PET_TP-F) at 6.21 kN ($\sigma$ = 0.09), and the lowest by the parent (uncoated) basalt (B-F) at 5.58 kN ($\sigma$ = 0.04). This indicates that reinforcing basalt with thermoplastic and thermoset fabric composites in FRCM specimens improves the average tensile load by 11.29% and 21.86%, respectively, compared to the parent basalt fabric.

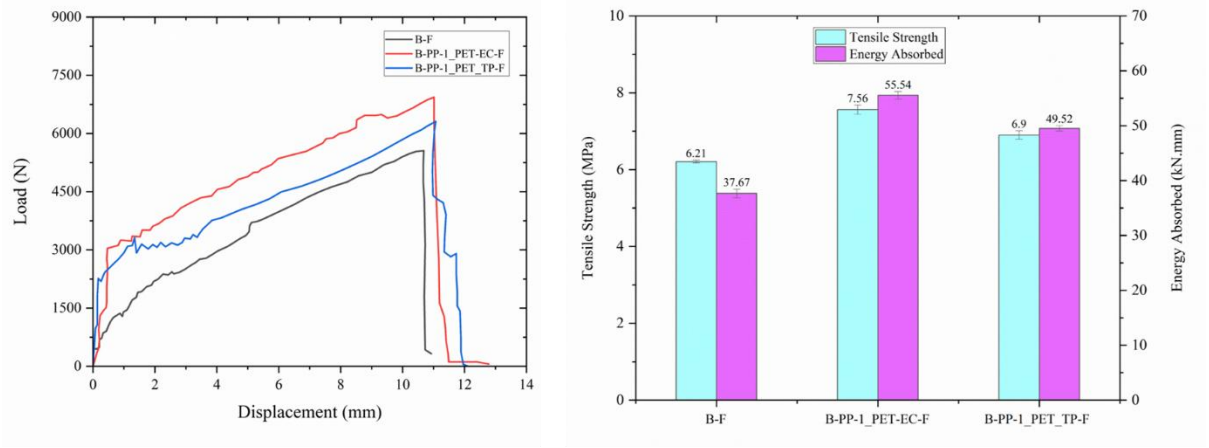


(a) (b)

*Figure 4.35 (a) Tensile load versus displacement plot for parent basalt, epoxy coated thermoset basalt fabric composite, and basalt hybrid yarn-based thermoplastic fabric*

*composite reinforced FRCM specimens, (b) plot representing average tensile strength and energy absorbed by these FRCM specimens during the uniaxial tensile test.*

Figure 4.35(b) represents the average tensile strength and energy absorbed by various basalt FRCM specimens. It shows a marked increase in tensile strength and energy absorption when parent basalt fabric is replaced by epoxy-coated TS fabric composite and hybrid yarn-based TP fabric composite for FRCM reinforcement. The tensile strength improves by 21.74% with epoxy-coated TS fabric composite and by 11.29% with hybrid yarn-based TP fabric composite. Similarly, energy absorption improves by 47.44% with epoxy-coated TS fabric composite and by 31.46% with hybrid yarn-based TP fabric composite. The epoxy resin coating and PP melt impregnation within the basalt filament bundle promotes fibre activation, facilitates efficient load transfer, and enhances load-sharing performance, enabling the fabric to sustain higher tensile loads in FRCM specimensand achieve greater displacement(ductility) in FRCM specimens.

Figures 4.34(a), and 4.36(b,c,d) display images of basalt yarn-based FRCM specimens after the uniaxial tensile test.

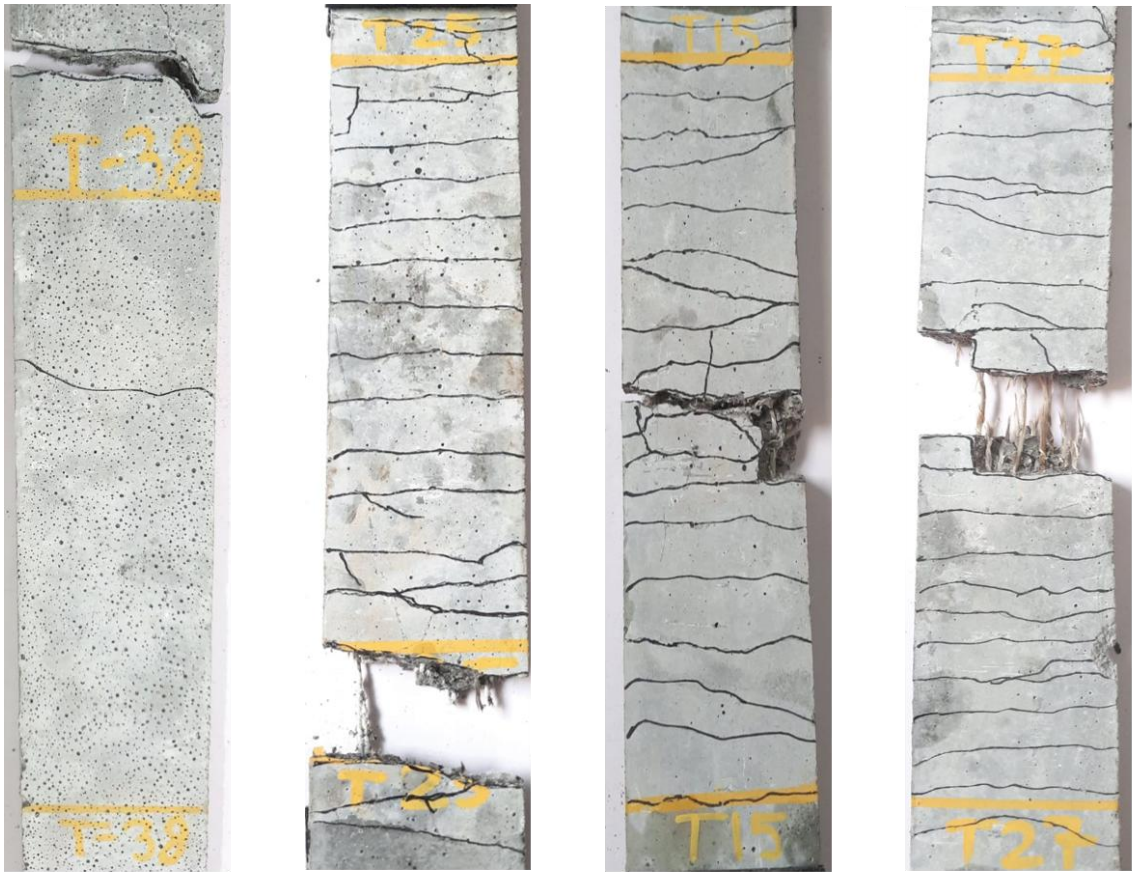

**(a) PP-FRC** **(b) B-PP-1_PET-EC-F** **(c) B-PP-1_PET_TP-F (10 mm x 12 mm)** **(d) B-PP-1_PET_TP-F (6 mm x 7 mm)**

*Figure 4.36 Photographs of various failed FRCM specimens reinforced PP-fibres, basalt thermoplastic, and thermoset fabric composites subjected to a uniaxial tensile test.*

The specimens reinforced with parent basalt (B-F), epoxy-coated TS fabric composite (B-PP-1_PET-EC-F), and hybrid yarn-based TP fabric composite (B-PP-1_PET_TP-F) all exhibit failure through a combination of fibre fracture (fabric rupture) and fibre pull-out, with cracks running along the width of the specimen.

Furthermore, replacing the parent basalt fabric with epoxy-coated TS and hybrid yarn-based TP fabric composites in mortar/concrete reinforcement resulted in an increase in fine microcracks, improved crack distribution, and reduced crack spacing. This indicates enhanced load transfer and stress redistribution, effectively preventing catastrophic (localized) failure.

### 4.7.4 Effect of number of layer reinforcement on tensile behaviour of FRCM specimens

The graph in Figure 4.37(a) shows the tensile load versus displacement behaviour of PP fibre reinforced concrete (PP-FRC, control specimen) without fabric reinforcement, and AR glass and basalt epoxy-coated FRCM specimens with one and two layers of fabric reinforcement [ARG-EC-F (1 L), ARG-EC-F (2 L), B-EC-F (1 L), and B-EC-F (2 L)]. The tensile peak load of the PP-FRC specimen was 0.54 kN ($\sigma = 0.04$), which increased to 1.89 kN ($\sigma = 0.10$) with one layer of AR glass epoxy-coated fabric reinforcement and to 4.54 kN ($\sigma = 0.13$) with two layers. Similarly, one layer of basalt epoxy-coated fabric reinforcement improved the tensile peak load to 2.88 kN ($\sigma = 0.03$) and 6.44 kN ($\sigma = 0.02$) with two layers. The improvement in tensile peak load of FRCM specimens with one layer of AR glass and basalt epoxy-coated fabric is 250% and 433%, respectively. With two layers, the improvement was 740% and 1092%, respectively.As the number of layers in FRCM specimens increases from one to two, the reinforcement ratio (fibre volume fraction) also increases, enhancing the tensile load-bearing capacity of TRC specimens. This improvement allows them to resist higher forces before failure. Additionally, the increased number of fabric layers contributes to better deflection-hardening behaviour, improved ductility (displacement), and greater energy absorption, making the specimens more resilient under tensile loading.

Figure 4.37(b) shows the average tensile strength and energy absorbed of PP-FRC, ARG-EC-F (1 L), ARG-EC-F (2 L), B-EC-F (1 L), and B-EC-F (2 L) FRCM specimens. There is a marked increase in tensile strength and energy absorption when PP-FRC is

reinforced with one layer of ARG-EC-F or B-EC-F. The improvement is even greater with two layers. Energy absorption capacity is significantly enhanced with one layer of AR glass and basalt epoxy-coated fabric by 470% and 1485%, respectively. With two layers, the improvement is 2292% and 7234%, respectively.Reinforcing FRCM with continuous fabrics significantly enhances its tensile properties. Fabrics made from high-performance fibres, combined with PP fibres added as secondary reinforcement in mortar mixing, synergistically improve load-bearing capacity, energy absorption, and ductility (elongation behaviour).

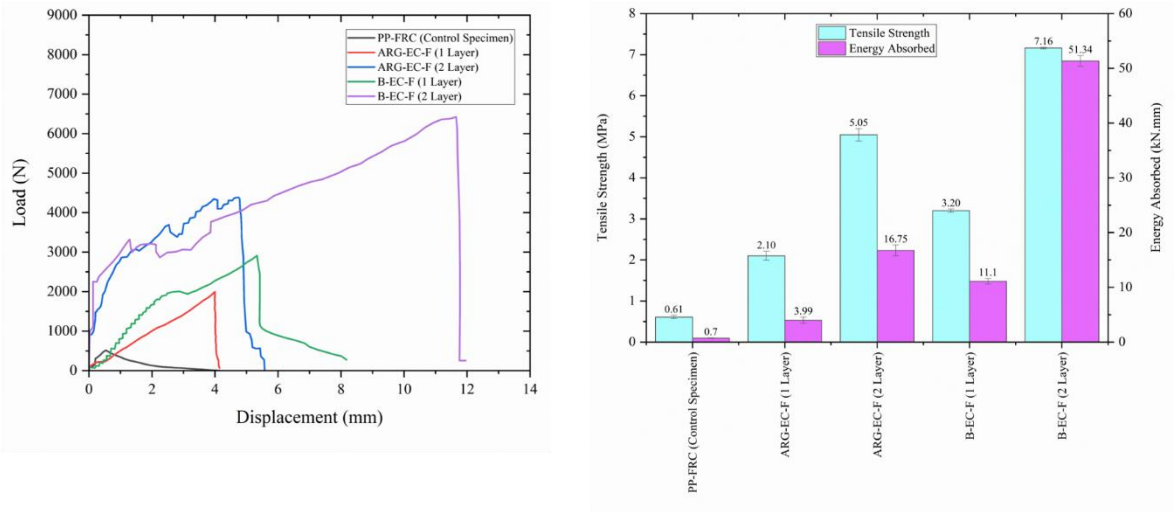


(a) (b)

*Figure 4.37 (a) Tensile load versus displacement plot for PP-FRC, ARG-EC-F (1 L), ARG-EC-F (2 L), B-EC-F (1 L), and B-EC-F (2 L) FRCM specimens, (b) plot representing average tensile strength and energy absorbed by these FRCM specimens during the uniaxial tensile test.*

Figures 4.32(b, c), 4.34(b, c) and 4.36(a) depict images of ARG-EC-F (1 L), ARG-EC-F (2 L), B-EC-F (1 L), B-EC-F (2 L) FRCM specimens, and PP-FRC, after uniaxial tensile test. The PP-FRC specimen (without fabric reinforcement) exhibited tensile failure with two cracks, one leading to failure (Figure 4.36, a). All ARG and basalt FRCM specimens showed failure through a combination of fibre fracture (fabric rupture) and fibre pull-out, with multiple fine cracks running along the width of the specimen. The images indicate that the number of cracks increases and crack spacing decreases as the number of fabric layers increases from one to two layers, regardless of fibre type (AR glass or basalt).

### 4.7.5 Effect of mesh size opening of fabric on tensile behaviour of FRCM specimens

Figure 4.38(a) illustrates the tensile load versus displacement behaviour of basalt hybrid yarn-based thermoplastic fabric composite reinforced FRCM specimens with varying mesh opening sizes (6 mm x 7 mm and 10 mm x 12 mm). As the mesh opening size decreases from 10 mm x 12 mm to 6 mm x 7 mm, the average tensile peak load of the B-PP-1_PET_TP-F (10 mm x 12 mm) FRCM specimen increased from 6.21 kN ($\sigma$ = 0.09) to 7.46 kN ($\sigma$ = 0.20), marking a 20% improvement.

Figure 4.38(b) displays the average tensile strength and energy absorption of B-PP-1_PET_TP-F (10 mm x 12 mm) and B-PP-1_PET_TP-F (6 mm x 7 mm) FRCM specimens. There is a notable increase in tensile strength by 20.2% and energy absorption by 43.25% when the mesh size reduces from 10 mm x 12 mm to 6 mm x 7 mm. This improvement is attributed to the increased number of warp and weft yarns in the fabric, while maintaining the same dimensions of the FRCM specimen. Specifically, the fabric with a 10 mm x 12 mm mesh had four load-bearing warp yarns, whereas the 6 mm x 7 mm mesh had six.

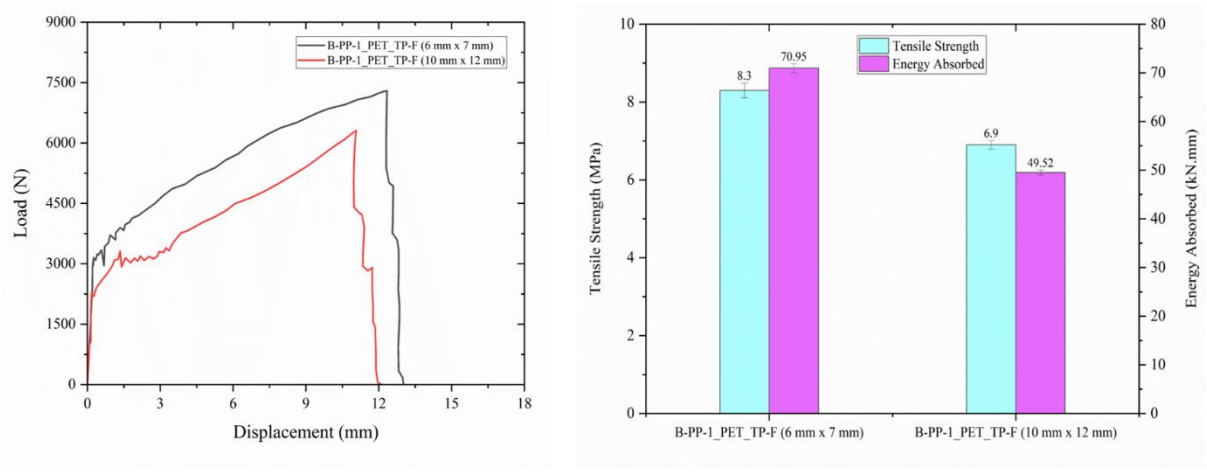


(a) (b)

*Figure 4.38 (a) Tensile load versus displacement plot for basalt hybrid yarn-based thermoplastic fabric composite reinforced FRCM specimens of varying mesh opening sizes (6 mm x 7 mm, and 10 mm x 12 mm), (b) plot representing average tensile strength and energy absorbed by these FRCM specimens during the uniaxial tensile test.*

Figure 4.36(c, d) depicts images of B-PP-1_PET_TP-F (10 mm x 12 mm) and B-PP-1_PET_TP-F (6 mm x 7 mm) FRCM specimens after uniaxial tensile testing. Both specimens exhibited failure through a combination of fibre fracture (fabric rupture) and fibre pull-out, with multiple fine cracks running along the width of the specimen, indicating improved load

transfer and stress redistribution, effectively mitigating catastrophic (localized) failure.The images highlight a slight increase in the number of cracks and a decrease in slight crack spacing as the fabric mesh opening size decreases from 10 mm x 12 mm to 6 mm x 7 mm.

### 4.7.6 Uniaxial tensile behaviour of Carbon FRCM specimens

The graph in Figure 4.39(a) illustrates the tensile load versus displacement behaviour of different carbon yarn-based FRCM specimens: uncoated, epoxy-coated, and hybrid. The parent (uncoated) carbon yarn based FRCM specimen exhibited an average tensile load of 10.80 kN ($\sigma$ = 0.06), which increased to 11.53 kN ($\sigma$ = 0.03) with epoxy coating. The addition of twisted PET yarn helically wrapped around the carbon yarn core, along with epoxy coating, further enhanced the load to 13.32 kN ($\sigma$ = 0.41). Finally, the DREF yarn with a carbon filament core, a sheath of PP fibres, helically wrapped with twisted PET yarn and epoxy coating, achieved the highest peak load of 17.57 kN ($\sigma$ = 1.23), representing a 63% increase in tensile load over the parent uncoated carbon FRCM specimen. FRCM specimens reinforced with hybrid carbon yarn-based fabrics exhibited larger displacement before failure, enhancing ductility compared to parent uncoated carbon FRCM specimens.

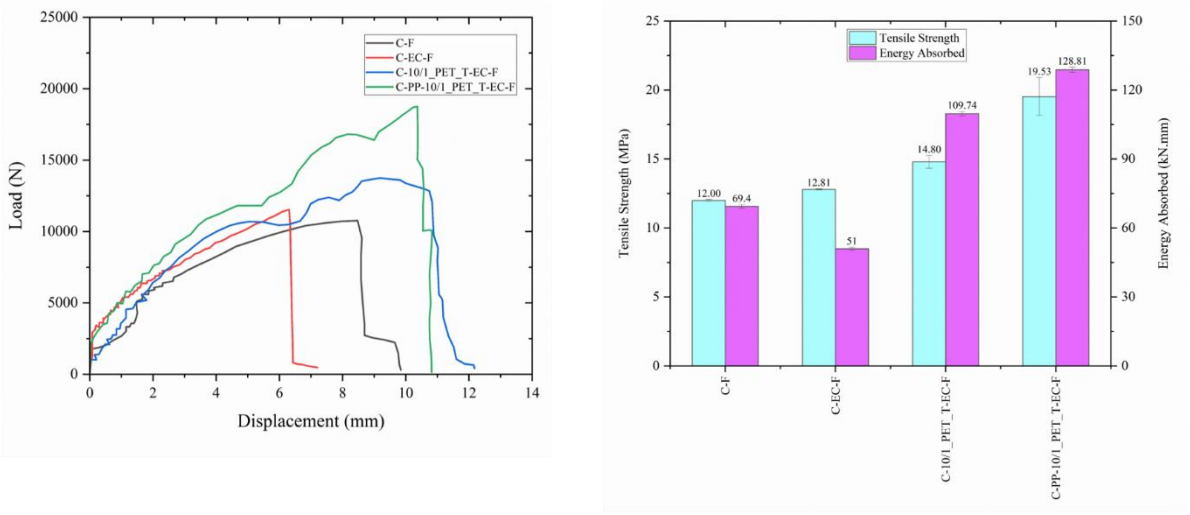


(a) (b)

*Figure 4.39 (a) Tensile load versus displacement plot for parent carbon, epoxy coated carbon fabric, and carbon hybrid yarn-based fabric reinforced FRCM specimens, (b) plot representing average tensile strength and energy absorbed by these FRCM specimens during the uniaxial tensile test.*

Figure 4.39(b) represents the average tensile strength and energy absorbed by uncoated, epoxy-coated, and hybrid carbon yarn-based FRCM specimens. It shows that the

average tensile strength and energy absorbed significantly increase from fabric made with parent carbon yarn to epoxy-coated and hybrid yarn. The carbon hybrid yarn-based FRCM specimen (C-PP-10/1_PET_T-EC-F) exhibits a 63% increase in tensile strength and an 86% increase in energy absorbed compared to the parent (uncoated) carbon FRCM specimen (C-F). The reasons for this improvement in tensile load, tensile strength, ductility (displacement), and energy absorption are similar to those discussed for ARG yarn-based FRCM specimens (see section 4.7.1).

Figure 4.40 displays images of carbon yarn-based FRCM specimens after the uniaxial tensile test. The specimens reinforced with parent carbon fabric (C-F) and hybrid yarn-based fabric (C-PP-10/1_PET_T-EC-Y) exhibited failure through a combination of fibre fracture (fabric rupture) and fibre pull-out. However, the FRCM specimens C-EC-F and C-10/1_PET_T-EC-Y did not undergo complete fabric rupture (complete separation after failure) and maintained very strong bonding with the mortar matrix, indicating their true potential might be greater than reported. The superior mechanical properties and strong bonding of carbon fabrics with mortar were evident.

(a) C-F (b) C-EC-F (c) C-10/1_PET_T_EC_F (d) C-PP-10/1_PET_T_EC_F

*Figure 4.40 Photographs of various failed FRCM specimens reinforced with carbon fabric, epoxy-coated carbon fabric, and hybrid yarn-based carbon fabrics subjected to a uniaxial tensile test.*

### 4.7.7 Comparison of uniaxial tensile behaviour of different FRCM specimens

The graph in Figure 4.41(a) illustrates the tensile load versus displacement behaviour of various parent (uncoated) and hybrid AR glass, basalt, and carbon FRCM specimens. The parent (uncoated) FRCM specimens exhibit the highest tensile peak load for carbon (C-F) at 10.80 kN (σ = 0.06), followed by basalt (B-F) at 5.58 kN (σ = 0.04), and AR glass (ARG-F) at 3.78 kN (σ = 0.08). Among the hybrid FRCM specimens, carbon (C-PP-10/1_PET_T-EC-Y) shows the highest tensile peak load at 17.57 kN (σ = 1.23), followed by basalt (B-PP-10/1_PET_T-EC-Y) at 9.41 kN (σ = 0.31), and AR glass (ARG-PP-10/1_PET_T-EC-Y) at 6.15 kN (σ = 0.14).

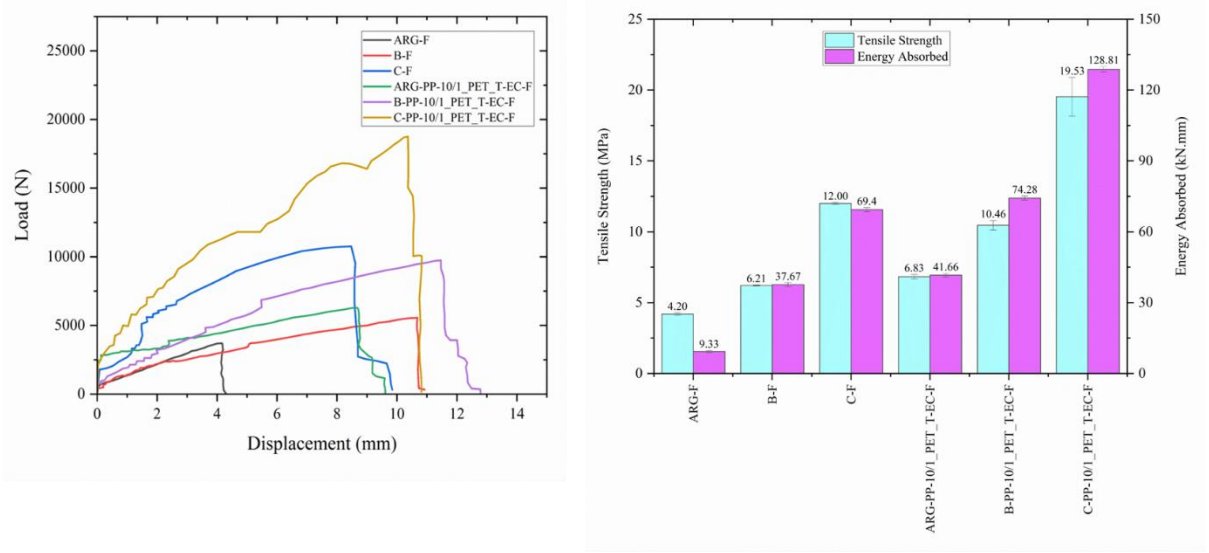


(a) (b)

*Figure 4.41 (a) Tensile load versus displacement plot for AR glass, basalt and carbon parent, and hybrid FRCM specimens, (b) plot representing average tensile strength and energy absorbed by these FRCM specimens during the uniaxial tensile test.*

Figure 4.41(b) presents the tensile strength and energy absorbed by these specimens. Consistent with the tensile peak load values, carbon FRCM specimens have the highest tensile strength and energy absorption, followed by basalt, and the lowest for AR glass. Hybrid yarn-based FRCM specimens exhibit higher tensile strength and energy absorption than their parent counterparts, regardless of fibre type (AR glass, basalt, and carbon). This

tensile behaviour of FRCM specimens aligns with the tensile properties observed in the fabric tensile test results. This suggests that the tensile properties of the fabric have been effectively transferred to the FRCM specimens.

### 4.7.8 Crack pattern of FRCM specimenssubjected touniaxial tensiletest

The details of cracks observed in various failed FRCM specimens under tensile loading, including average number of cracks and crack spacing, are listed in Table 4.4.

*Table 4.4 Crack details of failed FRCM specimens after uniaxial tensile test. (n – number of specimens considered for average readings)*

| Tensile specimen name | Average number of cracks (n=3) | Average crack spacing (mm) (n=3) |
|---|---|---|
| PP-FRC (without fabric reinforcement) | 2 | 93 |
| ARG-F | 6 | 28 |
| ARG-EC-F (1 Layer) | 7 | 35.4 |
| ARG-EC-F (2 Layer) | 8 | 27.8 |
| ARG-10/1_PET_T-EC-F | 10 | 22.2 |
| ARG-PP-10/1_PET_T-EC-F | 12 | 23 |
| B-F | 8 | 39.2 |
| B-EC-F (1 Layer) | 6 | 45 |
| B-EC-F (2 Layer) | 11 | 18.6 |
| B-10/1_PET_T-EC-F | 12 | 21.5 |
| B-PP-10/1_PET_T-EC-F | 16 | 18.9 |
| B-PP-8_PET_B_1S-EC-F | 16 | 17 |
| B-PP-8_PET_B_2S-EC-F | 16 | 16.5 |
| B-PP-1_PET-EC-F | 17 | 14.8 |
| B-PP-1_PET_TP-F (10 mm x 12 mm) | 19 | 12 |

| | | |
|---|---|---|
| B-PP-1_PET_TP-F (6 mm x 7 mm) | 21 | 11.1 |
| C-F | 8 | 30.8 |
| C-EC-F | 11 | 15.4 |
| C-10/1_PET_T-EC-F | 16 | 16.2 |
| C-PP-10/1_PET_T-EC-F | 17 | 11.4 |

Figure 4.42 presents the average number of cracks and crack spacing in various FRCM specimens reinforced with: (a) parent AR glass, epoxy-coated, and hybrid yarn-based fabric; (b) parent basalt, epoxy-coated, and hybrid yarn-based fabric; and (c) parent carbon, epoxy-coated, and hybrid yarn-based fabric. The results indicate that replacing the parent fabric with epoxy-coated and hybrid yarn-based fabric increases the average number of cracks while reducing crack spacing, regardless of the fibre type.Microcracks formed during the uniaxial tensile test are often difficult to identify and locate after the load is removed (i.e., upon test completion). This behaviour suggests a more uniform load transfer from the fabric to the mortar matrix, leading to even tensile stress distribution in FRCM specimens. The formation of multiple fine cracks instead of a single localized failure helps prevent sudden catastrophic failure. This desirable cracking behaviour is particularly evident in hybrid yarn-based specimens, demonstrating their effectiveness in enhancing the structural performance of FRCM composites.

Figure 4.42(d) shows the average number of cracks and crack spacing of PP-FRC, ARG-EC-F (1 L), ARG-EC-F (2 L), B-EC-F (1 L), and B-EC-F (2 L) FRCM specimens. It was observed that the PP-FRC specimen (without fabric reinforcement) experienced tensile failure with two cracks, one leading to failure. In contrast, the FRCM specimens exhibited a greater number of cracks compared to the PP-FRC specimen. As the number of fabric layers increased from one to two layers, regardless of fibre type (AR glass or basalt), the number of cracks increased and crack spacing decreased.The formation of multiple fine cracks instead of a single localized failure helps prevent sudden catastrophic failure.

Figure 4.42(e) shows the average number of cracks and crack spacing of FRCM specimens reinforced with parent basalt (B-F), epoxy-coated thermoset fabric (B-PP-1_PET-EC-F), and thermoplastic fabric composite [B-PP-1_PET_TP-F (10 mm x 12 mm), B-PP-

1_PET_TP-F (6 mm x 7 mm)]. Among these specimens, the average number of cracks increases and crack spacing decreases from B-F to B-PP-1_PET-EC-F to B-PP-1_PET_TP-F. This observation suggests that resin coating and impregnation improves load distribution from fabric to mortar matrix in FRCM specimens. Additionally, reducing the fabric mesh opening size from 10 mm x 12 mm to 6 mm x 7 mm slightly increases the number of cracks and decreases crack spacing. This effect is attributed to the increased number of warp and weft yarns in the fabric with a smaller mesh opening, which enhances uniformity in load sharing and transfer between the fabric and mortar during tensile loading.

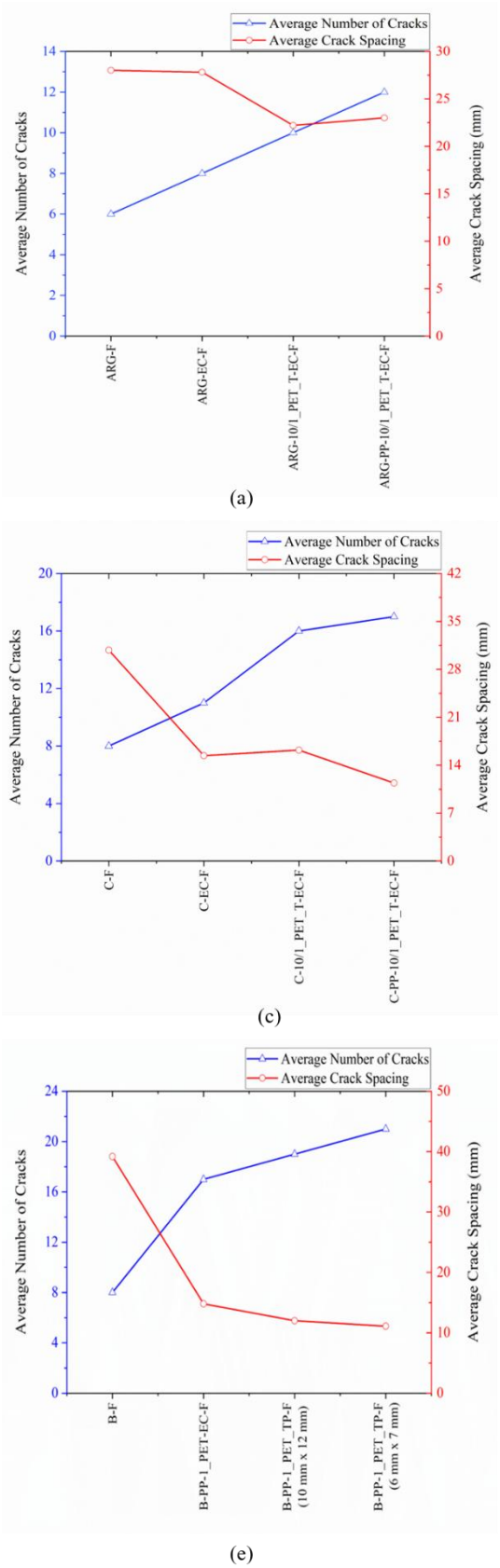


*Figure 4.42 Plot showing number of cracks and crack spacing in various FRCM specimens: (a) AR glass, (b) basalt, (c) carbon; (d) PP-FRC and number of layers comparison; (e) parent basalt, thermoplastic and thermoset fabric composite.*

## 4.8 Flexural behaviour of FRCM specimens

This section discusses the flexural behaviour of FRCM specimens (plate specimen, dimensions – 30 mm x 100 mm x 500 mm, three-point bending test). In this test, each FRCM specimen is reinforced with three layers of fabric, except for the specimens used for comparison, the details of which are mentioned. The test procedure is described in Section 3.12, Chapter 3. The specimens are reinforced with various fabrics made of uncoated parent AR glass, basalt, carbon, and their epoxy coated and hybrid yarn structures. The flexural load versus mid-span deflection behaviour, along with the average flexural strength and energy absorbed, are plotted and analysed. It was observed that the crack size (width) increases during flexural loading and reduces after the test (removal of load). Therefore, individual fine cracks (microcracks) are difficult to identify and locate in the images and are highlighted with colour markings for ease of identification and understanding of the number of cracks, crack spacing, and crack pattern.

### 4.8.1 Flexural behaviour of AR glass FRCM specimens

The graph in Figure 4.43(a) illustrates the flexural load versus mid-span deflection behaviour of different ARG yarn-based FRCM specimens: uncoated, epoxy-coated, and hybrid. The parent (uncoated) ARG yarn based FRCM specimen exhibited an average flexural load of 2.02 kN ($\sigma$ = 0.02), which increased to 3.38 kN ($\sigma$ = 0.07) with epoxy coating. The addition of twisted PET yarn helically wrapped around the AR glass yarn core, along with epoxy coating, further enhanced the load to 4.16 kN ($\sigma$ = 0.07). Finally, the DREF yarn with an ARG filament core, a sheath of PP fibres, helically wrapped with twisted PET yarn and epoxy coating, achieved the highest peak load of 4.40 kN ($\sigma$ = 0.05), representing a 118% increase in flexural load over the parent uncoated ARG FRCM specimen.

Figure 4.43(b) illustrates the significant increase in average flexural strength and energy absorbed from fabric made with parent ARG yarn to epoxy-coated and hybrid yarn. The AR glass hybrid yarn-based FRCM specimen (ARG-PP-10/1_PET_T-EC-F) exhibits a 118% increase in flexural strength and a 355% increase in energy absorbed compared to the parent (uncoated) ARG FRCM specimen (ARG-F).

Based on the flexural load versus mid-span deflection plot (Figure 4.43a), all ARG yarn-based FRCM specimens exhibit deflection-hardening (strain-hardening) behaviour under flexural loading. After the first crack formation (matrix cracking), the specimens

continue to sustain increasing load with the development of fine multiple cracks, preventing sudden localized failure. The bending load induces tensile stresses in the bottom face of the FRCM plate specimen, where the fabric reinforcement is placed during casting. The tensile load is then transferred to the fabric, which bears the applied load during the flexural test. This behaviour is characterized by progressive stress redistribution, multiple crack formations, and enhanced load-bearing capacity, ultimately improving ductility and energy absorption.

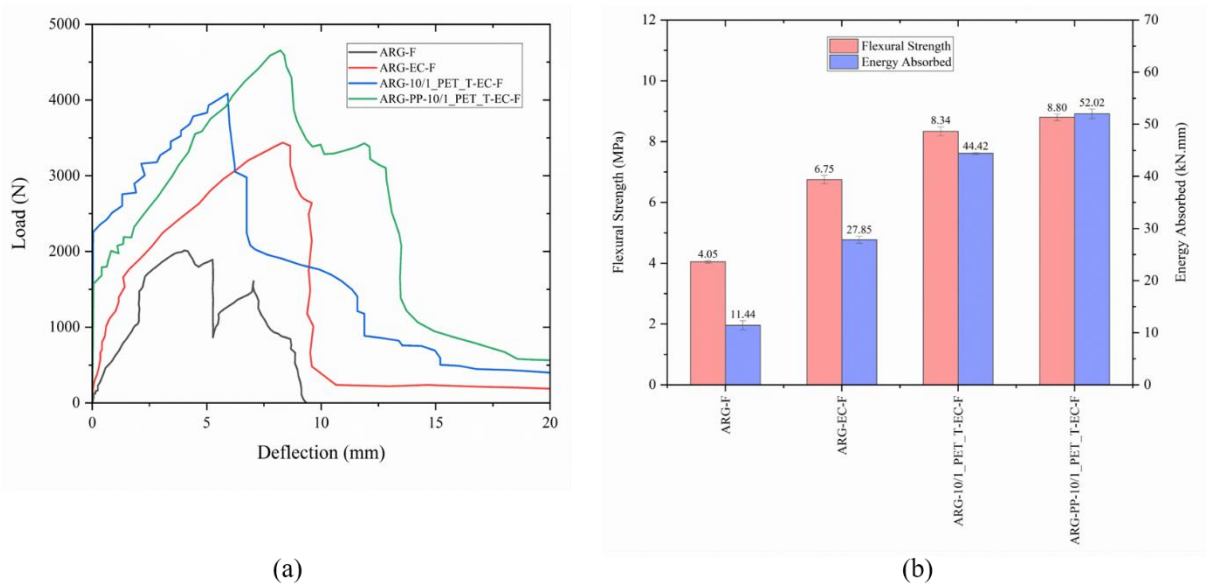


(a) (b)

*Figure 4.43 (a) Flexural load versus mid-span deflection plot for parent AR glass fabric, epoxy coated AR glass fabric, and AR glass hybrid yarn-based fabric reinforced FRCM specimens, (b) plot representing average flexural strength and energy absorbed by these FRCM specimens during the flexural test.*

The FRCM specimen reinforced with a hybrid yarn structure (ARG-PP-10/1_PET_T-EC-F), featuring surface-twisted PET yarn secured by an epoxy resin coating, enhances mechanical anchorage within the mortar matrix, leading to higher flexural load-bearing capacity, flexural strength and energy absorption. This improvement suggests that incorporating a hybrid yarn structure and epoxy coating promotes fibre activation, facilitates efficient load transfer, and enhances load-sharing performance. Additionally, the helically wrapped twisted PET yarns contribute to increased surface roughness, further improving the mechanical anchorage of the yarn within the mortar matrix.

Moreover, the woven fabric structure – specifically the weft yarns – introduces undulations that enhance bonding with the mortar matrix. These undulations are more

pronounced (higher crimp) in fabrics woven with hybrid yarns, which have a nearly circular cross-section (low shape factor, see Table 4.4), compared to parent yarns that exhibit a flatter cross-sectional geometry. The increased undulation in hybrid yarns results in greater surface contact between the weft yarn and the cementitious matrix, leading to improved bond behaviour, higher flexural strength, and enhanced energy absorption in FRCM specimens.

Furthermore, the inclusion of low-modulus ductile fibres (PP and PET) in hybrid yarn-based FRCM specimens enhances their ductility during flexural testing. Fabrics incorporating hybrid yarns exhibit greater mid-span deflection before failure, significantly improving ductility compared to parent uncoated ARG FRCM specimens. This increased ductility also enhances the energy absorption capacity of hybrid yarn-based FRCM specimens.

Figure 4.44 presents images of AR glass FRCM specimens after the flexural test.

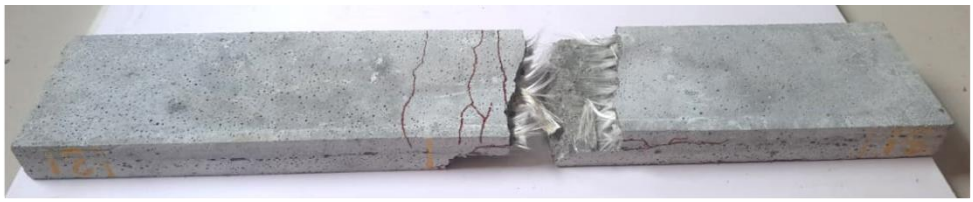

(a) ARG-F

(b) ARG-EC-F

(c) ARG-10/1_PET_T_EC_F

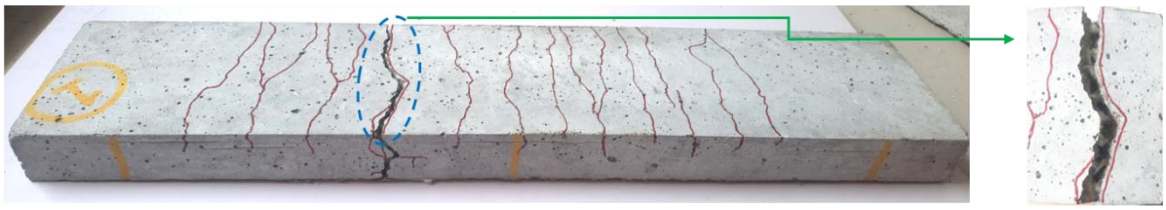

(d) ARG-PP-10/1_PET_T_EC_F Magnified view of failure region

*Figure 4.44 Photographs of various failed FRCM specimens reinforced with AR glass fabric, epoxy-coated AR glass fabric, and hybrid yarn-based AR glass fabrics subjected to a flexural test.*

Similar to the pull-out and tensile tests of ARG-reinforced FRCM specimens, fabrics made from parent AR glass yarn (ARG-F), epoxy-coated AR glass yarn (ARG-EC-F), and twisted PET helically wrapped ARG yarn (ARG-10/1_PET_T-EC-F) failed through a combination of fibre fracture (fabric rupture) and fibre pull-out. However, the FRCM specimen reinforced with fabric made from ARG hybrid yarn (ARG-PP-10/1_PET_T-EC-F), featuring an ARG-PP DREF spun yarn core, exhibited telescopic failure (as shown in the magnified image) under flexural loading. This failure mode suggests inadequate epoxy resin penetration through the PP sheath in the hybrid ARG yarn. Additionally, the zirconium coating on the ARG bundle hindered effective bonding between the filaments and the resin, resulting in poor wetting of the AR glass filaments. Consequently, the inner core filaments slipped out, leaving the outer PP sleeve embedded in the mortar during the flexural test. Due to this failure mechanism, no significant crack development, damage, or spalling was observed in the concrete specimen. Furthermore, an increase in the number of fine microcracks and improved crack distribution was observed when transitioning from parent AR glass fabric to epoxy-coated and hybrid yarn-based fabric.

### 4.8.2 Flexural behaviour of Basalt FRCM specimens

The graph in Figure 4.45(a) illustrates the flexural load versus mid-span deflection behaviour of different basalt yarn-based FRCM specimens: uncoated, epoxy-coated, and hybrid. The parent (uncoated) basalt yarn-based FRCM specimen exhibited an average flexural load of 2.30 kN ($\sigma$ = 0.07), which increased to 3.08 kN ($\sigma$ = 0.03) with epoxy coating. The fabric with twisted PET yarn (10/1_PET) helically wrapped around the basalt yarn core, combined with epoxy coating, further enhanced the load to 3.12 kN ($\sigma$ = 0.06). The fabric made of DREF yarn with a basalt filament core, a sheath of PP fibres, helically wrapped with twisted PET yarn (10/1_PET) and epoxy coating, achieved a load of 4.70 kN ($\sigma$ = 0.11). Similarly, fabric with a braided PET structure over the basalt-PP DREF yarn core, combined with epoxy coating, demonstrated a load of 4.74 kN ($\sigma$ = 0.05), while fabric with two braided PET structures crossing each other increased the load to 5.30 kN ($\sigma$ = 0.12), representing a 130% increase in flexural load over the parent (uncoated) basalt FRCM specimen. All the FRCM specimens reinforced with hybrid basalt yarn-based fabrics (B-PP-10/1_PET_T-EC-F, B-PP-

8_PET_B_1S-EC-F, and B-PP-8_PET_B_2S-EC-F) exhibited larger mid-span deflection before failure, enhancing ductility compared to parent uncoated basalt FRCM specimens.

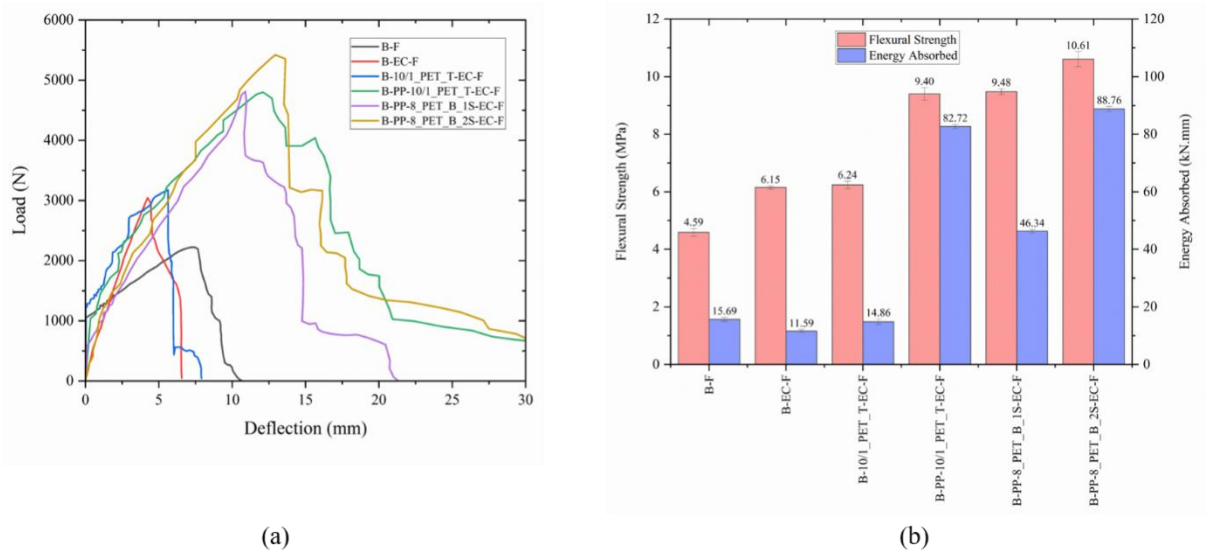


(a) (b)

*Figure 4.45 (a) Flexural load versus mid-span deflection plot for parent basalt fabric, epoxy coated basalt fabric, and basalt hybrid yarn-based fabric reinforced FRCM specimens, (b) plot representing average flexural strength and energy absorbed by these FRCM specimens during the flexural test.*

Figure 4.45(b) represents the average flexural strength and energy absorbed by various basalt FRCM specimens. It shows that the average flexural strength and energy absorbed markedly increase from fabric made with parent basalt yarn to epoxy-coated and hybrid yarn. The hybrid yarn-based fabric reinforced FRCM specimen (B-PP-10/1_PET_T-EC-F) exhibits a 105% increase in flexural strength and a 427% increase in energy absorbed compared to the parent (uncoated) basalt-based FRCM specimen (B-F). Similarly, another basalt hybrid yarn-based fabric reinforced FRCM specimen (B-PP-8_PET_B_2S-EC-F) shows a 131% increase in flexural strength and a 465% increase in energy absorbed compared to the parent (uncoated) basalt-based FRCM specimen (B-F). The reasons for this improvement in flexural load, flexural strength, mid span deflection (ductility) and energy absorption are similar to those discussed for ARG yarn-based FRCM specimens (see section 4.8.1).

Figure 4.46 shows images of basalt yarn-based FRCM specimens after the flexural test. The specimens reinforced with parent basalt (B-F) exhibited complete failure through fibre fracture (fabric rupture). The epoxy-coated basalt (B-EC-F) and hybrid yarns failed

through a combination of fibre fracture and fibre pull-out, with warp yarn bridging preventing complete separation of the FRCM plate specimen (as shown in the magnified image).

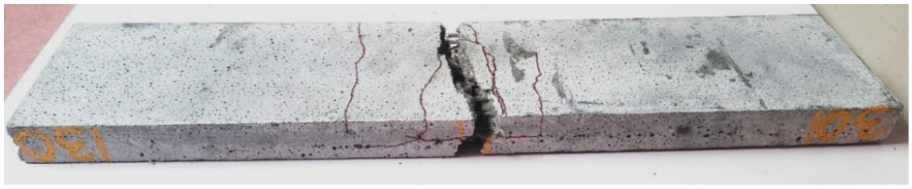

(a) B-F

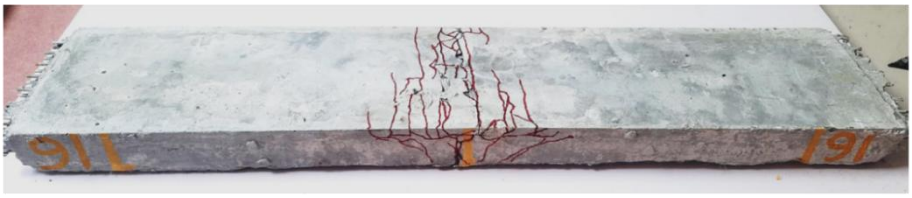

(b) B-EC-F

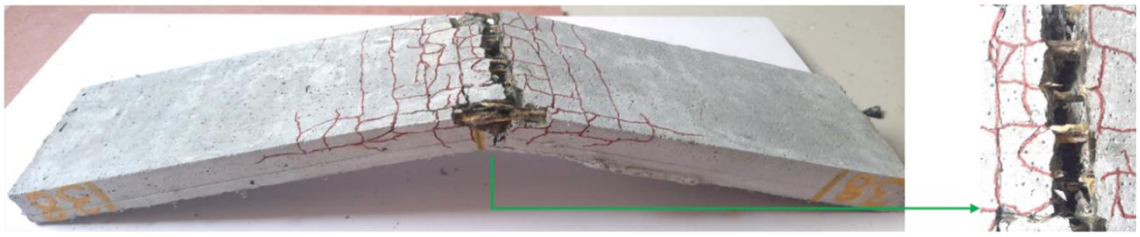

(c) B-10/1_PET_T_EC_F Magnified view of failure region

(d) B-PP-10/1_PET_T_EC_F

(e) B-PP-8_PET_B_1S_EC_F

(f) B-PP-8_PET_B_2S_EC_F

*Figure 4.46 Photographs of various failed FRCM specimens reinforced with basalt fabric, epoxy-coated basalt fabric, and hybrid yarn-based basalt fabrics subjected to a flexural test.*

The hybrid yarn-based FRCM specimens (B-10/1_PET_T-EC-Y) displayed mortar damage, with cracks running in both axial and transverse directions and minor spalling. This indicates strong bonding of warp-weft yarn in the fabric and highlights the support provided by the weft yarn. The number of fine microcracks in FRCM increases from parent basalt yarn to epoxy-coated and hybrid yarn.

### 4.8.3 Comparison of flexural behaviour of parent basalt fabric, hybrid yarn-based basalt TP and TS fabric composite based FRCM specimens

The graph in Figure 4.47(a) illustrates the flexural load versus mid-span deflection behaviour of different basalt yarn-based FRCM specimens: parent (uncoated) (B-F), epoxy-coated thermoset (TS) fabric composite (B-PP-1_PET-EC-F), and hybrid yarn-based thermoplastic(TP)fabric composite (B-PP-1_PET_TP-F). Among the three basalt specimens, hybrid yarn-based thermoplastic(TP) fabric composite (B-PP-1_PET_TP-F) exhibited the highest flexural load of 3.41 kN ($\sigma$ = 0.07), followed by the epoxy-coated thermoset (TS) fabric composite (B-PP-1_PET_EC-F) at 3.18 kN ($\sigma$ = 0.01), and the lowest by the parent (uncoated) basalt (B-F) at 2.30 kN ($\sigma$ = 0.07). This indicates that reinforcing basalt with thermoplastic and thermoset fabrics in FRCM specimens improves the average flexural load by 48% and 38%, respectively, compared to the parent basalt fabric.

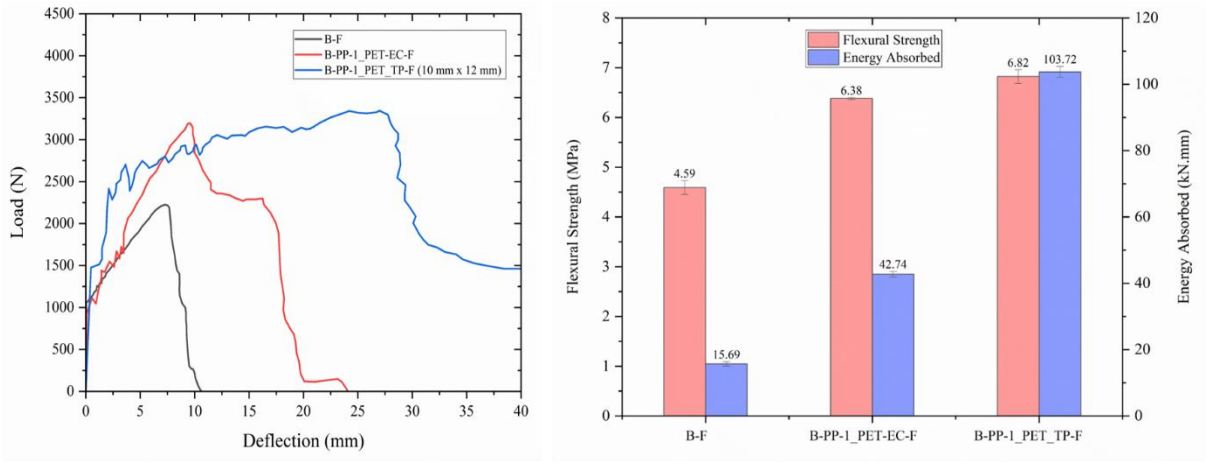


(a) (b)

*Figure 4.47 (a) Flexural load versus mid-span deflection plot for parent basalt, epoxy coated thermoset basalt fabric composite, and basalt hybrid yarn-based thermoplastic fabric*

*composite reinforced FRCM specimens, (b) plot representing average flexural strength and energy absorbed by these FRCM specimens during the flexural test.*

Figure 4.47(b) represents the average flexural strength and energy absorbed by various basalt FRCM specimens. It shows a marked increase in flexural strength and energy absorption when parent basalt fabric is replaced by epoxy-coated TS fabric composite (B-PP-1_PET-EC-F) and hybrid yarn-based TP fabric composite (B-PP-1_PET_TP-F) for FRCM reinforcement. The flexural strength improves by 38% with B-PP-1_PET-EC-F and by 48% with B-PP-1_PET_TP-F. Similarly, energy absorption improves by 172% with B-PP-1_PET-EC-F and by 561% with B-PP-1_PET_TP-F. The epoxy resin coating in the B-PP-1_PET-EC-F specimen and PP melt impregnation in the B-PP-1_PET_TP-F specimen within the basalt filament bundle promote fibre activation, facilitate efficient load transfer, and enhance load-sharing, enabling the fabric composite to sustain higher flexural loads and achieve greater mid-span deflection in FRCM specimens. Additionally, the ductile behaviour of the thermoplastic PP polymer in the hybrid yarn-based TP fabric composite (B-PP-1_PET_TP-F) enhances mid-span deflection (ductility) and increases energy absorption in FRCM specimens.

Figures 4.46(a) and 4.48(a, d) present images of parent basalt (B-F), basalt thermoset (TS) fabric composite (B-PP-1_PET-EC-Y), and basalt hybrid yarn-based thermoplastic (TP) fabric composite (B-PP-1_PET_TP-F) FRCM specimens after the flexural test. The specimen reinforced with parent basalt (B-F) exhibited complete failure due to fibre fracture (Figure 4.46a). In contrast, the hybrid yarn-based TP fabric composite (B-PP-1_PET_TP-F) failed through a combination of fibre fracture and fibre pull-out, with fabric bridging preventing complete separation of the FRCM specimen (Figure 4.48d). Meanwhile, the TS fabric composite (B-PP-1_PET-EC-Y) did not experience complete fabric rupture and maintained strong bonding with the mortar matrix, suggesting its actual load-bearing potential may be higher than reported (Figure 4.48a).

Furthermore, replacing the parent basalt fabric with epoxy-coated thermoset and hybrid yarn-based thermoplastic fabric composites in mortar/concrete reinforcement resulted in an increase in fine microcracks, improved crack distribution, and reduced crack spacing. This indicates enhanced load transfer and stress redistribution, effectively preventing catastrophic (localized) failure.

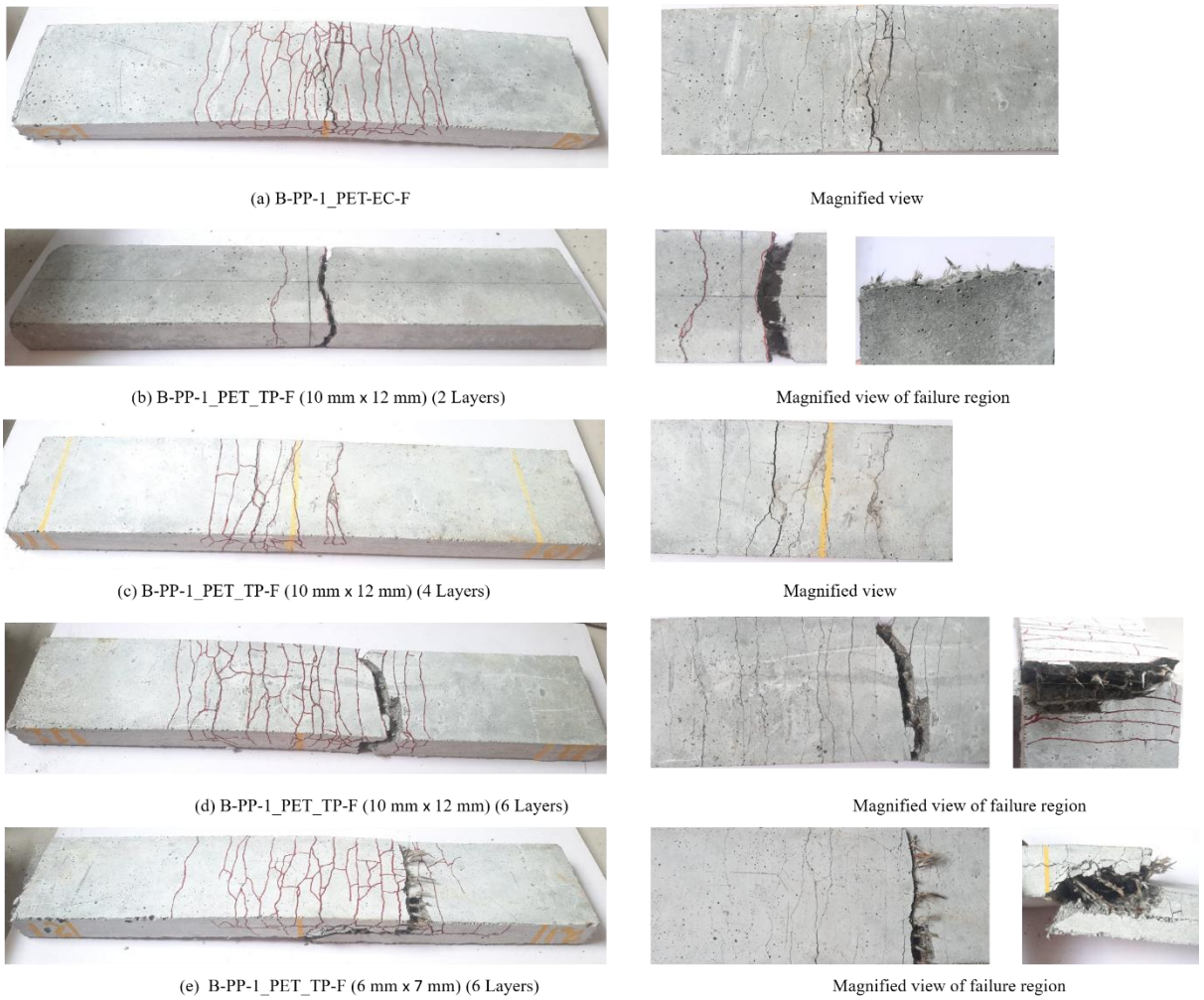


*Figure 4.48 Photographs of failed basalt epoxy coated FRCM and basalt thermoplastic fabric composite-based FRCM after flexural test.*

### 4.8.4 Effect of mesh size opening of fabric on flexural behaviour of FRCM specimens

Figure 4.49(a) illustrates the flexural load versus mid-span deflection behaviour of basalt hybrid yarn-based thermoplastic fabric composite reinforced FRCM specimens with varying mesh opening sizes (6 mm x 7 mm and 10 mm x 12 mm). As the mesh opening size decreases from 10 mm x 12 mm to 6 mm x 7 mm, the average flexural peak load of the B-PP-1_PET_TP-F (10 mm x 12 mm) FRCM specimen increased from 3.41 kN ($\sigma$ = 0.07) to 4.47 kN ($\sigma$ = 0.06), marking a 31% improvement.

Figure 4.49(b) displays the average flexural strength and energy absorption of B-PP-1_PET_TP-F (10 mm x 12 mm) and B-PP-1_PET_TP-F (6 mm x 7 mm) FRCM specimens. There is a notable increase in tensile strength by 31% and energy absorption by 72% when the mesh size reduces from 10 mm x 12 mm to 6 mm x 7 mm. This improvement is attributed

to the increased number of warp and weft yarns in the fabric, while maintaining the same dimensions of the FRCM specimen. Specifically, the fabric with a 10 mm x 12 mm mesh had six load-bearing warp yarns, whereas the 6 mm x 7 mm mesh had ten yarns.

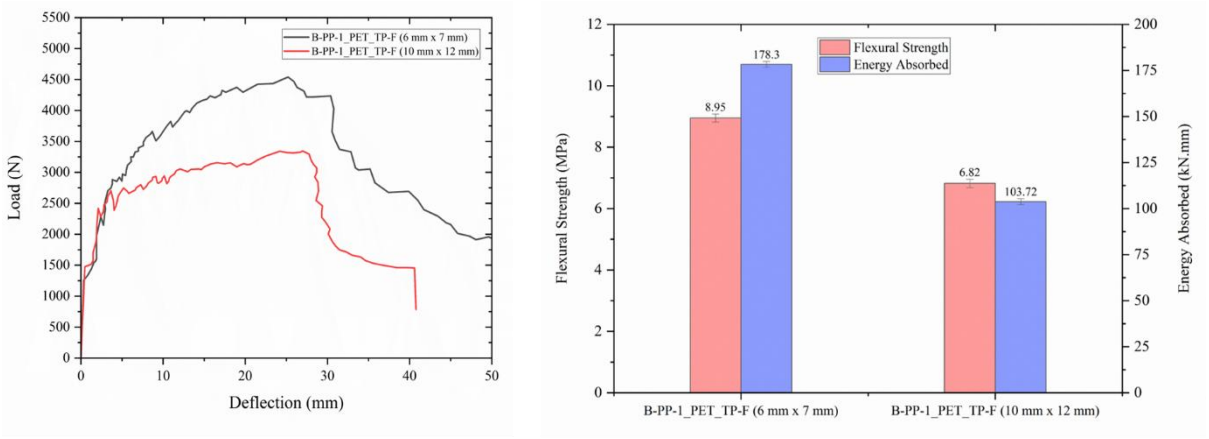


(a) (b)

*Figure 4.49 (a) Flexural load versus mid-span deflection plot for basalt hybrid yarn-based thermoplastic fabric composite reinforced FRCM specimens of varying mesh opening sizes (6 mm x 7 mm, and 10 mm x 12 mm), (b) plot representing average flexural strength and energy absorbed by these FRCM specimens during the flexural test.*

Figure 4.48(d,e) presents images of B-PP-1_PET_TP-F (10 mm x 12 mm) and B-PP-1_PET_TP-F (6 mm x 7 mm) FRCM specimens after flexural testing. Both specimens exhibited failure through a combination of fibre fracture and fibre pull-out, with fabric bridging preventing complete separation. Additionally, multiple fine microcracks formed along the width of the specimens, indicating improved load transfer and stress redistribution, effectively mitigating catastrophic (localized) failure.

### 4.8.5 Effect of number of layer reinforcement on flexural behaviour of FRCM specimens

The graph in Figure 4.50(a) shows the flexural load versus mid-span deflection behaviour of unreinforced plain mortar (PC), PP fibre reinforced mortar (PP-FRC) without fabric reinforcement, and FRCM specimens reinforced with basalt hybrid yarn-based thermoplastic fabric composites – B-PP-1_PET_TP-F (2 Layers), B-PP-1_PET_TP-F (4 Layers), and B-PP-1_PET_TP-F (6 Layers). The flexural peak load of PC was 0.43 kN ($\sigma$ = 0.02), which increased by 123% to 0.96 kN ($\sigma$ = 0.008) with the PP-FRC specimen. With two layers of basalt thermoplastic fabric composite reinforcement, the load increased by 297% to 1.71 kN

(σ = 0.04), by 490% to 2.54 kN (σ = 0.07) with four layers, and by 693% to 3.41 kN (σ = 0.07) with six layers. There is a significant improvement in flexural load when unreinforced mortar is replaced by PP-FRC, with further enhancements observed as the number of fabric layers increases.As the number of layers in FRCM specimens increases from two to six, the reinforcement ratio (fibre volume fraction) also increases, enhancing the flexural load-bearing capacity of TRC specimens. This improvement allows them to resist higher forces before failure. Additionally, the increased number of fabric layers contributes to better deflection-hardening behaviour, improved ductility (mid-span deflection), and greater energy absorption, making the specimens more resilient under flexural loading.

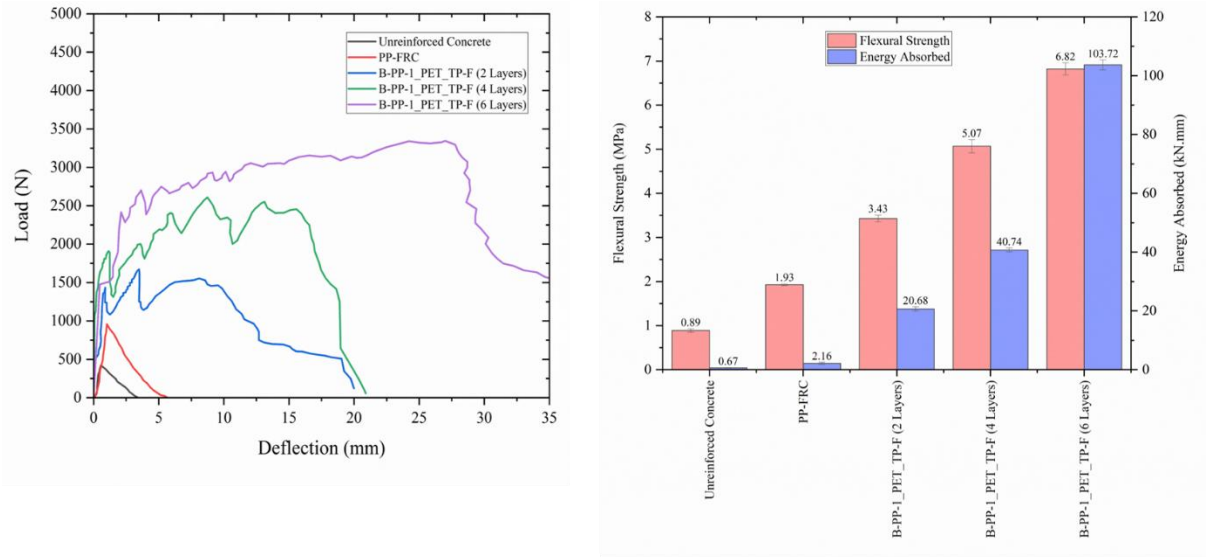


(a) (b)

*Figure 4.50 (a) Flexural load versus mid-span deflection plot for unreinforced plain mortar, PP-FRC, and FRCM specimens reinforced with B-PP-1_PET_TP-F (2 L), B-PP-1_PET_TP-F (4 L), and B-PP-1_PET_TP-F (6 L), (b) plot representing average flexural strength and energy absorbed by these FRCM specimens during the flexural test.*

Figure 4.50(b) depicts the average flexural strength and energy absorbed by plain mortar (PC), PP fibre reinforced mortar (PP-FRC) without fabric reinforcement, and FRCM specimens reinforced with basalt hybrid yarn-based thermoplastic fabric composites – B-PP-1_PET_TP-F (2 Layers), B-PP-1_PET_TP-F (4 Layers), and B-PP-1_PET_TP-F (6 Layers). Replacing PC with PP-FRC significantly increases tensile strength and energy absorption, and this improvement is even greater with more fabric layers. The flexural energy absorption of PC increased by 222% with the PP-FRC specimen, by 2986% with two layers of basalt TP fabric composite reinforcement, by 5980% with four layers, and by 15380% with six layers.

Fabrics made from high-performance fibres, combined with PP fibres added as secondary reinforcement in mortar mixing, synergistically improve load-bearing capacity, energy absorption, and ductility (mid-span deflection).

Figures 4.51(a,b), and 4.48(b,c,d) show images of plain mortar (PC), PP fibre reinforced mortar (PP-FRC) without fabric reinforcement, and FRCM specimens reinforced with basalt hybrid yarn-based TP fabric composites – B-PP-1_PET_TP-F (2 Layers), B-PP-1_PET_TP-F (4 Layers), and B-PP-1_PET_TP-F (6 Layers) – after flexural testing.

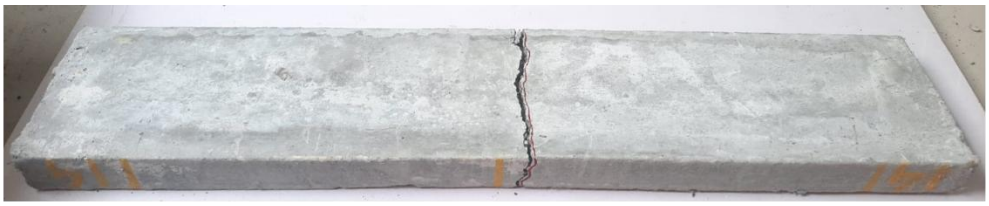

(a) PP fiber reinforced mortar specimen (PP-FRC)

(b) Unreinforced mortar specimen (without PP fibers)

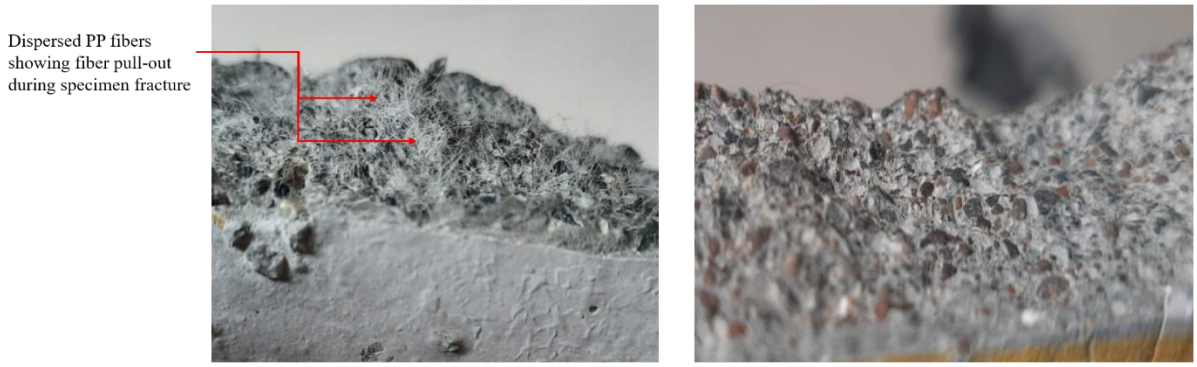


(c) Magnified view of fractured surface after flexural test – PP-FRC (left), unreinforced concrete (right)

*Figure 4.51 Photographs of failed unreinforced concrete and PP-FRC specimens after flexural test.*

The unreinforced PC and PP-FRC specimens exhibited failure with a single major crack leading to complete separation, although the PP-FRC showed some resistance with fibre pull-out behaviour (Figure 4.49, c). All FRCM specimens reinforced with TP fabric composites [B-PP-1_PET_TP-F (2 Layers), B-PP-1_PET_TP-F (4 Layers), and B-PP-

1_PET_TP-F (6 Layers)] failed through a combination of fibre fracture (fabric rupture) and fibre pull-out, with multiple fine cracks along the width. Increasing the number of fabric layers in the FRCM specimens led to more fine cracks, better crack distribution, and reduced crack spacing (Figure 4.47, b-d). The FRCM specimen with two layers showed complete separation, but with four and six layers, the fabric bridging effect prevented complete separation, improving the effectiveness of the FRCM specimens.

### 4.8.6 Flexural behaviour of Carbon FRCM specimens

The graph in Figure 4.52(a) illustrates the flexural load versus mid-span deflection behaviour of different carbon yarn-based FRCM specimens: uncoated, epoxy-coated, and hybrid.

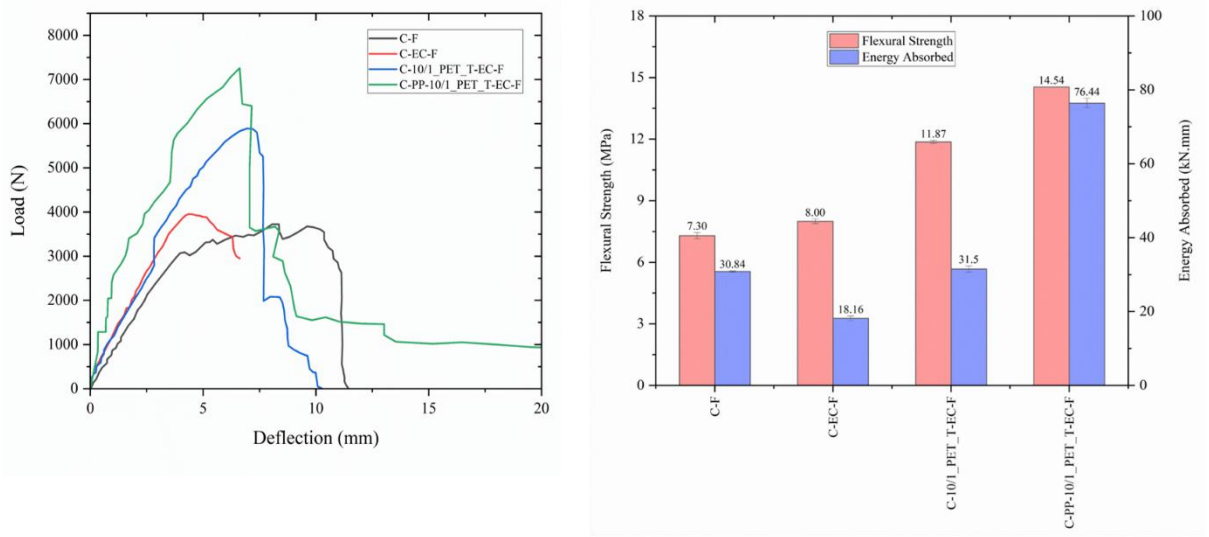


(a) (b)

*Figure 4.52 (a) Flexural load versus mid-span deflection plot for parent carbon fabric, epoxy coated carbon fabric, and carbon hybrid yarn-based fabric reinforced FRCM specimens, (b) plot representing average flexural strength and energy absorbed by these FRCM specimens during the flexural test.*

The parent (uncoated) carbon yarn based FRCM specimen exhibited an average flexural load of 3.65 kN ($\sigma$ = 0.08), which increased to 3.99 kN ($\sigma$ = 0.05) with epoxy coating. The addition of twisted PET yarn helically wrapped around the carbon yarn core, along with epoxy coating, further enhanced the load to 5.93 kN ($\sigma$ = 0.04). Finally, the DREF yarn with a carbon filament core, a sheath of PP fibres, helically wrapped with twisted PET yarn and epoxy coating, achieved the highest peak load of 7.27 kN ($\sigma$ = 0.01), representing a 99% increase in flexural load over the parent uncoated carbon FRCM specimen. FRCM specimens

reinforced with hybrid carbon yarn-based fabrics exhibited larger mid-span deflection before failure, enhancing ductility compared to parent uncoated carbon FRCM specimens.

Figure 4.52(b) illustrates the significant increase in average flexural strength and energy absorbed from fabric made with parent carbon yarn to epoxy-coated and hybrid yarn. The carbon hybrid yarn-based FRCM specimen (C-PP-10/1_PET_T-EC-F) exhibits a 99% increase in flexural strength and a 148% increase in energy absorbed compared to the parent (uncoated) carbon FRCM specimen (C-F). The reasons for this improvement in flexural load, flexural strength, mid span deflection (ductility) and energy absorption are similar to those discussed for ARG yarn-based FRCM specimens (see section 4.8.1).

Figure 4.53 shows images of carbon yarn-based FRCM specimens after the flexural test. Specimens reinforced with parent carbon fabric (C-F) exhibited complete separation due to a combination of fibre fracture (fabric rupture) and fibre pull-out. However, the carbon epoxy-coated and hybrid yarn-based FRCM specimens (C-EC-F, C-10/1_PET_T-EC-Y, and C-PP-10/1_PET_T-EC-Y) did not undergo complete fabric rupture and maintained strong bonding with the mortar matrix, suggesting their true potential may be greater than reported. The superior mechanical properties and strong bonding of carbon fabrics with mortar were evident. The number of fine microcracks and crack distribution improved from parent carbon fabric to epoxy-coated and hybrid yarn-based fabric.

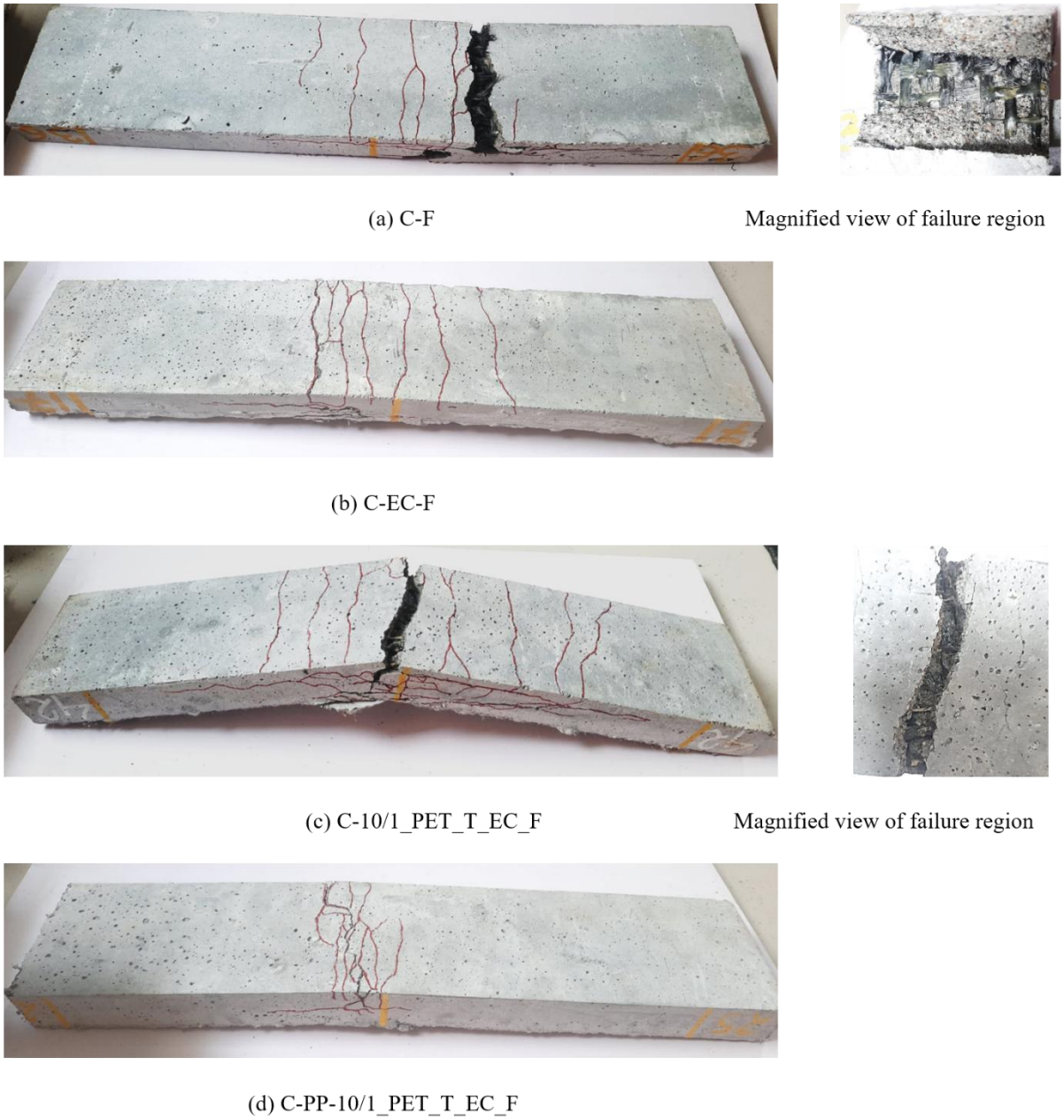

(a) C-F

Magnified view of failure region

(b) C-EC-F

(c) C-10/1_PET_T_EC_F

Magnified view of failure region

(d) C-PP-10/1_PET_T_EC_F

*Figure 4.53 Photographs of various failed FRCM specimens reinforced with carbon fabric, epoxy-coated carbon fabric, and hybrid yarn-based carbon fabrics subjected to a flexural test.*

### 4.8.7 Comparison of flexural behaviour of different FRCM specimens

The graph in Figure 4.54(a) illustrates the flexural load versus mid-span deflection behaviour of various parent (uncoated) and hybrid AR glass, basalt, and carbon FRCM specimens. The parent (uncoated) FRCM specimens exhibit the highest flexural peak load for carbon (C-F) at 3.65 kN ($\sigma$ = 0.08), followed by basalt (B-F) at 2.30 kN ($\sigma$ = 0.02), and AR glass (ARG-F) at 2.02 kN ($\sigma$ = 0.02). Among the hybrid FRCM specimens, carbon (C-PP-10/1_PET_T-EC-Y)

shows the highest tensile peak load at 7.27 kN (σ = 0.01), followed by basalt (B-PP-10/1_PET_T-EC-Y) at 4.70 kN (σ = 0.11), and AR glass (ARG-PP-10/1_PET_T-EC-Y) at 4.40 kN (σ = 0.05).

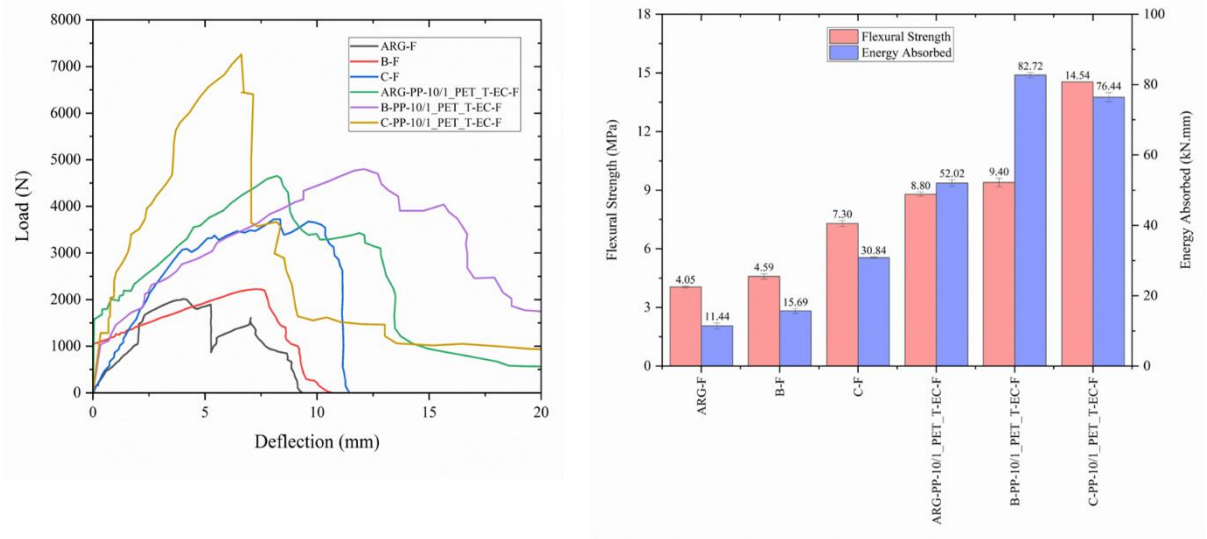


(a) (b)

*Figure 4.54 (a) Flexural load versus mid-span deflection plot for AR glass, basalt and carbon parent, and hybrid FRCM specimens, (b) plot representing average flexural strength and energy absorbed by these FRCM specimens during the flexural test.*

Figure 4.54(b) presents the flexural strength and energy absorbed by these specimens. Consistent with the flexural peak load values, carbon FRCM specimens have the highest flexural strength and energy absorption, followed by basalt, with AR glass being the lowest. Hybrid yarn-based FRCM specimens exhibit higher flexural strength and energy absorption than their parent counterparts, regardless of fibre type (AR glass, basalt, and carbon). This flexural behaviour of FRCM specimens aligns with the tensile properties observed in the fabric tensile test results and the tensile behaviour of FRCM specimens. This suggests that the tensile properties of the fabric have been effectively transferred to the FRCM specimens.